Multimodal analysis of neuroimages in Alzheimer's disease

Multimodal analysis of neuroimages in Alzheimer's disease

ACADEMIC DISSERTATION

to obtain the degree of Doctor at the Maastricht University, on the authority of the Rector Magnificus, Prof. Dr. G.P.M.F. Mols, in accordance with the decision of the Board of Deans,
to be defended in public on Friday
October 15th 2010 at 12:00 hrs

by

ANNA CAROLI

born in Bergamo (Italy) on October 25th 1979

Promotor:

Prof. Frans R.J. Verhey (Maastricht University)

Co-promotores

Dr. Andrea Remuzzi (Mario Negri Institute, Italy)

Dr. Giovanni B. Frisoni (IRCCS Fatebenefratelli, Italy)

Assessment committee

Prof. Eric Griez (chairman)

Dr. Martin van Boxtel

Prof. Marc DeBaets

Prof. Eric Salmon (University of Liège)

Dr. Pieter-Jelle Visser (Maastricht University and VU Amsterdam)

The research for this thesis was performed at the Laboratory of Epidemiology, Neuroimaging and Telemedicine of the IRCCS Centro San Giovanni di Dio – Fatebenefratelli in Brescia, Italy. The discussion of this PhD thesis at Maastricht University was made possible thanks to an active cooperation between Maastricht University, the Netherlands, and Mario Negri Institute for Pharmacological Research in Bergamo, Italy.

To my family

Abbreviations

AD = Alzheimer’s disease
ADAS-Cog = Alzheimer's disease assessment scale-cognitive subscale
ADC = apparent diffusion coefficient
ApoE = apolipoprotein E
ARWMC = age related white matter changes
BOLD = blood oxygenation level dependent
BPM = biological parametric mapping
BBSI = brain boundary shift integral
CDT = clock drawing test
CES-D = center for epidemiologic studies depression scale
COWAT = controlled oral word association test
CSF = cerebrospinal fluid
CTAC = CT-based attenuation correction
DTI = diffusion tensor imaging
ECD = ethyl cysteinate dimer
ECG = electrocardiogram
FA = fractional anisotropy
FDG = fluorodeoxyglucose
FDR = false discovery rate
FLAIR = fluid attenuation inversion recovery
fMRI = functional magnetic resonance imaging
FTD = frontotemporal dementia
FWE = family-wise error
FWHM = full width at half maximum
GM = grey matter
ICA = independent component analysis

MCI = mild cognitive impairment

MMSE = mini mental state exam

MRI = magnetic resonance imaging

MTA = medial temporal lobe atrophy

MTI = magnetization transfer imaging

MTL = medial temporal lobe

NC = normal control

PET = positron emission tomography

PVE = partial volume effect

PIB = Pittsburgh compound B

ROI = region of interest

SPECT = single photon emission computed tomography

SPM = statistical parametric mapping

SSP = stereotactic surface projection

TIV = total intracranial volume

TMT = trail making test

VBA = voxel-based analysis

VBM = voxel-based morphometry

WFU = wake forest university

WM = white matter

WMH = white matter hyperintensity

Table of contents

Chapter 1	Introduction	9
Chapter 2	Quantitative evaluation of Alzheimer's disease	17
Chapter 3	Cerebral perfusion predictors of conversion to Alzheimer's Disease in amnestic Mild Cognitive Impairment	57
Chapter 4	Brain perfusion correlates of medial temporal lobe atrophy and white matter hyperintensities in mild cognitive impairment	77
Chapter 5	In vivo mapping of amyloid toxicity in Alzheimer's disease	95
Chapter 6	Functional compensation in incipient Alzheimer's disease	111
Chapter 7	Metabolic compensation and depression in Alzheimer's Disease	133
Chapter 8	General discussion	149
Chapter 9	Acknowledgments	165
Chapter 10	Summary	169
	Curriculum vitae	173

Chapter 1

Introduction

Alzheimer's disease: an overview

More than 35 million people worldwide are affected by Alzheimer's disease (AD), a deterioration of memory and other cognitive domains that leads to death within 3 to 10 years after diagnosis [1]. AD is the most common form of dementia, accounting for 42 to 54% of cases at autopsy [2] and in the clinical setting [3]. AD combined with intracerebral vascular disease accounts for another 15 to 22% of cases [2,3].

The principal risk factor for Alzheimer's disease is age. The incidence of the disease doubles every 5 years after 65 years of age, with the diagnosis of 1275 new cases per year per 100,000 persons older than 65 years of age [4]. Data on centenarians show that Alzheimer's disease is not necessarily the outcome of aging [5]; however, the age of peak incidence is ≥80 years, and more than one third of elderly people aged 85 years or older receive the diagnosis of Alzheimer's disease.

At the individual level, AD significantly shortens life expectancy and is one of the principal causes of physical disability, institutionalization, and decreased quality of life among the elderly. Moreover, the social, health and economic burden due to AD are a worldwide problem, with some of the greatest burden coming from the developing world, where people live longer. Throughout the world, as the population is aging, the projected growth of Alzheimer's disease is dramatic [6,7]. AD is a top priority public health problem, which needs to be faced.

AD: need for an early diagnosis

Alzheimer's disease can be definitively diagnosed only by histopathologic examination of brain tissue [8]. Post-mortem studies have identified the major hallmarks of late-stage Alzheimer's disease, including amyloid plaques, neurofibrillary tangles, neuronal cell loss, and gliosis [9]; however, to date, the initiating mechanisms that trigger disease onset and drive its progression have not been fully understood, yet. Efforts to understand and track the early changes associated with AD will greatly increase our understanding of disease-causing mechanisms and lead to the identification of novel targets for pharmaceutical intervention which could delay disease progression.

During the last ten years most of the Alzheimer's disease research has been focused on finding biomarkers that could be reliably used to diagnose AD, monitor its progression, and possibly predict its onset [10,11].

The diagnosis of AD is especially challenging in its early stages, because of the

difficulty in distinguishing AD from mild memory decline that can occur in normal aging and from mild cognitive manifestations of other neuropsychiatric conditions, such as depression, as well as other causes of dementia [12,13]. Early diagnosis is extremely relevant as patients at the earliest stage of the disease have the most to gain from therapies that intervene in the course of inexorably progressive and irreversible brain damage.

Imaging in AD

Advances in neuroscience and neuroimaging have led to an increasing recognition that certain neuroanatomical structures may be affected preferentially by particular disease. Neurodegenerative brain diseases mark the brain with a specific morphological "signature", detection of which may be useful to enhance diagnosis. The two main morphostructural aspects in the clinical diagnosis of AD are regional atrophy (especially assessed in the medial temporal lobe) [14] and subcortical cerebrovascular damage [15]. Structural imaging (mainly magnetic resonance imaging - MRI) enables to investigate both aspects, providing markers to track the biological progression of disease [16].

As functional alterations precede structural changes [17], functional imaging (mostly single photon emission computed tomography - SPECT, fluorodeoxyglucose-positron emission tomography - FDG-PET [18,19] and functional MRI - fMRI [20]) is playing an increasingly relevant role in detecting the dysfunction that characterizes the earliest stage of AD, providing pathophysiological information on synapse dysfunction in AD in vivo that cannot be detected by structural imaging. Furthermore, functional imaging provides the chance to objectively determine the extent to which clinically effective treatments attenuate or potentially compensate for disease progression.

Grey matter (GM) loss assessed by structural MRI has a limited ability to capture the whole range of morphostructural changes associated with neurodegeneration in AD; it cannot discriminate neuronal from glial and axonal loss, or neuronal loss from age-associated shrinkage of healthy neurons, and it cannot appreciate white matter (WM) damage that might arise from neurofilament tau pathology. Recently, several microstructural imaging techniques probing into the finer structure of the brain have been developed, such as diffusion tensor (DTI) and magnetization transfer imaging (MTI). Microstructural imaging enables investigation of the brain microstructure [21],

providing increasingly precious information to elucidate the pathophysiology of AD.

Currently, protein concentration (i.e. extracellular amyloid plaques and intracellular neurofibrillary tangles load) is assessed by lobar puncture followed by CSF (Cerebrospinal Fluid) laboratory analysis, an invasive procedure not suitable for all patients. Research is indeed very active into molecules labelled with radioactive isotopes that might enter the brain, bind selectively to β-amyloid, be visualized with PET scanners and analyzed with PET imaging tools, enabling in vivo quantification of amyloid plaque load in AD, the compound at the most advanced stage of validation being Pittsburgh compound B (PIB) [22]. Amyloid imaging could hopefully replace lobar puncture for the investigation of the pathological processes occurring at the cellular level, identifying in vivo neuroanatomic evidence of AD at a very early stage.

The more and more relevant role of imaging in the diagnosis of AD has been further pointed out in the revised diagnostic criteria for probable AD recently proposed by Dubois and colleagues, currently used in research and still undergoing validation for clinical application, developed to capture both the earliest stages and the full spectrum of the illness: the new criteria stipulate that, beyond a clinical core of early and significant episodic memory impairment, there must be at least one or more abnormal biomarkers, among cerebrospinal fluid analysis of beta-amyloid or tau proteins and imaging biomarkers (i.e. medial temporal lobe atrophy - MTA, temporo-parietal metabolism and amyloid PET) [23].

Multimodal imaging

Single imaging techniques enable to study single cerebral alterations; in order to investigate the overall cerebral damage, several techniques should be combined. There is considerable promise that early and specific diagnosis of AD will be rendered possible through the combination of a number of different imaging biomarkers for AD, such as medial temporal or cortical atrophy on MRI, functional defects in the temporoparietal and posterior cingulate cortex on PET, SPECT, or fMRI, microstructural pathology on DTI or MTI, high amyloid load on PIB-PET, and non-imaging ones, such as low memory performance on comprehensive neuropsychological tests, and high concentrations of Aβ or tau protein in the CSF. A few studies have already tried to combine biomarkers, showing an increase in prognostic power [24,25] and diagnostic accuracy [26], but much work still needs to be done.

Aims of this thesis are:

1. To review the main neuroimaging tools currently available for quantitative evaluation of AD for both research and clinical purposes
2. To point out the relevance of multimodal imaging to increase single imaging technique prognostic power and diagnostic accuracy
3. To investigate the relationship between different imaging modalities
4. To find cerebral perfusion correlates of conversion to dementia in patients with amnestic mild cognitive impairment based on both SPECT and MR imaging
5. To assess the association of medial temporal lobe atrophy and white matter hyperintensities with grey matter perfusion in mild cognitive impairment
6. To study the relationship between grey matter atrophy and amyloid deposition in AD
7. To compare on a voxel-by-voxel basis grey matter atrophy and perfusion deficits in incipient AD in order to investigate the functional compensation and depression mechanism in the regions affected by AD neuropathology
8. To further investigate compensation and depression mechanisms in AD in terms of glucose metabolism

Overview of this thesis

Chapter 2 reviews the main neuroimaging techniques currently available for quantitative evaluation of AD for both research and clinical purposes, pointing out the need of assessing the relationship between single imaging modalities to increase prognostic power and diagnostic accuracy. Chapter 3 addresses SPECT prognostic power, identifying cerebral perfusion correlates of conversion to dementia in patients with amnestic mild cognitive impairment, and shows the voxel-wise relationship between atrophy and hypoperfusion patterns. Chapter 4 investigates the association of MR-based measures of medial temporal lobe atrophy and white matter lesions, assessed through visual rating scales, with voxel-wise grey matter perfusion in mild cognitive impairment. Chapter 5 looks into structural and amyloid imaging, studying the relationship between decreased grey matter density and increased [11C]-PIB uptake and assessing the regional distribution of amyloid toxicity. Chapter 6 and 7 voxel-wise compare grey matter atrophy and functional deficits in order to investigate the perfusion (chapter 6) and metabolic (chapter 7) compensation and depression mechanisms in the regions affected by AD neuropathology. Chapter 8 includes a general discussion, future perspectives and conclusion. Chapter 9 summarises this thesis.

References

1. Zanetti O, Solerte SB, Cantoni F. Life expectancy in Alzheimer's disease (AD). Arch Gerontol Geriatr 2009; 49 Suppl 1:237-243.
2. Brunnström H, Gustafson L, Passant U, Englund E. Prevalence of dementia subtypes: a 30-year retrospective survey of neuropathological reports. Arch Gerontol Geriatr 2009; 49:146-149.
3. Lobo A, Launer LJ, Fratiglioni L, et al. Prevalence of dementia and major subtypes in Europe: A collaborative study of population-based cohorts. Neurologic Diseases in the Elderly Research Group. Neurology 2000; 54:S4-S9.
4. Hirtz D, Thurman DJ, Gwinn-Hardy K, Mohamed M, Chaudhuri AR, Zalutsky R. How common are the "common" neurologic disorders? Neurology 2007; 68:326-337.
5. Den Dunnen WF, Brouwer WH, Bijlard E, et al. No disease in the brain of a 115-year-old woman. Neurobiol Aging 2008; 29:1127-1132.
6. Hebert LE, Scherr PA, Bienias JL, Bennett DA, Evans DA. Alzheimer disease in the US population: prevalence estimates using the 2000 census. Arch Neurol 2003; 60:1119-1122.
7. Alzheimer's Association. 2009 Alzheimer's Disease Facts and Figures. Available at: www.alz.org.
8. McKhann G, Drachman D, Folstein M, Katzman R, Price D, Stadlan EM. Clinical diagnosis of Alzheimer's disease: report of the NINCDS-ADRDA Work Group under the auspices of Department of Health and Human Services Task Force on Alzheimer's Disease. Neurology 1984; 34:939-944.
9. Goedert M, Spillantini MG. A century of Alzheimer's disease. Science 2006; 314:777-781.
10. Hampel H, Burger K, Teipel SJ, Bokde AL, Zetterberg H, Blennow K. Core candidate neurochemical and imaging biomarkers of Alzheimer's disease. Alzheimers Dement 2008; 4:38-48.
11. Shaw LM, Korecka M, Clark CM, Lee VM, Trojanowski JQ. Biomarkers of neurodegeneration for diagnosis and monitoring therapeutics. Nat Rev Drug Discov 2007; 6:295-303.
12. Callahan CM, Hendrie HC, Tierney WM. Documentation and evaluation of cognitive impairment in elderly primary care patients. Ann Intern Med 1995; 122:422-429.
13. McDaniel LD, Lukovits T, McDaniel KD. Alzheimer's disease: the problem of incorrect clinical diagnosis. J Geriatr Psychiatry Neurol 1993; 6:230-234.
14. Duara R, Loewenstein DA, Potter E, et al. Medial temporal lobe atrophy on MRI scans and the diagnosis of Alzheimer disease. Neurology 2008; 71:1986-1992.
15. Frisoni GB, Galluzzi S, Pantoni L, Filippi M. The effect of white matter lesions on cognition in the elderly – small but detectable. Nat Clin Pract Neurol 2007; 3: 620-627.
16. Frisoni GB, Fox NC, Jack CR Jr, Scheltens P, and Thompson PM. The clinical use of structural MRI in Alzheimer disease. Nat Rev Neurol 2010; 6:67-77.
17. Small SA. Alzheimer disease, in living color. Nat Neurosci 2005; 8:404-405.
18. Herholz K, Carter SF, Jones M. Positron emission tomography imaging in dementia. Br J Radiol 2007; 80:S160-S167.
19. Jagust WJ, Reed B, Mungas D, Ellis W, Decarli C. What does fluorodeoxyglucose PET imaging add to a clinical diagnosis of dementia? Neurology 2007; 69:871-877.
20. Liu Y, Wang K, Yu C, et al. Regional homogeneity, functional connectivity and imaging markers of

Alzheimer's disease: a review of resting state fMRI studies. Neuropsychologia 2008; 46:1648-1656.

21. Stahl R, Dietrich O, Teipel SJ, Hampel H, Reiser MF, Schoenberg SO. White matter damage in Alzheimer disease and mild cognitive impairment: assessment with diffusion-tensor MR imaging and parallel imaging techniques. Radiology 2007; 243:483-492.
22. Ikonomovic MD, Klunk WE, Abrahamson EE, et al. Post-mortem correlates of in vivo PiB-PET amyloid imaging in a typical case of Alzheimer's disease. Brain 2008; 131:1630-1645.
23. Dubois B, Feldman HH, Jacova C, et al. Research criteria for the diagnosis of Alzheimer's disease: revising the NINCDS-ADRDA criteria. Lancet Neurol 2007; 6:734-746.
24. Okamura N, Arai H, Maruyama M, et al. Combined Analysis of CSF Tau Levels and [(123)I]Iodoamphetamine SPECT in Mild Cognitive Impairment: Implications for a Novel Predictor of Alzheimer's Disease. Am J Psychiatry 2002; 159:474-476.
25. Borroni B, Anchisi D, Paghera B, et al. Combined 99mTc-ECD SPECT and neuropsychological studies in MCI for the assessment of conversion to AD. Neurobiol Aging 2006; 27:24-31.
26. Schmidt R, Ropele S, Pendl B, et al. Longitudinal multimodal imaging in mild to moderate Alzheimer disease: a pilot study with memantine. J Neurol Neurosurg Psychiatry 2008; 79:1312-1317.

Chapter 2

Quantitative evaluation of Alzheimer's disease

Caroli A and Frisoni GB

Expert Reviews in Medical Devices 2009; 6:569-588

Abstract

Alzheimer's disease can be definitively diagnosed only by histopathologic examination of brain tissue, and the identification and differential diagnosis of AD is especially challenging in its early stages. Neuroimaging is playing a more and more relevant role in the identification and quantification of AD in vivo, especially in preclinical stages, when a therapeutical intervention could be more effective. Neuroimaging enables to quantify brain volume loss (structural imaging), to detect early cerebral dysfunction (functional imaging), to probe into the finest cerebral structures (microstructural imaging), and to investigate amyloid plaque and neurofibrillary tangle build-up (amyloid imaging). Throughout the years, several imaging tools have been developed, ranging from simple visual rating scales to sophisticated computerized algorithms. As recently revised criteria for AD require quantitative evaluation of biomarkers mostly based on imaging, this paper provides an overview of the main neuroimaging tools which might be used presently or in the future in routine clinical practice for AD diagnosis.

Introduction

It is well known that Alzheimer's Disease can be definitively diagnosed only by histopathologic examination of brain tissue [1]. The identification and differential diagnosis of AD is especially challenging in its early stages, because of the difficulty in distinguishing AD from mild memory decline that can occur in normal aging and from mild cognitive manifestations of other neuropsychiatric conditions, such as depression, as well as other causes of dementia [2-5].

The need for an early, accurate diagnosis has become even more important now that several medications for the treatment of mild to moderate AD are available. Patients with neurodegenerative disease have the most to gain from therapy that intervenes as early as possible in the course of inexorably progressive, irreversible damage to brain tissue.

Recently, advances in neuroscience and neuroimaging have led to an increasing recognition that certain neuroanatomical structures may be affected preferentially by particular diseases. Neurodegenerative brain diseases mark the brain with a specific morphological "signature"; detecting this may be useful to enhance diagnosis, particularly in diseases lacking in other diagnostic tools. Moreover, structural imaging provide markers to track the biological progression of disease. As in AD functional alterations precede structural changes [6], functional imaging is playing a more and more relevant role in detecting the dysfunction that characterizes the earliest stage of AD, providing pathophysiological information on the distribution of neuronal death and synapse dysfunction in AD in vivo which cannot be detected by structural imaging yet. Recently, several techniques to probe into the finer structure of the brain have been developed, such as diffusion tensor and magnetization transfer imaging. Microstructural imaging enables to investigate the brain microstructure, providing increasingly precious information to elucidate the pathophysiology of AD. Finally, as AD is neuropathologically characterised by extracellular amyloid plaques and intracellular neurofibrillary tangles, amyloid imaging enables the investigation of the pathological processes occurring at the cellular level. It could help in identifying in vivo neuroanatomic evidence of AD at a very early stage and could even enable to detect any change in the natural history of amyloid deposition induced by anti-amyloid therapies.

Throughout the years, a number of imaging tools of varying technological level have

been developed to rate structural, functional, microstructural and amyloid changes taking place in the brains of patients with AD, ranging from simple subjective rating scales to sophisticated computerized algorithms. Which tools should be used in the clinical practice is not obvious. Aim of this paper is to review the main neuroimaging tools that clinical neurologists might use presently or in the future in their routine clinical practice for quantitative evaluation of AD.

The current review becomes particularly prominent in light of the revised diagnostic criteria for AD recently proposed by Dubois [7], currently used in research and still in course of validation for clinical application, developed to capture both the earliest stages and the full spectrum of the illness, which stipulate that there must be at least one or more abnormal biomarkers (among structural neuroimaging with MRI, molecular neuroimaging with PET, and cerebrospinal fluid analysis of β-amyloid or tau proteins) beyond a clinical core of early and significant episodic memory impairment. According to Dubois criteria even just one validated biomarker would be sufficient to diagnose AD. However, none of the proposed biomarkers has been adequately validated yet and a unique reliable biomarker still need to be identified. Revised criteria are flexible enough that any of the imaging methods described in this paper could be used, once adequately validated.

In view of the use of the new diagnostic criteria in the clinical practise, clinicians dealing with AD patients must get more and more familiar with available imaging techniques and equip themselves to use quantitative tools.

Structural imaging

The two main morphostructural issues of relevance in the clinical diagnosis of Alzheimer's Disease are regional atrophy (especially the medial-temporal one) [8] and subcortical cerebrovascular damage [9]. Both aspects can be accurately studied through magnetic resonance (MR) imaging, using a number of different tools. Structural imaging tools described in this section have been categorized based on increasing levels of technological intensivity and practical usability, and summarized in table 1.

Table 1: summary of the main structural MR imaging tools, ordered by increasing technical requirements.

Parameter	Technical requirements	Regional atrophy measure	Subcortical cerebrovascular disease measure
Visual rating	Routine acquisition	Scheltens MTL atrophy rating scale	ARWMC rating scale
Volumetry	3D T1 and Flair PD-T2 acquisition Manual or semiautomatic post-processing	Hippocampal and enthorinal cortex tracing	Thresholding of WMHs WMH volumetric measurement
Computational neuroanatomy	3D T1 and Flair PD-T2 acquisition Software for computerised post-processing serial scans	VBM Cortical pattern matching Cortical thickness measurement Hippocampal radial atrophy mapping BBSI	WMH segmentation and mapping

ARWMC: Age-related white matter change; BBSI: Brain-boundary shift integral; FLAIR: fluid attenuation inversion recovery; MTL: Medial temporal lobe; VBM: voxel-based morphometry; WMH: white matter hyperintensity

Visual rating scales

An easy and not much time-consuming way to quantitatively evaluate morphostructural changes on MRI is the use of specific visual rating scales.

Medial temporal atrophy. Magnetic resonance can directly visualise the hippocampus and other critical medial temporal lobe (MTL) structures in substantial cytoarchitectonic detail. Scheltens and colleagues [10] have developed a subjective visual rating scale to assess MTL atrophy on plain MR films (the subjective MTL atrophy score).

T1 weighted sequences are used and six coronal slices (slice thickness of 5 mm) parallel to the brainstem axis are acquired from a midsagittal scout image, the first image being acquired directly adjacent to the brainstem. The score (increasing with MTL atrophy) is assigned based on visual rating of the width of the choroid fissure, width of the temporal horn, and height of the hippocampal formation (figure 1).

In 41 patients with AD and 66 non-demented controls the subjective MTL atrophy score showed a correct classification of 96%, comparing favourably with volumetry (93%) [11]. In a prospective study of 31 patients with minor cognitive impairment, the subjective MTL atrophy score improved the predictive accuracy of age and delayed recall score for AD at follow-up [12]. More recently, DeCarli and coll. found MTL atrophy assessment to be helpful in estimating the risk of progressing from mild cognitive impairment (MCI) to dementia in 190 patients with MCI [13].

Figure 1. Visual rating of medial temporal lobe atrophy (MTA) on patient-specific MRI images. Figures displayed, from the left top to the right bottom, show increasing levels of MTA, rated from 0 (normality) to 4 (severe MTA) according to the Scheltens scale [10].

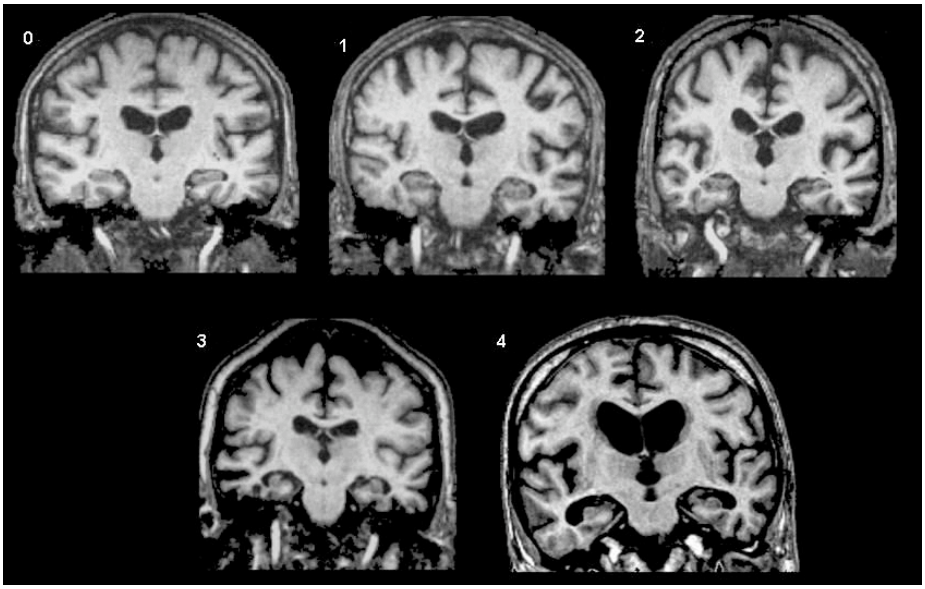

Subcortical cerebrovascular disease. White matter hyperintensities (WMHs) can be grouped according to morphologic features into smooth caps or halo, punctate, and confluent [14]. The smooth caps and halo are located in the periventricular white matter adjacent to the ependimal layer. Caps are usually less than 10 mm thick, and the halo tends to be progressively thinner from anterior to posterior (figure 2). Punctate and confluent lesions can be located in the periventricular or deep white matter (figure 2). Punctate hyperintensities are small (diameter less than 5 mm), round, with a regular boundary, and tend to be multiple in the same patient. Confluent lesions are larger than punctate (usually >5 mm), have irregular shape and boundaries, and seem to be originated by the confluence of smaller lesions. When periventricular, confluent lesions tend to be separated by the ventricles or the smooth periventricular halo by a more or less thin region of apparently normal white matter.

The European Task Force on Age Related White Matter Changes [15] has developed the age-related white matter changes (ARWMC) scale [16]. This is a 4-point scale requiring to rate white matter changes separately in five areas: frontal, parieto-occipital, temporal, infratentorial/cerebellum, and "basal ganglia" (striatum, globus pallidus, thalamus, internal/external capsule, and insula). The first three areas are

scored as 0: no lesions (including symmetrical, well-defined caps or bands), 1: focal lesions, 2: beginning confluence of lesions, 3: diffuse involvement of the entire region, with or without involvement of U fibres. The infratentorial/cerebellum and basal ganglia are scored as 0: no lesions, 1: only one focal lesion (>5 mm), 2: more than one focal lesion, 3: confluent lesions.The final results of the rating are 5 separate scores to grade white matter hyperintensities in the different brain regions in each hemisphere (figure 3).

Figure 2. MR images showing different combinations of white matter hyperintensities (WMHs): periventricular caps (c), caps and halo (ch), punctate (p) and confluent (cnf). Lacunes can also be appreciated within the confluent hyperintensities (right-bottom image). Modified from [14].

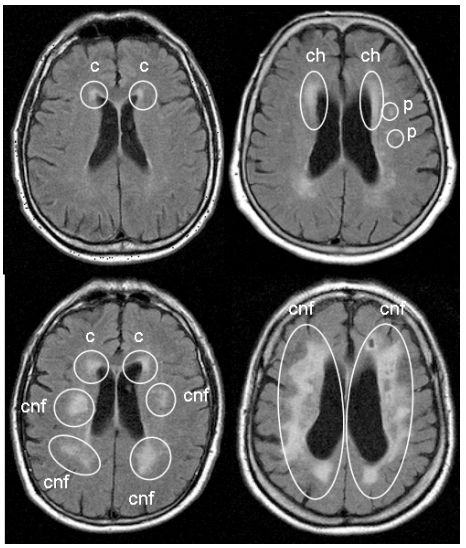

Figure 3. Visual rating of white matter hyperintensities (WMHs) on flair MRIs. Figures displayed show increasing levels of WMHs, rated according to the ARWMC scale [16]: (A) no white matter lesions (ARWMC score=1), (B1) mild (ARWMC score=5), (B2) moderate (ARWMC score=7), and (B3) severe white matter lesions (ARWMC score=9).

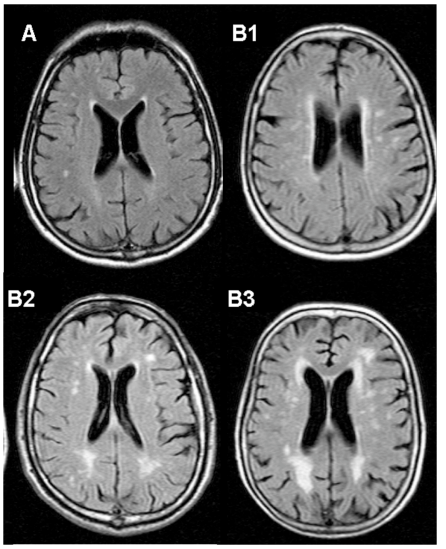

Volumetry

Qualitative MRI estimate of regional atrophy and subcortical cerebrovascular disease with visual rating scales may not fully appreciate the pathophysiology and pathology complexity of the diseases under investigation. Quantification of the patient-specific volumes based on MR can provide an objective measure of the severity of the underlying disease.

Medial temporal atrophy. A T1-weighted 3D-technique is employed for MR image acquisition (MP-RAGE or SPGR). After acquisition, the digital images need to be

reconstructed on coronal, 1-2 mm-thick slices. The hippocampus is then manually traced on all the contiguous slices where it can be appreciated (figure 4).

Figure 4. Single patient volumetric measure of the hippocampus based on digital MR: manual tracing.

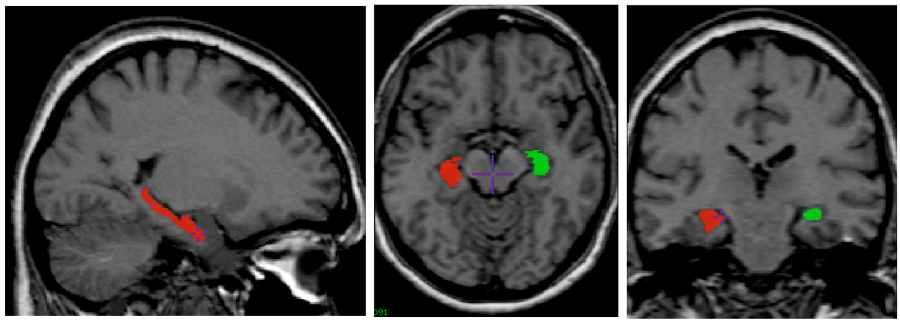

In expert hands, the reliability is high, intraclass correlation coefficients for hippocampal measurements being 0.95 for intrarater and 0.90 for interrater variability [17]. Sensitivity and specificity values of hippocampal volumes in a relative large series of 55 AD patients and 42 controls were 94 and 90%, respectively [18]. Small hippocampal volume has been found to be predictive of subsequent conversion to AD in 139 patients with MCI independently of age, education, and memory tests [19]. Of the 46 MCI patients with small hippocampal volume, nearly 55% converted to AD within the following 3 years, while of the 47 with medium hippocampal volume, converters were 35%, and of the 46 with large hippocampal volume 15% converted [19].

These findings suggest that serial measurements of the hippocampal volume enable to detect stable versus declining normal controls, MCI, and AD patients, and may therefore be a useful tool for AD diagnosis, even at the earliest stage, as well as for monitoring the progression of the disease.

Similarly, the enthorinal cortex, which is known to be the earliest site to be affected by AD, even at a preclinical stage, before hippocampus and neocortex [20,21], can be manually traced on MR images. AD was found to be associated with a greater rate of ERC atrophy than normal aging, and longitudinal ERC measurements were found to be better than cross-sectional measurements in separating AD from normal controls [22].

Subcortical cerebrovascular disease. A number of semi-automated methods have been developed to quantify the volume of WMHs, most based on the notion that pixels of

normal white matter can be accurately separated from those of hyperintense white matter. A conventional spin-echo, double-echo T2 or FLAIR sequence in the axial orientation is used for MR acquisition. De carli and colleagues developed a method based on manual tracing followed by automatic thresholding. Manual tracing is carried out crudely defining region of interest (ROI) within the white matter that completely includes all the hyperintense white matter (figure 5).

Figure 5. Semi-automated method developed by De Carli and collegues to quantify the volume of single patient white matter hyperintensities. A region of interest completely including all the hyperintense white matter is manually drawn. Automatic thresholding is than applied to the selected ROI in order to segment WMHs De Carli and collegues [23]

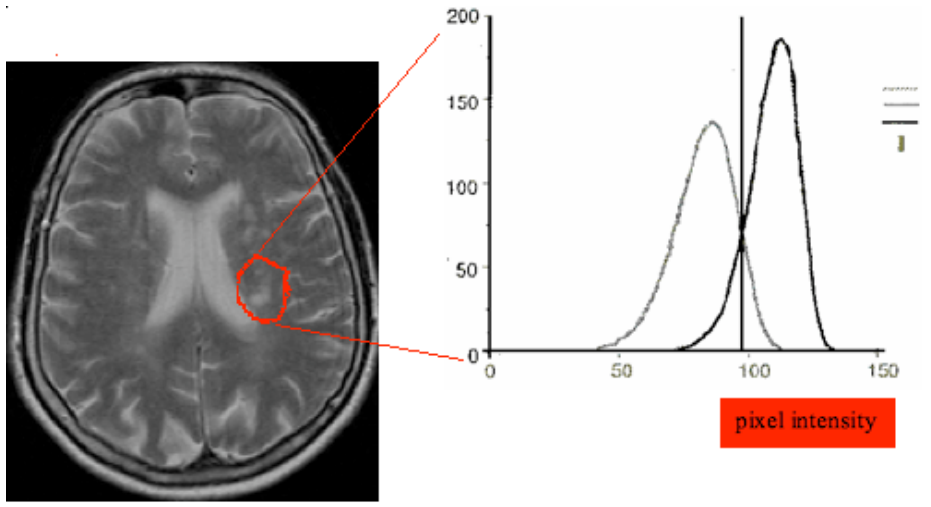

Intrarater and interrater reliabilities of this method are good [23]. WMH volume has been found to be predictive of cognitive impairment in a group of 369 cognitively intact community-dwelling older men [24].

Computational neuroanatomy

Recent developments in computer science may help to detect early sensitive and specific markers for AD. The new approaches are automated, avoiding error-prone and labour-intensive manual measurements. The effort to develop such algorithms has been referred to as computational neuroanatomy [25].

The individual algorithms can be categorized into two broad classes: algorithms devised to detect group differences at one point in time and algorithms devised to detect prospective changes over time. The first category may be useful to define disease-specific signatures. The second can be applied to one or more individuals to

track natural disease progression or as modified by treatment. While most tools have been developed to compare groups, some are being adapted to analyse individual cases, an issue of the greatest interest for the practicing physician.

Computational anatomy algorithms generally involve some or all of the following steps: a) brain extraction, b) tissue segmentation, c) spatial normalization, and d) statistical comparison of different subject groups or points in time. The pivotal step of all methods is registration. Here, cross-sectional methods match images of interest to a reference sterotactic template (a typical brain or a typical hippocampus, etc.) or vice versa, while prospective methods match sequential images of the same patients taken at different times.

Registration strategies differ in scope (i.e., analysis of the whole brain or preselected regions-of-interest) and mathematical approach (accounting for global or local variability of the brain's size and shape). Some cross-sectional methods that account for global variability are completely automated (such as voxel-based morphometry based on statistical parametric mapping by Ashburner and Friston [26] or cortical thickness measurement by Lerch et al [27]), while those that account for local variability often require manually positioned landmarks to precisely match the image to the template (such as the Cortical Pattern Matching) [28]. Longitudinal methods use the complexity of each individual's brain structure to align accurately an individual's serial images (such as the brain-boundary shift integral – BBSI – algorithm) [29].

To perform well, all methods need high spatial resolution and clear differentiation between tissue types. Usually, 3D high-resolution T1-weighted MR images (spoiled gradient – SPGR – or magnetization prepared rapid acquisition gradient recalled echo – MP-RAGE) acquired with conventional 1.5T MR scanners and 1 mm3 voxels (ideally isotropic) across the cranium provide sufficient detail and contrast.

Voxel-based morphometry (VBM) is a completely automatic method developed by Ashburner & Friston [26] based on the general linear model. All images are normalized to the same customized template, segmented into grey matter, white matter and cerebral spinal fluid, smoothed; the two groups are compared through a voxel-by-voxel t-test, and regions of tissue with significant increased or decreased density or concentration are identified. Like every statistical test, the larger the effect and group size, the higher the sensitivity of the method for identifying differences. This method has been implemented in the statistical parametric mapping software (SPM,

www.fil.ion.ucl.ac.uk/spm) running under Microsoft Windows or UNIX. Through voxel-based morphometry, the AD pattern of atrophy (figure 6) was found to involve hippocampus, posterior cingulate gyrus, adjacent precuneus, and temporoparietal association cortex [30,31].

Figure 6. Atrophy pattern related to a group of 25 AD patients compared with a group of 21 normal controls, assessed by voxel-based morphometry (SPM) and expressed in terms of t-scores: the higher is the t-score, the more significant is the GM volume reduction, i.e. GM atrophy.

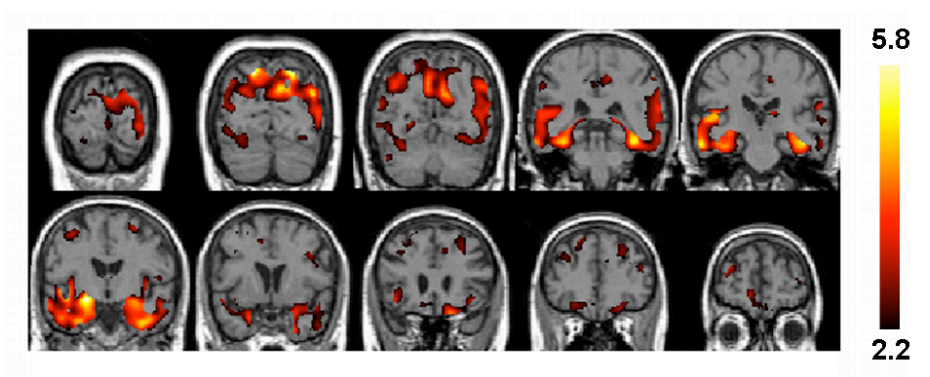

The VBM method could be used to assess differences among groups (e.g. AD patients vs normal controls) as well as within a group of subjects scanned at baseline and follow-up, in order to monitor the disease progression. In a recent prospective study, Chetelat et al. studied 18 patients with MCI for 18 months [32]. At the end of the follow-up period, 7 had converted to probable AD, and 11 remained MCI. Converters showed greater grey matter loss than non-converters in the temporal neocortex, medial temporal lobe structures, posterior cingulate, and precuneus, bilaterally.

In order to use VBM as a routine diagnostic tool, single subjects should be compared with the normal control group. The "single case" procedure is being used for research purposes; however, it is in course of validation to be used in the clinical practise, for both the AD and MCI diagnosis (figure 7).

Figure 7. Surface rendering of regions of atrophy of one AD patient (left) and one amnestic MCI patient (right) in comparison with a database of normal elderly subjects, assessed by voxel-based morphometry (SPM). Atrophy is expressed in terms of t-scores: the higher is the t-score, the more significant is the GM density reduction.

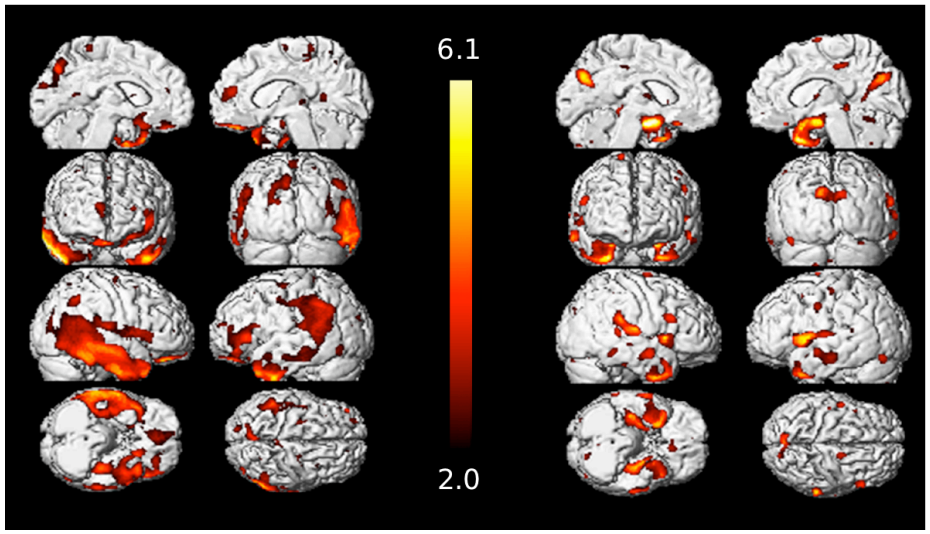

Cortical pattern matching is a sensitive approach that measures the topologic variability of the cortex [33-36]. The approach consists of cortical flattening and sulcal matching that aim to obtain an average cortical model for a group of subjects; measures of grey matter density can then be analyzed with statistical tools similar to those used by voxel-based morphometry. This technique can be executed on high-end desktop machines such as the Macintosh G4, as well as Silicon Graphics Interface or Sun workstations running UNIX. These algorithms are often used in client-server mode, connecting to a supercomputer for very large-scale analyses [37].

Cortical pattern matching allows to map changes of cortical grey matter density or thickness in AD as compared to normal controls with great accuracy (figure 8) [38,39]. As it provides quantitative and dynamic visualization of cortical atrophy rates, cortical pattern matching could be used to better localize disease effects within cortex over time. Thompson et al. longitudinally studied 12 AD patients and 14 elderly normal controls, and found that cortical atrophy occurred in a well-defined sequence as the disease progressed, from temporal and limbic cortices into frontal and occipital brain regions [40], mirroring the temporal sequence of beta-amyloid and neurofibrillary tangle accumulation observed at autopsy. Furthermore, local grey matter loss rates (5.3±2.3% per year in AD versus 0.9±0.9% in controls) extremely strongly correlated

with progressively declining cognitive status. More recently, we mapped the topography of cortical atrophy throughout the stages of severity, finding that the polysynaptic hippocampal pathway is affected in incipient AD, while the direct pathway and sensorimotor and visual networks are affected in moAD [41].

Figure 8. Grey matter loss of a group of early onset AD (left) and a group of late onset AD patients (right) compared with a group of normal controls assessed by cortical pattern matching. Modified from [39]

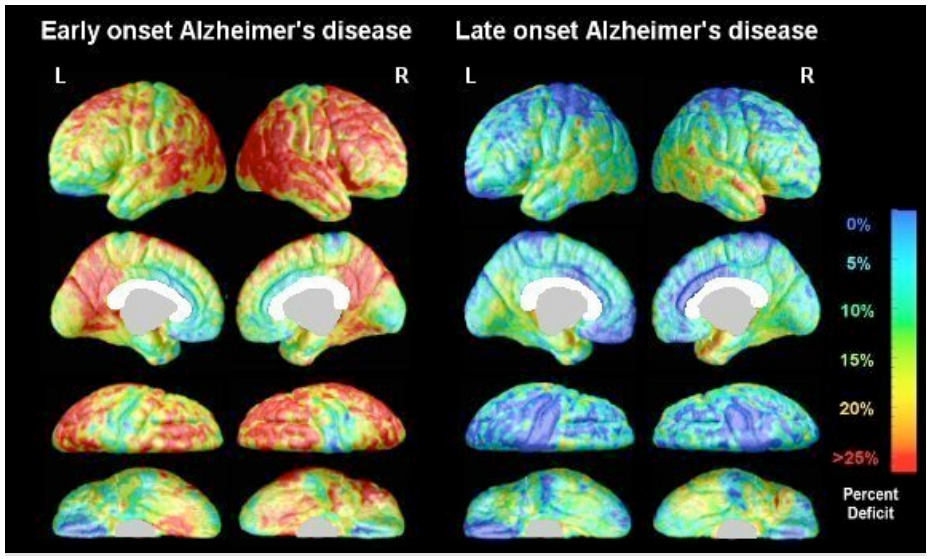

Ideally, apart from statistical issues, cortical pattern matching could be used to precisely assess single patient topologic variability of the cortex, through the comparison of a single patient with a group of normal controls. However, requiring manual tracing of the main sulci for each subject, the method is really time-consuming, needs experienced operator, and is then difficult to fit in the clinical practise.

Cortical thickness measurement. Lerch et al. developed a fully automated method to measure cortical thickness on MR images [27,42]. Native MRIs are registered to stereotaxic space and classified into white matter, grey matter, and CSF. Deformable initial spherical models are fit to the white matter and pial surfaces, which are then used to measure cortical thickness in 3D throughout the brain.

Statistically significant widespread cortical atrophy, with a specific focus on the temporal lobe and limbic cortex, was found in 19 AD patients as compared with 17 normal controls [27,42]. The patterns of thinning co-locate well with the putative presence of microscopic pathological features (plaques and tangles), increasing

confidence in these results.

Despite requiring high technology, the automated measurement of cortical thickness provides a potentially helpful tool for the diagnosis of AD, as well as an objective, reproducible in vivo metric of disease progression and remission.

Hippocampal radial atrophy mapping is a new 3-dimensional (3D) approach that allows to accurately localize atrophy within the hippocampus, reflecting pathological involvement, and thus enabling to better investigate the biological basis of functional disruption. After manual tracing of the hippocampus, a medial curve is automatically defined, and radial distance of each hippocampal surface point is computed. Statistical maps showing local group differences in radial hippocampal distance are displayed, with shorter radial distances indicative of atrophy.

Figure 9. Topographic distribution of atrophy in the hippocampal formation of a group of 28 patients with Alzheimer's disease compared to 40 elderly controls, assessed by hippocampal radial mapping. This technique allows to accurately localize atrophy within the hippocampus, thus enabling to carry out in vivo macroscopic neuropathology of the hippocampus. The figure shows that in AD significant atrophic changes amounting to tissue loss of 20% or more (in red) were found in regions of the hippocampal formation corresponding to the CA1 field and part of the subiculum. Regions corresponding to the CA2-3 fields were remarkably spared (in blue). Modified from [43].

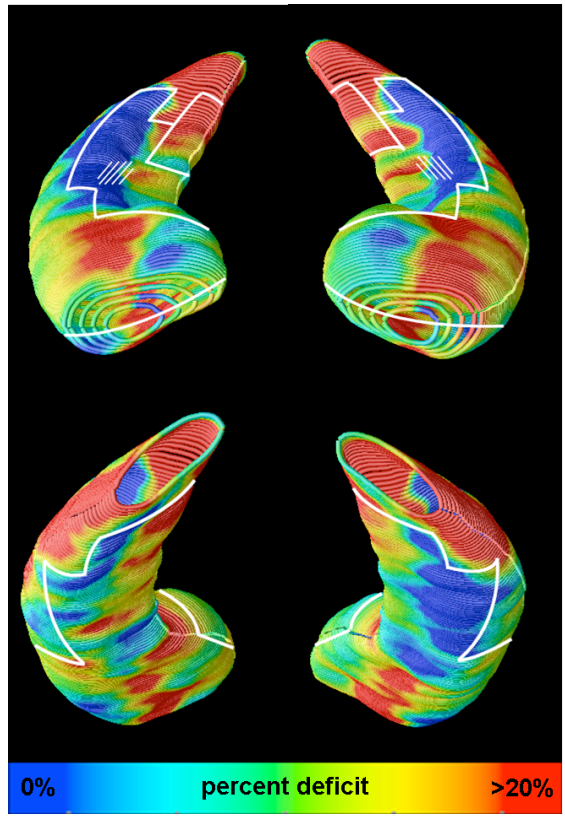

Recently, we found significant atrophic changes in 28 patients with mild to moderate AD as compared to 40 normal controls amounting to tissue loss of 20% or more in regions of the hippocampal formation corresponding to the CA1 field and part of the subiculum, known to be affected from pathological studies. Regions corresponding to

the CA2– 3 fields were remarkably spared [43] (figure 9).

Hippocampal atrophy in Alzheimer's disease was found to map to areas in the body and tail that partly overlap those affected by normal aging. Specific areas in the anterior and dorsal CA1 subfield involved in Alzheimer's disease were not in normal aging, probably indicative of a differential neural systems involved in Alzheimer's disease and aging [44]. These findings support the possibility of carrying out in vivo macroscopic neuropathology of the hippocampus.

Hippocampal radial mapping technique is suitable for group analysis only, and it can thus used in research but not in clinical activity.

Whole brain assessment with the brain boundary shift integral (BBSI). Serial scans within the same subject have the advantage that the wide inter-individual variability of brain morphology is not an issue, and comparing pre-post images of the same subject(s) carries much less error than comparing a case to controls. Fox et al. recently developed BBSI technique to monitor rates of cerebral atrophy [30,45]. Information on prospective global changes can be obtained by rigidly matching serial scans and subtracting the superimposed images, and the difference reflects the volume of brain tissue lost or gained [46]. Cerebral volume loss is then expressed as a percentage of initial total brain volume and annualized to give a rate of global atrophy. Compared to region of interest (ROI) techniques used to measure atrophy, this automated BBSI technique doesn't require a-priori decisions about relevant ROI, has high repeatability and is insensitive to the operator. On the other hand, it has the limit to investigate the whole brain, including white matter, in the evaluation of cerebral atrophy.

The rate of atrophy in a group of 18 AD patients was found to be significantly greater than in 31 controls (2.78% vs 0.24%) [47]. Moreover, the rate of global cerebral volume loss was strongly correlated with rate of cognitive change measured with the Mini Mental State Exam (MMSE) score in 29 AD patients [48].

The BBSI technique enables to compute the atrophy rate of any specific patient followed throughout years.

This method might be particularly useful to detect disease in asymptomatic subjects at high risk of developing AD. Prospective measurements of brain atrophy have become a very relevant issue with the advent of drugs that might alter the natural history of AD by slowing its progression. Rates of brain atrophy measured from serial registered MR are being used as a surrogate outcome of drug effectiveness in clinical trials.

WMH segmentation and mapping. DeCarli and coll. [49,50] developed an image segmentation and nonlinear image mapping technique to determine the extent and spatial location of WMHs. Briefly, image segmentation using previously described algorithms was applied to the FLAIR sequences to segment WMH. After affine coregistration of the FLAIR image to the high-resolution T1 image, WMH voxels were used to correct intensity changes in the T1 image to reduce any adverse impact of the WMH voxel values on the accuracy of the nonlinear warping algorithm.

Data analysis included quantification of WMH volume, nonlinear mapping onto a common anatomic image, and spatial localization of each WMH voxel to create an anatomically precise frequency distribution map. Twenty-six mild Alzheimer's disease, 28 mild cognitive impairment patients, and 33 controls were studied. The Authors found that the overall burden of WMH was increased with both vascular risk factors and the degree of cognititve impairment. Regarding spatial distribution, WMHs are common to the periventricular area of cognitively normal and cognitively impaired individuals. WMHs were also most prevalent in frontal areas of cognitively normal, whereas more posterior regions and the corpus callosum were minimally affected [50].

Functional imaging

As functional alterations precede structural changes [6], functional imaging (both PET/ SPECT and functional MR imaging) is playing a more and more relevant role in detecting the dysfunction that characterizes the earliest stage of AD, providing pathophysiological information on the distribution of neuronal death and synapse dysfunction in AD in vivo which cannot be detected by structural imaging yet.

Functional scans can be investigated using several different methods, from visual inspection of the film to highly sophisticated computational instruments.

Functional imaging tools described in this section have been categorized based on imaging technique and increasing levels of technological intensivity and practical usability.

PET-SPECT imaging

Through the estimation of the local cerebral blood flow and metabolic rate of glucose consumption, respectively, SPECT and PET imaging techniques provide pathophysiological information on the distribution of cerebral dysfunction in AD.

SPECT has historically been the functional imaging modality most widely used in the

clinical evaluation of dementia [51]. In the recent years, PET has become more and more popular due to its higher resolution, sensitivity and accuracy [52-55], especially relevant for identifying disease in its earliest stages. In 2007 FDG-PET was included in the diagnostic criteria revised by Dubois and colleagues as one of the three biomarkers for AD [7], and it has been shown more than others to have diagnostic value. Recently, it has been shown in patients with pathologically verified disease that progressive metabolic reductions occur years in advance of clinical AD symptoms [56], suggesting PET power in early diagnosis.

Although the specific radiopharmaceuticals and instrumentation used in SPECT differ from those used in PET, the principles of interpretation, as well as the underlying neurobiologic processes, are similar. All the analysis tools presented hereafter for PET images could be applied to SPECT, too. They are summarized in table 2.

Table 2: summary of PET imaging tools, ordered by increasing technical requirements.

Regional function measure technique	Technical requirements	Output measure
ROI-based method	PET scan and 3D T1 MRI Manual or semi-automatic post-processing	ROI mean metabolism
Voxel-based analysis	PET scan SPM or NEUROSTAT software	voxel-by-voxel hypometabolism
PALZ	PET scan PALZ software	AD/non-AD

AD: Alzheimer's disease; PALZ: PMOD Alzheimer's discrimination analysis tool; ROI: region of interest; SPM: Statistical parametric mapping software

ROI-based methods. Historically, the AD-associated PET pattern has been defined based on visual inspection, which is an operator-dependent method and enables a qualitative but not quantitative evaluation of functional damage. In order to overcome visual inspection limitations, ROI-based methods have been developed, relying upon Region Of Interest (ROI) tracing on MR images and within-subject coregistration of PET and MRI scans. ROIs identified on PET scans can be used both to visually inspect metabolism in specific regions (ROI-based qualitative evaluation) and to calculate the mean metabolism within them (ROI-based semiautomatic quantitative method).

Several ROI-based studies showed that, in the resting state, brain metabolism is abnormally lower throughout the cortex in AD patients as compared with matchednormal control (NC) subjects, with a typical pattern of parieto-temporal and

posterior cingulate cortex reduced function [57-59]. Despite heterogeneity among studies, FDG-PET measures in those cortical regions were shown to provide excellent separation of AD from NC, with an overall sensitivity of 86% (95%CI 76%, 93%) and specificity of 86% (95%CI 72%, 93%) [60].

More recent reports, employing last-generation PET equipments, reported hypometabolsim in AD patients even in medial temporal regions [61-63]. Hippocampal metabolism at baseline was found to reliably predict decline both from normal controls (NC) to AD (with 83% sensitivity and 81% specificity) and from NC to MCI (with 74% sensitivity and 70% specificity) in a cohort of 77 normal elderly subjects (aged 50-80) followed over a 14 year period [64].

ROI-based methods could be used to investigate single subject metabolism and compare it with normal control one. However they are time-consuming, and intense skilled labour is necessary to draw ROIs; ROI analysis is limited by the need to make a priori assumptions about regions of particular interest.

Voxel-based analysis. In order to overcome ROI-based method limitations, fully automated, voxel-based analytical techniques have been developed; they enable examination of the whole brain at the single voxel level with no need for regional a-priori hypothesis. Voxel-based analysis (VBA) methods are the functional analogous of voxel-based morphometry previously described for structural imaging; they rely on spatial normalisation aimed to anatomically standardise all images onto a standard brain atlas while preserving metabolic counts [65]. Statistical comparisons are performed on a voxel-by-voxel basis, with the resultant creation of statistical parametric maps of significant effects.

There are two main automated software to perform VBA: statistical parametric mapping (SPM), which creates statistical parametric maps of significant effects [66-67], and NEUROSTAT, which includes a three-dimensional stereotactic surface projection routine (3D-SSP) to project maximal grey matter activity onto the surface [68].

VBA is currently used to compare groups of patients with normal controls [69] (figure 10). In order to use PET as a routine diagnostic tool, single subjects should be compared with the normal controls group. The "single case" procedure is being used for research purposes; however, it is in course of validation to be used in the clinical practise, for both AD and MCI diagnosis.

Figure 10. Hypometabolism pattern related to a group of 25 AD patients compared with a group of 21 normal controls, assessed by SPM voxel-based analysis and expressed in terms of t-scores: the higher is the t-score, the more significant is the FDG uptake reduction, i.e. hypometabolism

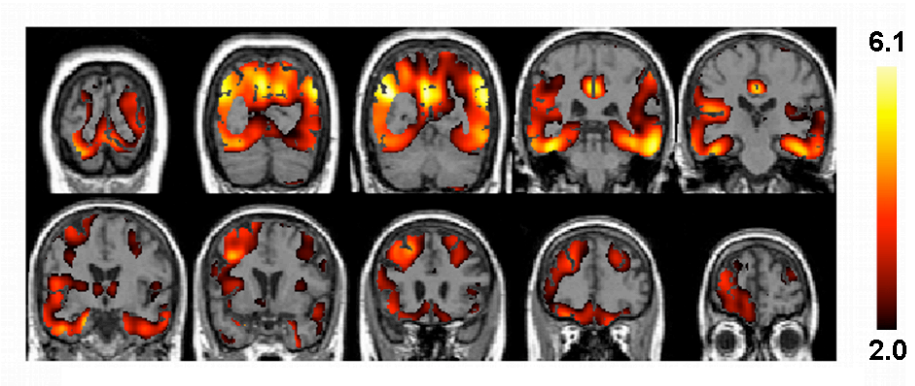

Herholz and colleagues [70] developed the PALZ automatic tool (part of PMOD technologies, http://www.pmod.com) for early diagnosis of AD, combining the virtues of voxel-based parametric mapping with the diagnostic information about brain regions that are typically affected in AD. After comparing a single patient PET scan with a group of normal control PET scans, PALZ software automatically compute the voxel-by-voxel sum of T-scores over an AD-pattern mask, and use the result, corrected by age, as indicator to distinguish AD from non-AD. In a cohort of 395 AD patients and 110 normal controls recruited for a longitudinal multicentric study PALZ could identify mild to moderate AD with 93% sensitivity and specificity, and very mild AD with 84% sensitivity and 93% specificity [70]. Being accurate, completely automatic, and designed for single patient analysis, PALZ seems to be a powerful tool which could be used in the clinical practise to help in AD diagnosis.

Differential diagnosis of AD using PET. Several reports have provided evidence for distinctive patterns of perfusion and metabolic abnormalities able to distinguish AD from other dementias.

AD vs frontotemporal dementia: Frontotemporal dementia (FTD) is characterised on PET examination by an earlier and more severe frontal and anterior and/or mesiotemporal hypometabolism as compared with the parieto-temporal cortex, with relative sparing of primary visual and sensorimotor cortex. The temporal and frontal variants are associated with more severe temporal or frontal hypometabolism on PET, respectively [71-73]. Visual interpretation of FDG-PET was found to be more reliable

and accurate in distinguishing FTD from AD than clinical methods, thus increasing diagnostic confidence [74].

AD vs dementia with Lewy bodies: Several studies have shown that PET deficits in dementia with Lewy bodies are similar to those of AD, but with less sparing of the occipital primary cortex and cerebellum. These findings have been replicated with [75,76].

AD vs vascular dementia: Vascular dementia is characterised by diffuse hypometabolism in several cortical regions, as well as subcortical and cerebellar areas, which are instead usually spared in AD [77,78].

AD vs depression: PET studies have shown that metabolism in frontal lobe regions, such as the dorsolateral prefrontal cortex, is lower in both unipolar and bipolar depression as compared with AD [79]. Other SPECT studies have found reduced rCBF in the parieto-temporal cortex for AD as compared with depressed patients [80,81].

Despite a certain degree of overlap concerning the parieto-temporal hypometabolism, PET/SPECT investigations can be helpful in supporting the clinical differential diagnosis in vivo [82]. Some years ago Charpentier and collegues developed a sensitive automatic classification tool based on a decision rule deduced from factorial discriminant analysis to differentiate AD from FTD based on SPECT scan [83]. Further accurate automatic classification tools would be very welcome.

Functional MRI

Functional magnetic resonance imaging (fMRI) is a quite recent technique that allows to study the brain function, i.e. "to look at the brain while it works", by exploiting the principles of traditional MRI.

fMRI is based on the acquisition of the BOLD (Blood Oxygenation Level Dependent) signal, given the assumption that cortical activation produces changes of the oxy-/ deoxyhemoglobin ratio in brain tissue. fMRI activation maps, showing a signal proportional to neuronal activation, can be computed as the difference between the active map and that acquired in resting conditions.

Functional MRI studies are providing unprecedented insight into the physiological mechanisms of the brain in a variety of conditions, from traditional neuropsychological task to emotional perceptions to ethical choices, mapping activation with around 1 mm spatial resolution (3.0 Tesla) or even less (4-7 Tesla), and determining functions exploited to carry out a given task. Most imaging tools used for fMRI analysis are the

same described for PET/SPECT imaging, from visual rating to automated voxel-based analysis. Recently, some more specific tools have been developed [84].

Neurodegenerative disorders affect the normal activation pattern in a number of ways. As predictable, in AD patients functional activation is decreased in the areas most affected by AD pathology [85-90]. Interestingly, medial temporal activation patterns in MCI patients during a memory task have been found as much reduced as in AD patients, possibly suggesting that the functional damage of AD neuropathology in the medial temporal lobe is very early [86].

Several studies have provided evidence that in AD and frontotemporal dementia reduced activation of normally active areas is accompanied by cortical reorganization [87-89,91-97], consistently with the recruitment of wider networks in the attempt to preserve function. Such compensatory mechanism is most likely to occur in the early stages of the disease [91,98].

The regional coherence of the fMRI signal, in terms of functional connectivities based on ROI and whole brain analysis, was found to be significantly altered in AD patients, indicating that AD may be a disconnection syndrome [99].

One of the most interesting findings obtained through the use of fMRI in AD relates to the involvement of the default network (figure 11), a specific set of regions (including large sections of the lateral parietal, medial parietal and frontal cortex) which consistently shows deactivation in normal people across a wide range of different tasks and stimulus modalities [100-104]. Lustig and colleagues investigated the default network in 32 young, 27 elderly healthy subjects, and 23 elderly mild AD patients through fMRI during an active semantic classification and a passive fixation baseline task. Deactivation in lateral parietal regions was equivalent across groups; in medial frontal regions, it was reduced by aging but was not further reduced by AD. Of greatest interest, the posterior cingulate region showed differences between young and older healthy subjects, and an even more marked difference with AD [93]. AD patients might be unable to deactivate the default network to selectively allocate specific cognitive resources to a given task, and its activation might interfere with the activation of task-specific regions leading to poor performance in cognitive tasks. Further studies showed that the default network response significantly differed in MCI from both normal controls and AD patients, suggesting that altered activity in the default mode network may act as an early marker for AD pathology [105,106].

Figure 11. Visualization of the default network, assessed by GIFT independent component analysis (ICA), in a group of 8 patients with moderate AD who underwent resting state fMRI.

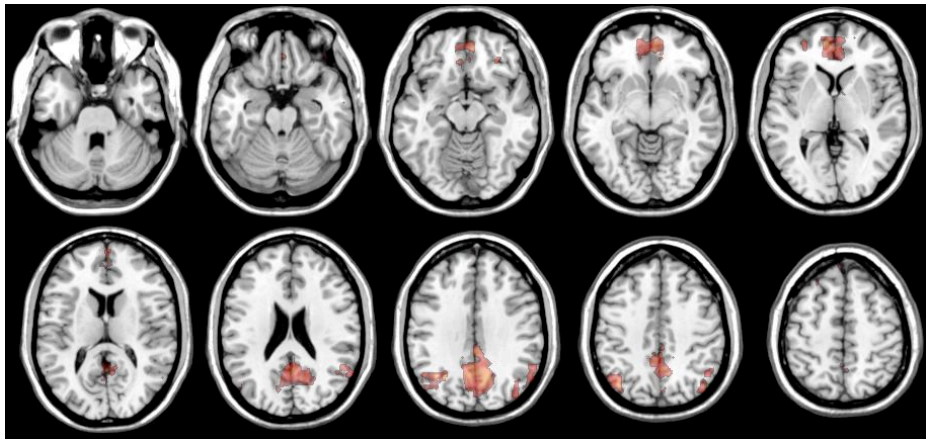

There are few longitudinal studies using functional MRI in AD, and they all showed that fMR imaging is a reliable tool for differentiating groups at risk for AD. Fleisher et al. found increased BOLD signal in the left medial temporal lobe associated with novel encoding among individuals at high AD-risk [107]. Smith et al. found significant reduced activation in the inferotemporal regions in the high AD-risk group, despite identical neuropsychological performance [108]. High AD-risk and low AD-risk groups were found to have further diverged fMRI activations at 1-year followup, suggesting that fMRI may report on the presence and progression of neuropathology in the ventral temporal cortex or in functionally connected regions in presymptomatic AD [109].

Some issues should always be kept in mind when interpreting fMRI results in neurodegenerative conditions. First, fMRI does not allow to discriminate areas of excitation and areas of inhibition, as all active areas look the same. Second, even in normal persons, the same task gives rise to greater activation based on subjective difficulty [110,111] and, unfortunately, the specific contribution of subjective task difficulty cannot be assessed with current experimental designs. Thus, the fMRI signal of AD patients is the summation of three trends: (i) lower activation due to neuronal or synaptic damage, (ii) greater activation due to compensatory recruitment, and (iii) greater activation due to subjective task difficulty. Their contribution to brain activation remains to be investigated.

By now, fMR imaging is just used for research purposes. However, the research

findings described above are really promising, and fMRI could probably be used soon even in clinical settings.

Microstructural imaging

Diffusion and magnetization transfer imaging

Grey matter loss assessed by structural MR imaging has limited ability to capture the whole range of morphostructural changes associated with neurodegeneration in AD; it cannot discriminate neuronal from glial and axonal loss as well as neuronal loss from age-associated shrinkage of healthy neurons, and it cannot appreciate white matter damage that might arise from neurofilament tau pathology.

More recent techniques probing into the finer structure of the brain, such as diffusion tensor and magnetization transfer imaging, are providing increasingly precious information to elucidate the pathophysiology of AD.

Diffusion tensor imaging (DTI) is based on the physical properties of moving water protons. Motion is higher where protons have no constraints (e.g. in the CSF) and lower where protons are confined within organized tissues such as the intracellular matrix or the axonal cytoplasm. MR imaging can detect and quantify such motion through the apparent diffusion coefficient (ADC). In the white matter, not only the ADC is lower than in the CSF, but proton motion is highly oriented in the direction of the axonal fibre (i.e. anisotropic), and the direction of the motion can be quantified through the fractional anisotropy index (FA). Axonal loss and demyelination due to wallerian degeneration are picked up as increased ADC and decreased FA. Gliosis of the white matter, by disrupting the normal axonal structure, also gives rise to decreased FA, but the ADC is normal or decreased due to the boundaries to proton motion represented by glial cell membranes. Neurofilament pathology is associated with normal ADC and FA, cell membranes being intact.

Magnetization transfer imaging (MTI) is based on the exchange of magnetization between free and macromolecule bound protons and allows to indirectly observe semisolids, such as protein matrices and cell membranes. Changes in tissue structural integrity such as gliosis lead to decreased bound and increased free protons which show as decreased magnetization transfer ratio.

Over the last decade, DTI has arisen as one of the biggest advances in clinical imaging. Consistent with a decline of cortical connectivity and impairment of axonal

and dendritic integrity early in the disease process of AD [112], studies using DTI found a decline of fractional anisotropy as a marker of fibre loss in posterior corpus callosum, fasciculus longitudinalis superior, temporal lobe and cingulate white matter [113-115].

Figure 12. DTI color-maps, showing the fiber direction in the brain. The left figure shows the main fibers in the inferio-superior (blu, e.g. pyramidal tract), left-right (red, e.g. bundles in the splenium), and anterior-posterior (green, e.g. large bundles connecting anterior to posterior cortex) directions. The right figure shows in more details the fiber trajectory in the corpus callosum splenium. Fiber tracking is extremely interesting for the investigation of AD, as it enables to identify white matter changes and to go deep into the comprehension of cerebral connectivity

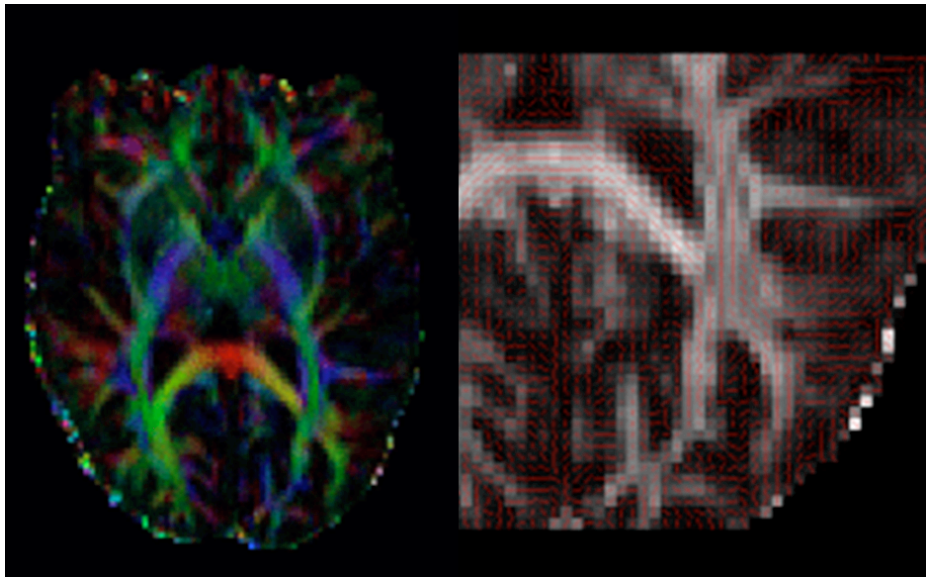

One study using voxel-based analysis of low-dimensionally normalised FA maps found significant reductions of FA in posterior white matter areas [116]. Using the multivariate information of diffusion tensors, in vivo fibre tracking can be performed, which allows reconstructing the fibre tracts originating from selected white matter areas based on individual DTI scans (figure 12). Through multivariate analysis of high-dimensionally normalised FA maps, significant decline of FA was found in intracortical projecting fibre tracts in the AD patients compared to the controls [117].

DTI has not yet been widely employed for the early diagnosis of AD. Müller et al. [118] have compared the ability of FA and mean diffusivity measures in the hippocampus with hippocampus volume to discriminate between 18 subjects with MCI and 18 controls. They found superior accuracy of group separation based on diffusion

compared to volume measurements.

There is ground to believe that microstructural pathology is strongly correlated with cognitive performance. Of the two pathological hallmarks of the disease, senile plaques and neurofibrillary tangles, the latter involves the cytoskeleton and neurobiological studies have shown that it affects axonal transport [119]. Moreover, pathological studies have shown that neurofibrillary tangle density is more strictly related with cognitive performance than senile plaques [120].

As for fMRI, by now DTI have been used for research purpouses only. However, these findings encourage further research in the possible application of DTI as a useful diagnostic tool in AD.

Amyloid imaging

AD is neuropathologically characterised by extracellular amyloid plaques and intracellular neurofibrillary tangles, which are associated with progressive neuronal loss. Currently, protein concentration is assessed by lobar puncture followed by CSF laboratory analysis, an invasive procedure not suitable for all patients. Amyloid imaging could hopefully replace lobar puncture, could help in identifying in vivo neuroanatomic evidence of AD at a very early stage and could even enable to detect any change in the natural history of amyloid deposition induced by anti-amyloid therapies.

Pittsburgh compound-B-PET

Research is indeed very active into molecules labelled with radioactive isotopes that might enter the brain, bind selectively to β-amyloid, be visualised with PET scanners and analysed with PET imaging tools, enabling in vivo quantification of amyloid plaque load in AD [121-123]. The compound at the most advanced stage of validation is the Pittsburgh compound B (PIB), a carbon-11-labelled benzothiazole derivative, which was shown to correlate with two of the more traditional Alzheimer's markers, β-amyloid in the cerebral spinal fluid [124] and progressive brain atrophy [125], suggesting that the presence of beta amyloid as detected with 11C-PIB-PET is associated with neuronal destruction over time. Higher 11C-PIB uptake also correlated with lower glucose metabolism in temporal and parietal cortices [126]. We recently further studied the relationship between grey matter atrophy and amyloid deposition in AD, finding that medial temporal lobe might be highly susceptible to amyloid toxicity, whereas neocortical areas might be more resilient (figure 13) [127].

Figure 13. Correlation between grey matter density and [11C]PIB uptake in a group of 23 AD patients and 17 normal controls. The correlation is highest and most significant in the medial temporal region. Modified from [127].

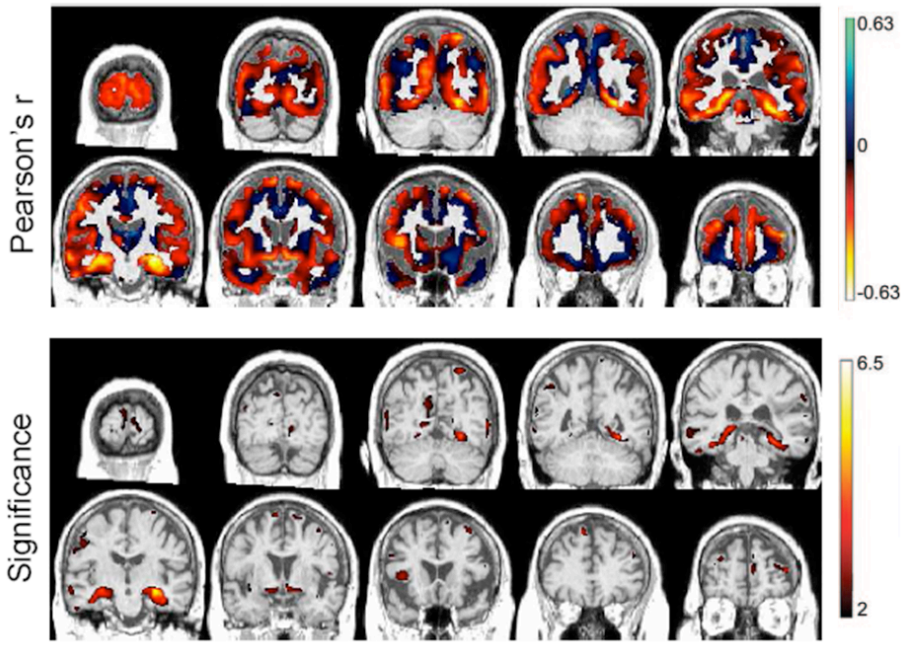

High 11C-PIB retention was found in mild cognitive impairment (MCI) patients, suggesting that a maximum amyloid load in brain is reached almost in the prodromal stage of AD disease [128-131], providing evidence for in vivo measurement of senile plaques as a potential diagnostic test for early or presymptomatic detection of AD patients.

18F-labeled PIB analogues

Another promising radioligand applicable to imaging Abeta plaques in living human brain with PET is [(18)F]FDDNP (2-(1-{6-[(2-[18F]Fluoroethyl)(methyl)amino]-2-naphthyl} ethylidene)malononitrile). [(18)F]FDDNP-PET signal was found to be highly correlated with cognitive performance, especially in regions deteriorating earliest in AD, suggesting the potential utility of [(18)F]FDDNP for early diagnosis. [(18)F]FDDNP signal growth mirrored the classic Braak and Braak trajectory in lateral temporal, parietal, and frontal cortices [132]. FDDNP-PET binding was shown to differentiate MCI from AD patients and normal controls better than did metabolism on FDG-PET or volume on MRI [133].

However, differences in ligand uptake between patients with AD, patients with MCI, and controls were more pronounced for 11C-PIB than for FDDNP [134], and FDDNP was shown to be only weakly retained by the hallmark neuropathology because of its low affinity for amyloid structures [135].

More recently, new F-18-labeled Abeta ligands have been identified. The first one is (18)F-BAY94-9172, whose binding was reported to match the reported post-mortem distribution of Abeta plaques in AD, and for whom sensitivity and specificity for detection of AD at visual rating (within a cohort of subjects including AD, FTD patients and normal controls) was reported to be 100% and 90% respectively [136]. The radiation dosimetry of this new radioligand was found to be comparable with 11C-PIB dosimetry and suitable for clinical and research applications [137]. (18)F-GE067 was recently tested on a cohort of healthy elderly human subjects: the mean effective dose was acceptable and comparable to that of many other (18)F-labeled radiopharmaceuticals; relatively low variability between subjects was observed [138].

Other F18-amyloid imaging radioligand are under development, currently at a preclinical validation step. A (18)F-labeled biphenylalkyne, [(18)F]AV-138, showed high binding signal specifically due to A beta plaques in vitro autoradiography of postmortem AD brain sections; fluorescent staining of plaques with TF-S correlated well with the radiolabeling in AD brain sections, suggesting that [(18)F]AV-138 is potentially useful for imaging A beta plaques in the living human brain [139]. 2-(4'-[(18)F]fluorophenyl)-1,3-benzothiazole was synthesized as a fluorine-18 labelled derivative of the Pittsburg Compound-B, and showed excellent preclinical characteristics comparable with those of the (11)C-labelled PIB [140].

F-18-labeled radioligand might facilitate integration of Abeta imaging into clinical practice.

Multimodal imaging

All individual imaging modalities described above could be of help in the diagnosis of AD. The combination of different imaging modalities could increase the accuracy of each modality alone.

Moreover, there is considerable promise that early and specific diagnosis of AD will be rendered possible through the combination of a number of different biomarkers for AD from different fields of research, both imaging and not, such as hippocampal or cortical

atrophy on MRI, functional defects in the temporoparietal and posterior cingulate cortex on PET, SPECT, or fMRI, microstructural pathology on DTI or MTI, high amyloid load on amyloid ligand PET, as well as low memory performance on comprehensive neuropsychological tests, and high concentrations of tau protein in the CSF.

Several studies have already tried to combine more than one Alzheimer's disease biomarker, in order to prove a great increase in the prognostic power and diagnostic accuracy.

A combination of regional cerebral blood flow and CSF tau levels [141], SPECT uptake and brain structure volume on MRI [142], as well as functional imaging and neuropsychological tests [143-145] was shown to achieve higher sensitivity and specificity than each marker alone in discriminating converters to AD from non-converters.

As far as the diagnostic accuracy, De Leon and colleagues showed that the combination of hippocampal volume and P-tau231 concentration in the CSF could improve the early diagnosis of AD [146]. Hippocampal hypometabolism and medial temporal atrophy can predict normal controls future transition to MCI; moreover, the combination of conventional imaging with CSF biomarkers significantly improve the early and specific diagnosis of AD [147]. Schmidt and colleagues further supported the use of multimodal imaging including MRI and PET in longitudinal studies to monitor the progression of moderate AD [148]. The combination approach could greatly enhance the understanding of both the pathophysiology of neurodegenerative disorder and the functional and structural basis of normal cognition in the human brain.

In a recent paper we investigated the relationship between structural and functional loss in incipient AD, finding relatively preserved perfusion, indicative of compensation in the setting of neuronal loss, in the neocortex, and functional depression in the medial temporal lobe [69]. A better understanding of compensatory mechanisms, taking into account the overall cerebral alteration rather than any specific structural or functional damage, could help to go more deep into the comprehension of the AD underlying pathology, hopefully opening the way to a more accurate disease marker than atrophy or metabolism alone or suggesting novel therapeutic strategies to improve the resilience of the brain to neurodegenerative damage.

Further studies would be needed to determine a fully reliable, unique biomarker for AD, based on the combination of all different biomarkers available nowadays.

Expert commentary

At this point the diagnostic pathway for AD cannot fail to quantify biomarkers, both imaging and not.

Biomarker assessment could be especially helpful in the first stages of the disease, making an early and accurate diagnosis possible and any early therapeutic intervention more likely to be effective. Moreover, as most of the biomarkers are shown to be abnormal even at a preclinical stage, biomarker evaluation in patients with mild cognitive impairment could be predictive of clinical outcome, and the underlying Alzheimer's disease could be identified even prior to the arising of any clinical symptom. Apart from diagnosis, quantitative evaluation of the disease is particular relevant in clinical trials, aimed to assess the specific effect of any new drug on the brain as well as on the disease progression, before and beyond clinical symptoms.

The revised diagnostic criteria for AD, recently proposed by Dubois and colleagues [7], identified relevant biomarkers for early diagnosis, in addition to the presence of early and significant episodic memory impairment: medial temporal lobe atrophy, temporo-parietal hypometabolism, and β-amyloid and tau protein abnormal concentration in cerebro-spinal fluid.

Most of the quantification techniques presented throughout the paper are currently used for research in AD, some of them are still quite far from routine clinical practise due to the high technology required and to their suitability for group analysis only, but some others are already available or pretty close to clinical application. Currently, in order to quantify medial temporal atrophy, beyond visual rating scales, right and left hippocampus of each patient could be manually traced on MR images using low-technology tools, and their volume could be compared with those of a normative population in order to have an accurate measure of atrophy; each patient MR image could be compared with a group of normal control images on a voxel-by-voxel level by performing VBM using one of the freely downloadable tools (e.g. SPM) in order to assess the patient-specific pattern of atrophy. Temporoparietal hypometabolism, which has been shown more than other biomarkers to have diagnostic value, could be assessed comparing mean metabolism within a specific temporoparietal region of interest, or rather performing a wholebrain or region of interest voxel-based analysis (e.g. using SPM); in case of suspect of AD, the PALZ tool [70], specifically designed for

clinical purposes, enables to distinguish AD from non-AD based on the FDG-PET image only with a single click. As for β-amyloid and tau protein build-up, the state of the art is still the assessment of abnormal concentration by lobar puncture and CSF laboratory analysis. However, the commercial distribution of radioligands applicable to imaging Abeta plaques will make amyloid imaging widely available to clinicians and is therefore likely to replace lobar puncture soon.

Five-year view

Research is indeed very active into more and more reliable biomarkers for AD, able to identify the disease from the earliest stages. Beyond markers included in the revised diagnostic criteria [7], several other cerebral changes, either structural, microstructural, functional, or histological are continuously being reported in the literature. Despite some of them being really far from routine clinical practice and used in research only, most novel biomarkers, from voxel-based image analysis to hippocampal volumetry and wholebrain atrophy rate assessment to DTI and amyloid imaging, could become more and more helpful in clinical practice, and could be included in the near future in the AD diagnostic pathway.

However, all biomarkers are indicators of single aspects of the pathology, rather than of the overall cerebral damage.

From now on, the challenge will be to identify an unique, fully reliable biomarker for AD, a specific overall "signature" of the disease to be used for accurate diagnosis, based on the combination of all available biomarkers.

References

1. McKhann G, Drachman D, Folstein M, Katzman R, Price D, Stadlan EM. Clinical diagnosis of AD: report of the NINCDS-ADRDA Work Group under the auspices of Department of Health and Human Services task force on AD. Neurology 1984; 34:939-944.
2. Callahan CM, Hendrie HC, Tierney WM. Documentation and evaluation of cognitive imapirment in elderly primary care patients. Ann Intern Med 1995; 122:422-429.
3. Hoffman RS. Diagnostic errors in the evaluation of behavioral disorders. JAMA 1982; 248:964-967.
4. Lim A, Tsuang D, Kukull W, et al. Clinico-neuropathological correlation of Alzheimer's disease in a community-based case series. J Am Geriatr Soc 1999; 47:564-569.
5. McDaniel LD, Lukovits T, McDaniel KD. Alzheimer's disease: the problem of incorrect clinical diagnosis. J Geriatr Psychiatry Neurol 1993; 6:230-234.
6. Small AS. Alzheimer disease, in living color. Nature Neuroscience 2005; 8:404-405.
7. Dubois B, Feldman HH, Jacova C, et al. Research criteria for the diagnosis of Alzheimer's disease: revising the NINCDS-ADRDA criteria. Lancet Neurol 2007; 6:734-746.
8. Duara R, Loewenstein DA, Potter E, et al. Medial temporal lobe atrophy on MRI scans and the diagnosis of Alzheimer disease. Neurology 2008; 71:1986-1992.
9. Frisoni GB, Galluzzi S, Pantoni L, Filippi M. The effect of white matter lesions on cognition in the elderly—small but detectable. Nat Clin Pract Neurol 2007; 3:620-627.
10. Scheltens P, Leys D, Barkhof F, et al. Atrophy of medial temporal lobes on MRI in "probable" Alzheimer's disease and normal ageing: diagnostic value and neuropsychological correlates. J. Neurol. Neurosurg. Psychiatry 1992; 55:967-972.
11. Wahlund LO, Julin P, Johansson SE, Scheltens P. Visual rating and volumetry of the medial temporal lobe on magnetic resonance imaging in dementia: a comparative study. J Neurol Neurosurg Psychiatry 2000; 69:630-635.
12. Visser PJ, Verhey FR, Hofman PA, Scheltens P, Jolles J. Medial temporal lobe atrophy predicts Alzheimer's disease in patients with minor cognitive impairment. J Neurol Neurosurg Psychiatry 2002; 72:491-497.
13. DeCarli C, Frisoni GB, Clark CM, et al.; Alzheimer's Disease Cooperative Study Group. Qualitative estimates of medial temporal atrophy as a predictor of progression from mild cognitive impairment to dementia. Arch Neurol 2007; 64:108-115.
14. Galluzzi S, Lanni C, Pantoni L, Filippi M, Frisoni GB. White matter lesions in the elderly: pathophysiological hypothesis on the effect on brain plasticity and reserve. J Neurol Sci 2008; 273: 3-9.
15. Scheltens P, Erkinjunti T, Leys D, et al. White matter changes on CT and MRI: an overview of visual rating scales. European task force on age-related white matter changes. Eur Neurol 1998; 39:80-89.
16. Wahlund LO, Barkhof F, Fazekas F, et al.; European Task Force on Age-Related White Matter Changes. A new rating scale for age-related white matter changes applicable to MRI and CT. Stroke 2001; 32:1318-1322.
17. Laakso MP, Partanen K, Riekkinen P, et al. Hippocampal volumes in Alzheimer's disease, Parkinson's disease with and without dementia, and in vascular dementia: An MRI study. Neurology 1996; 46:

678-681.

18. Laakso MP, Soininen H, Partanen K, et al. MRI of the hippocampus in Alzheimer's disease: sensitivity, specificity, and analysis of the incorrectly classified subjects. Neurobiol Aging 1998; 19:23-31.
19. Devanand DP, Pradhaban G, Liu X, et al. Hippocampal and entorhinal atrophy in mild cognitive impairment: prediction of Alzheimer disease. Neurology 2007; 68:828-836.
20. Braak H, Braak E. Evolution of neuronal changes in the course of Alzheimer's disease. J Neural Transm Suppl 1998; 53:127-140.
21. Pennanen C, Kivipelto M, Tuomainen S, et al. Hippocampus and enthorinal cortex in mild cognitive impairment and early AD. Neurobiol Aging 2004; 25:303-310.
22. Du AT, Schuff N, Zhu XP, et al. Atrophy rates of entorhinal cortex in AD and normal aging. Neurology 2003; 60 481-486.
23. DeCarli C, Maisog J, Murphy DG, Teichberg D, Rapoport SI, Horwitz B. Method for quantification of brain, ventricular, and subarachnoid CSF volumes from MR images. J Comput Assist Tomogr 1992; 16:274-284.
24. DeCarli C, Miller BL, Swan GE, Reed T, Wolf PA, Carmelli D. Cerebrovascular and brain morphologic correlates of mild cognitive impairment in the National Heart, Lung, and Blood Institute Twin Study. Arch Neurol 2001; 58:643-647.
25. Ashburner J, Csernansky JG, Davatzikos C, Fox NC, Frisoni GB, Thompson PM. Computer-assisted imaging to assess brain structure in healthy and diseased brains. Lancet Neurol 2003; 2:79-88.
26. Ashburner J, Friston KJ. Voxel-Based Morphometry - The Methods. Neuroimage 2000; 14:805-821.
27. Lerch JP, Pruessner JC, Zijdenbos, et al. Focal decline of cortical thickness in Alzheimer's disease identified by computational neuroanatomy. Cerebral cortex 2005; 15:995-1001.
28. Thompson PM, Mega MS, Toga AW. Disease-specific brain atlases. In: Toga AW, Mazziotta JC, editors. Brain Mapping: The Disorders. Academic Press 2000; 131-177.
29. Freeborough PA, Fox NC, Kitney RI. Interactive algorithms for the segmentation and quantitation of 3-D MRI brain scans. Comput Methods Programs Biomed 1997; 53:15-25.
30. Frisoni GB, Testa C, Zorzan A, et al. Detection of grey matter loss in mild Alzheimer's disease with voxel based morphometry. J Neurol Neurosurg Psychiatry 2002; 73:657-664.
31. Karas GB, Burton EJ, Rombouts SA, et al. A comprehensive study of grey matter loss in patients with Alzheimer's disease using optimized voxel-based morphometry. Neuroimage 2003; 18:895-907.
32. Chetelat G, Landeau B, Eustache F. Using voxel-based morphometry to map the structural changes associated with rapid conversion in MCI: a longitudinal MRI study. Neuroimage 2005; 27:934-946.
33. Nichols TE, Holmes AP. Nonparametric permutation tests for functional neuroimaging: a primer with examples. Hum Brain Mapp 2002; 15:1-25.
34. Thompson PM, Toga AW. A surface-based technique for warping 3-dimensional images of the brain. IEEE Trans Med Imaging 1996; 15:1-16.
35. Thompson PM, Cannon TD, Narr KL, et al. Genetic influences on brain structure. Nat Neurosci 2001; 4:1253-1258.
36. Davatzikos C. Spatial normalization of 3D brain images using deformable models. J Comput Assist

Tomogr 1996; 20:656-665.

37. Thompson PM, Hayashi KM, de Zubicaray G, et al. Detecting dynamic and genetic effects on brain structure using high-dimensional cortical pattern matching. Proceedings of the International Symposium on Biomedical Imaging. July 7-10 2002; Washington, DC.
38. Thompson PM, Mega MS, Woods RP, et al. Cortical change in Alzheimer's disease detected with a disease-specific population-based brain atlas. Cereb Cortex 2001; 11:1-16.
39. Frisoni GB, Pievani M, Testa C, et al. The topography of grey matter involvement in early and late onset Alzheimer's disease. Brain 2007; 130:720-730.
40. Thompson PM, Hayashi KM, de Zubicaray G, et al. Dynamics of grey matter loss in Alzheimer's disease. J Neurosci 2003; 23:994-1005.
41. Frisoni GB, Prestia A, Rasser PE, Bonetti M, Thompson PM. In vivo mapping of incremental cortical atrophy from incipient to overt Alzheimer's disease. J Neurol 2009; 256:916-924.
42. Lerch JP, Pruessner JC, Zijdenbos, et al. Focal decline of cortical thickness in Alzheimer's disease identified by computational neuroanatomy. Cerebral cortex 2005; 15:995-1001.
43. Frisoni GB, Sabattoli F, Lee AD, Dutton RA, Toga AW, Thompson PM. In vivo neuropathology of the hippocampal formation in AD: a radial mapping MR-based study. Neuroimage 2006; 32:104-110.
44. Frisoni GB, Ganzola R, Canu E, et al. Mapping local hippocampal changes in Alzheimer's disease and normal aging with MRI at 3 Tesla. Brain 2008; 131:3266-3276.
45. Fox NC, Cousens S, Scahill R et al. Using serial registered brain magnetic resonance imaging to measure disease progression in Alzheimer Disease. Arch Neurol 2000; 57:339-344.
46. Fox NC, Freeborough PA, Rossor MN. Visualisation and quantification of rates of atrophy in Alzheimer's disease. Lancet 1996; 348:94–97.
47. Fox NC, Freeborough PA. Brain atrophy progression measured from registered serial MRI: validation and application to Alzheimer's disease. J Magn Reson Imaging 1997; 7:1069-1075.
48. Smith SM, De Stefano N, Jenkinson M, Matthews PM. Normalised accurate measurement of longitudinal brain change. J Comput Assist Tomogr 2001; 25:466-475.
49. DeCarli C, Fletcher E, Ramey V, Harvey D, Jagust WJ. Anatomical mapping of white matter hyperintensities (WMH): exploring the relationships between periventricular WMH, deep WMH, and total WMH burden. Stroke 2005; 36:50-55.
50. Yoshita M, Fletcher E, Harvey D, et al. Extent and distribution of white matter hyperintensities in normal aging, MCI and AD. Neurology 2006; 67:2192-2198.
51. Bonte FJ, Devous MD Sr, Holman BL. Single photon emission computed tomographic imaging of the brain. In: Sandler MP, Coleman RE, Wackers FJTh, Patton JA, Gottschalk A, Hoffer PB, eds. Diagnostic Nuclear Medicine. 4th ed. Baltimore MD: Williams and Wilkins. 2004
52. Jagust W, Thisted R, Devous MD Sr, et al. SPECT perfusion imaging in the diagnosis of AD: a clinical-pathologic study. Neurology 2001; 56:950–956.
53. Mielke R, Pietrzyk U, Jacobs A, et al. HMPAO SPET and FDG PET in Alzheimer's disease and vascular dementia: comparison of perfusion and metabolic pattern. Eur J Nucl Med 1994; 21:1052-1060.
54. Messa C, Perani D, Lucignani G, et al. High-resolution technetium-99m-HMPAO SPECT in patients with

probable Alzheimer's disease: comparison with fluorine-18-FDG PET. J Nucl Med 1994; 35:210–216.

55. Mielke R, Heiss WD. Positron emission tomography for diagnosis of AD and vascular dementia. J Neural Transm 1998; 53:237–250.
56. Mosconi L, Mistur R, Switalski R, et al. FDG-PET changes in brain glucose metabolism from normal cognition to pathologically verified Alzheimer's Disease. Eur J Nucl Med Mol Imaging 2009; 36: 811-822.
57. de Leon MJ, Ferris SH, George A, et al. Computed tomography and positron emission transaxial tomography evaluations of normal aging and Alzheimer's disease. J Cereb Blood Flow Metab 1993; 3:391–394.
58. Foster NL, Chase TN, Mansi L, et al. Cortical abnormalities in Alzheimer's disease. Ann Neurol 1984; 16:649–654.
59. Friedland RP, Brun A, Budinger TF. Pathological and positron emission tomographic correlations in Alzheimer's disease. Lancet 1985; 26:228.
60. Patwardhan MB, McCrory DC, Matchar DB, Samsa GP, Rutschmann OT. Alzheimer disease: operating characteristics of PET—a meta-analysis. Radiology 2004; 231:73–80.
61. de Leon MJ, Convit A, Wolf OT, et al. Prediction of cognitive decline in normal elderly subjects with 2-[18F]fluoro-2-deoxy-D-glucose/positron-emission tomography (FDG/PET). Proc Natl Acad Sci USA 2001; 98:10966–10971.
62. De Santi S, de Leon MJ, Rusinek H, et al. Hippocampal formation glucose metabolism and volume losses in MCI and AD. Neurobiol Aging 2001; 22:529–539.
63. Nestor PJ, Fryer TD, Smielewski P, Hodges JR. Limbic hypometabolism in Alzheimer's disease and mild cognitive impairment. Ann Neurol 2003; 54:343–351.
64. Mosconi L, De Santi S, Li J, et al. Hippocampal hypometabolism predicts cognitive decline from normal aging. Neurobiol Aging 2008; 29:676-692.
65. Ashburner J, Csernansky JG, Davatzikos C, Fox NC, Frisoni GB, Thompson PM. Computer-assisted imaging to assess brain structure in healthy and diseased brains. Lancet Neurol 2003; 2:79–88.
66. Friston KJ, Frith CD, Liddle PF, Frackowiak RSJ. Comparing functional (PET) images: the assessment of significant change. J Cereb Blood Flow Metab 1991; 11:690–699.
67. Friston K, Ashburner J, Frith C, Poline J-B, Heather J, Frackowiak R. Spatial registration and normalization of images. Hum Brain Map 1995; 3:165–189.
68. Minoshima S, Frey KA, Koeppe RA, Foster NL, Kuhl DE. A diagnostic approach in Alzheimer's disease using threedimensional stereotactic surface projections of fluorine-18-FDG PET. J Nucl Med 1995; 36:1238–1248.
69. Caroli A, Geroldi C, Nobili F, et al. Functional compensation in incipient Alzheimer's disease. Neurobiol Aging 2010; 31:387-397. Epub 2008.
70. Herholz K, Salmon E, Perani D, et al. Discrimination between Alzheimer dementia and controls by automated analysis of multicenter FDG PET. Neuroimage 2002; 17:302-316.
71. Barber R, Snowden JS, Craufurd D. Frontotemporal dementia and Alzheimer's disease: retrospective differentiation using information from informants. J Neurol Neurosurg Psychiatr 1995; 59:61–70.
72. Ishii K, Imamura T, Sasaki M, et al. Regional cerebral glucose metabolism in dementia with Lewy bodies

and Alzheimer's disease. Neurology 1998; 51:125–130.

73. Santens P, De Bleecker J, Goethals P, et al. Differential regional cerebral uptake of 18F-fluoro-2-deoxy-D-glucose in Alzheimer's disease and frontotemporal dementia at initial diagnosis. Eur J Neurol 2001; 45:19–27.
74. Foster NL, Heidebrink JL, Clark CM, et al. FDG-PET improves accuracy in distinguishing frontotemporal dementia and Alzheimer's Disease. Brain 2007; 130:2616-2635.
75. Minoshima S, Foster NL, Sima AA, Frey KA, Albin RL, Kuhl DE. Alzheimer's disease versus dementia with Lewy bodies: cerebral metabolic distinction with autopsy confirmation. Ann Neurol 2001; 50: 358–365.
76. Albin RL, Minoshima S, DAmato CJ, Frey KA, Kuhl DE, Sima AAF. Fluoro-deoxyglucose positron emission tomography in diffuse Lewy body disease. Neurology 1996; 47:462–466.
77. Barber R, Ballard C, McKeith IG, Gholkar A, O'Brien JT. MRI volumetric study of dementia with Lewy bodies: a comparison with AD and vascular dementia. Neurology 2000; 54:1304–1309.
78. Szelies B, Mielke R, Herholz K, Heiss W-D. Quantitative topographical EEG compared to FDG PET for classification of vascular and degenerative dementia. Electroencephalogr Clin Neurophysiol 1994; 91: 131–139.
79. Guze BH, Baxter LR, Schwartz JM, Szuba MP, Mazziotta JC, Phelps ME. Changes in glucose metabolism in dementia of the Alzheimer type compared with depression: a preliminary report. Psychiatry Res 1991; 40:195–202.
80. Ebmeier KP, Prentice N, Ryman A, et al. Temporal lobe abnormalities in dementia and depression: a study using high resolution single photon emission tomography and magnetic resonance imaging. J Neurol Neurosurg Psychiatr 1997; 63:597–604.
81. Ebmeier KP, Glabus M, Prentice N, Ryman A, Goodwin GM. A voxel-based analysis of cerebral perfusion in dementia and depression of old age. Neuroimage 1998; 7:199–208.
82. Herholz K, Carter SF, Jones M. Positron emission tomography imaging in dementia. Br J Radiol 2007; 80:S160-S167.
83. Charpentier P, Lavenu I, Defebvre L, et al. Alzheimer's disease and frontotemporal dementia are differentiated by discriminant analysis applied to (99m)Tc HmPAO SPECT data. J Neurol Neurosurg Psychiatry 2000; 69:661-663.
84. Rombouts SA, Damoiseaux JS, Goekoop R, Barkhof F, Scheltens P, Smith SM, Beckmann CF. Model-free group analysis shows altered BOLF FMRI networks in dementia. Hum Brain Mapp 2009; 30:256-266.
85. Grossman M, Koenig P, DeVita C, et al. Neural basis for verb processing in Alzheimer's disease: an fMRI study. Neuropsychology 2003; 17:658-674.
86. Machulda MM, Ward HA, Borowski B, et al. Comparison of memory fMRI response among normal, MCI, and Alzheimer's patients. Neurology 2003; 61:500-506.
87. Rombouts SA, van Swieten JC, Pijnenburg YA, Goekoop R, Barkhof F, Scheltens P. Loss of frontal fMRI activation in early frontotemporal dementia compared to early AD. Neurology 2003; 60: 1904-1908.
88. Sperling RA, Bates JF, Chua EF, et al. fMRI studies of associative encoding in young and elderly controls and mild Alzheimer's disease. J Neurol Neurosurg Psychiatry 2003; 74:44-50.
89. Kato T, Knopman D, Liu H. Dissociation of regional activation in mild AD during visual encoding: a

functional MRI study. Neurology 2001; 57:812-816.

90. Rombouts SA, Barkhof F, Veltman DJ, et al. Functional MR imaging in Alzheimer's disease during memory encoding. Am J Neuroradiol 2000; 21:1869-1875.
91. Dickerson BC, Salat DH, Bates JF, et al. Medial temporal lobe function and structure in mild cognitive impairment. Ann Neurol 2004; 56:27-35.
92. Lipton RB, Dodick D, Sadovsky R, et al.; ID Migraine validation study. A self-administered screener for migraine in primary care: The ID Migraine validation study. Neurology 2003; 61:375-382.
93. Lustig C, Snyder AZ, Bhakta M, et al. Functional deactivations: change with age and dementia of the Alzheimer type. Proc Natl Acad Sci USA 2003; 100:14504-14509.
94. Prvulovic D, Hubl D, Sack AT, et al. Functional imaging of visuospatial processing in Alzheimer's disease. Neuroimage 2002; 17:1403-1414.
95. Bookheimer SY, Strojwas MH, Cohen MS, et al. Patterns of brain activation in people at risk for Alzheimer's disease. N Engl J Med 2000; 343:450-456.
96. Thulborn KR, Martin C, Voyvodic JT. Functional MR imaging using a visually guided saccade paradigm for comparing activation patterns in patients with probable Alzheimer's disease and in cognitively able elderly volunteers. Am J Neuroradiol 2000;21:524-531.
97. Saykin AJ, Flashman LA, Frutiger SA, et al. Neuroanatomic substrates of semantic memory impairment in Alzheimer's disease: patterns of functional MRI activation. J Int Neuropsychol Soc 1999; 5:377-392.
98. Pihlajamäki M, Jauhiainen AM, Soininen H. Structural and functional MRI in mild cognitive impairment. Curr. Alzheimer Res 2009; 6:179-185.
99. Liu Y, Wang K, Yu C, et al. Regional homogeneity, functional connectivity and imaging markers of Alzheimer's disease: A review of resting-state fMRI studies. Neuropsychologia 2008; 46:1648–1656.
100. Cabeza R. Hemispheric asymmetry reduction in older adults: the HAROLD model. Psychol Aging 2002; 17:85–100.
101. Gusnard DA, Raichle ME, Raichle ME. Searching for a baseline: functional imaging and the resting human brain. Nat Rev Neurosci 2001; 2:685-694.
102. Mazoyer B, Zago L, Mellet E, et al. Cortical networks for working memory and executive functions sustain the conscious resting state in man. Brain Res Bull 2001; 54:287-298.
103. McKiernan KA, Kaufman JN, Kucera-Thompson J, Binder JR. A parametric manipulation of factors affecting task-induced deactivation in functional neuroimaging. J Cogn Neurosci 2003; 15:394-408.
104. Fox MD, Raichle ME. Spontaneous fluctuations in brain activity observed with functional magnetic resonance imaging. Nat Rev Neurosci 2007; 8:700-711.
105. Rombouts SA, Barkhof F, Goekoop R, Stam CJ, Scheltens P. Altered resting state networks in mild cognitive impairment and mild Alzheimer's disease: an fMRI study. Hum Brain Mapp 2005; 26: 231-239.
106. Greicius MD, Srivastava G, Reiss AL, Menon V. Default-mode network activity distinguishes Alzheimer's disease from healthy aging: evidence from functional MRI. Proc Natl Acad Sci USA 2004; 101:4637-4642.
107. Fleisher AS, Houston WS, Eyler LT, et al. Identification of Alzheimer disease risk by functional magnetic resonance imaging. Arch Neurol 2005; 62:1881-1888.

108. Smith CD, Andersen AH, Kryscio RJ. Altered brain activation in cognitively intact individuals at high risk for Alzheimer's disease. Neurology 1999; 53:1391-1396.
109. Smith CD, Kryscio RJ, Schmitt FA, et al. Longitudinal functional alterations in asymptomatic women at risk for Alzheimer's disease. J Neuroimaging 2005; 15:271-277.
110. Haier RJ, Jung RE, Yeo RA, Head K, Alkire MT. Structural brain variation and general intelligence. Neuroimage 2004; 23:425-433.
111. Grey JR, Thompson PM. Neurobiology of intelligence: science and ethics. Nat Rev Neurosci 2004; 5: 471-482.
112. Kowall NW, Kosik KS. Axonal disruption and aberrant localization of tau protein characterize the neuropil pathology of Alzheimer 's disease. Ann Neurol 1987; 22:639–643.
113. Stahl R, Dietrich O, Teipel SJ, Hampel H, Reiser MF, Schoenberg SO. White matter damage in Alzheimer 's disease and in mild cognitive impairment: assessment with diffusion tensor MRI using parallel imaging techniques. Radiology 2007; 243:483–492.
114. Bozzali M, Falini A, Franceschi M, et al. White matter damage in Alzheimer 's disease assessed in vivo using diffusion tensor magnetic resonance imaging. J Neurol Neurosurg Psychiatry 2002; 72:742–746.
115. Fellgiebel A, Muller MJ, Wille P, et al. Color-coded diffusion-tensor-imaging of posterior cingulate fiber tracts in mild cognitive impairment. Neurobiol Aging 2005; 26:1193–1198.
116. Medina D, Detoledo-Morrell L, Urresta F, et al. White matter changes in mild cognitive impairment and AD: a diffusion tensor imaging study. Neurobiol Aging 2006; 27:663–672.
117. Teipel SJ, Stahl R, Dietrich O, et al. Multivariate network analysis of fiber tract integrity in Alzheimer's disease. Neuroimage 2007;34:985–995.
118. Muller MJ, Greverus D, Weibrich C, et al. Diagnostic utility of hippocampal size and mean diffusivity in amnestic MCI. Neurobiol Aging 2007; 28:398–403.
119. Terwel D, Dewachter L, Van Leuven F. Axonal transport, tau protein, and neurodegeneration in Alzheimer's disease. Neuromolecular Med 2002; 2:151-165.
120. Berg L, McKeel DW Jr, Miller JP, Baty J, Morris JC. Neuropathological indexes of Alzheimer's disease in demented and nondemented persons aged 80 years and older. Arch Neurol 1993; 50:349-358.
121. Nordberg A. Amyloid plaque imaging in vivo: current achievement and future prospects. Eur J Nucl Med Mol Imaging 2008; 35:846-850.
122. Villemagne VL, Fodero-Tavoletti MT, Pike KE, Cappai R, Masters CL, Rowe CC. The ART of Loss: Aβ Imaging in the Evaluation of Alzheimer's Disease and other Dementias. Mol Neurobiol 2008; 38:1-15.
123. Frisoni GB. Imaging of amyloid comes of age. Lancet Neurol 2008; 7:114-115.
124. Svedberg MM, Hall H, Hellström-Lindahl E, et al. [(11)C]PIB-amyloid binding and levels of Abeta40 and Abeta42 in postmortem brain tissue from Alzheimer patients. Neurochem Int 2009; 54:347-357.
125. Archer A, Edison P, Brooks DJ. Amyloid load and cerebral atrophy in Alzheimer's Disease: an 11C-PIB positron emission tomography study. Ann Neurol 2006; 60:145-147.
126. Edison P, Archer HA, Hinz R, et al. Amyloid, hypometabolism, and cognition in Alzheimer disease. An [11C]PIB and [18F]FDG PET study. Neurology 2007; 68:501-508.
127. Frisoni GB, Lorenzi M, Caroli A, Kemppainen N, Någren K, Rinne JO. In vivo mapping of amyloid toxicity

in Alzheimer disease. Neurology 2009; 72:1504-1511.

128. Kempainen NM, Aalto S, Wilson IA, et al. PET amyloid ligand [11C]PIB uptake is increased in mild cognitive impairment. Neurology 2007; 68:1603–1606.
129. Forsberg A, Engler H, Almkvist O, et al. PET imaging of amyloid deposition in patients with mild cognitive impairment. Neurobiol Aging 2008; 29:1456-1465.
130. Pike KE, Savage G, Villemagne VL, et al. β-amyloid imaging and memory in non-demented individuals: evidence for preclinical Alzheimer 's disease. Brain 2007; 130:2837–2844.
131. Koivunen J, Pirttilä T, Kemppainen N, et al. PET amyloid ligand [11C]PIB uptake and cerebrospinal fluid beta-amyloid in mild cognitive impairment. Dement Geriatr Cogn Disord 2008; 26:378-383.
132. Braskie MN, Klunder AD, Hayashi KM, et al. Plaque and tangle imaging and cognition in normal aging and Alzheimer's disease. Neurobiol Aging 2008 Nov 10. [Epub ahead of print]
133. Small GW, Kepe V, Ercoli LM, et al. PET of brain amyloid and tau in mild cognitive impairment. N Engl J Med 2006; 355:2652-2663.
134. Tolboom N, Yaqub M, van der Flier WM, et al. Detection of Alzheimer pathology in vivo using both 11C-PIB and 18F-FDDNP PET. J Nucl Med 2009; 50:191-197.
135. Thompson PW, Ye L, Morgenstern JL, et al. Interaction of the amyloid imaging tracer FDDNP with hallmark Alzheimer's disease pathologies. J Neurochem 2009; 109:623-630.
136. Rowe, CC, Ackerman U, Browne W, et al. Imaging of amyloid [beta] in Alzheimer's disease with 18F-BAY94-9172, a novel PET tracer: proof of mechanism. Lancet Neurology 2008; 7:129-135.
137. O'Keefe GJ, Saunder TH, Ng S, et al. Radiation dosimetry of beta-amyloid tracers 11C-PIB and 18F-BAY94-9172. J Nucl Med 2009; 50:309-315.
138. Koole M, Lewis DM, Buckley C, et al. Whole-Body Biodistribution and Radiation Dosimetry of 18F-GE067: A Radioligand for In Vivo Brain Amyloid Imaging. J Nucl Med 2009; 50:818-822.
139. Wey SP, Weng CC, Lin KJ, et al. Validation of an 18F-labeled biphenylalkyne as a positron emission tomography imaging agent for beta-amyloid plaques. Nucl Med Biol 2009; 36:411-417.
140. Serdons K, Verduyckt T, Vanderghinste D, et al. Synthesis of 18F-labelled-2-(4'-fluorophenyl)-1,3-benzothiazole and evaluation as amyloid imaging agent in comparison with [11C]PIB. Bioorg Med Chem Lett 2009; 19:602-605.
141. Okamura N, Arai H, Maruyama M, et al. Combined analysis of CSF Tau levels and [123I]Iodoamphetamine SPECT in mild cognitive impairment: implications for a novel predictor of Alzheimer's disease. Am J Psychiatry 2002; 159:474-476.
142. El Fakhri G, Kijewski MF, Johnson KA, et al. MRI-guided SPECT perfusion measures and volumetric MRI in prodromal Alzheimer disease. Arch Neurol 2003; 60:1066-1072.
143. Arnaiz E, Jelic V, Almkvist O, et al. Impaired cerebral glucose metabolism and cognitive functioning predict deterioration in mild cognitive impairment. Neuroreport 2001; 12:851-855.
144. Cabranes JA, De Juan R, Encinas M, et al. Relevance of functional neuroimaging in the progression of mild cognitive impairment. Neurol Res 2004; 26:496-501.
145. Borroni B, Anchisi D, Paghera B, et al. Combined 99mTc-ECD SPECT and neuropsychological studies in MCI for the assessment of conversion to AD. Neurobiol Aging 2006; 27:24-31.

146. de Leon MJ, De SAnti S, Zinkowski Ret al. MRI and CSF studies in the early diagnosis of Alzheimer's disease. J Intern Med 2004; 256:205-223.
147. de Leon MJ, Mosconi L, Blennow K, et al. Imaging and CSF studies in the preclinical diagnosis of Alzheimer's disease. Ann NY Acad Sci 2007; 1097:114-145.
148. Schmidt R, Ropele S, Pendl B, et al. Longitudinal multimodal imaging in mild to moderate Alzheimer disease: a pilot study with memantine. J Neurol Neurosurg Psychiatry 2008; 79:1312-1317.

Websites

201. Statistical Parametric Mapping. Wellcome Trust Centre for Neuroimaging (2009). www.fil.ion.ucl.ac.uk/spm
202. Biomedical Imaging Quantification. PMOD Technologies Ltd (2009). www.pmod.com

Chapter 3

Cerebral perfusion predictors of conversion to Alzheimer's Disease in amnestic Mild Cognitive Impairment

Caroli A, Testa C, Geroldi C, Nobili F, Barnden LR, Guerra UP, Bonetti M, Frisoni GB

Journal of Neurology 2007; 254:1698-1707

Abstract

Objective: Aim of this study was to find cerebral perfusion correlates of conversion to dementia in patients with amnestic MCI. Methods: 17 healthy subjects (age=69±3, 9 females), and 23 amnestic MCI patients (age=70±6, 10 females) underwent brain MR scan and 99mTc ECD SPECT. Conversion to AD was ascertained on average 19±10 months after baseline: 9 had converted (age=69±3, 4 females), and 14 had not (age=71±8, 6 females). We processed SPECT images with SPM2 following an optimized protocol and performed a voxel-based statistical analysis comparing amnestic MCI patients converted to AD and non-converted to dementia vs controls. We assessed the effect of grey matter atrophy on the above results with SPM2 using an optimized Voxel-Based Morphometry protocol. We compared significant hypoperfusion with significant atrophy on a voxel-by-voxel basis. Results: In comparison with normal controls, amnestic MCI patients who converted to AD showed hypoperfusion in the right parahippocampal gyrus and left inferior temporal and fusiform gyri, whereas those who did not convert showed hypoperfusion in the retrosplenial cortex, precuneus and occipital gyri, mainly on the left side. We found no overlap between significant atrophy and significant hypoperfusion regions. Conclusions: Parahippocampal and inferior temporal hypoperfusion in amnestic MCI patients appears as a correlate of conversion to AD; hypoperfusion in the retrosplenial cortex is involved in memory impairment but does not seem the key prognostic indicator of conversion to dementia.

Introduction

Mild cognitive impairment (MCI) is a clinical syndrome characterized by cognitive deficits without functional impact on daily living, and thus not severe enough to allow a diagnosis of dementia [1].

MCI has often been considered a preclinical stage of Alzheimer Dementia, converting to dementia in the frequency of 10-15% per year [2] vs. 2% per year of cognitively intact persons [1,3]. However, as many as 50% of MCI patients do not progress to dementia [4], and some of them even improve over time [5,6].

Thus, the relevant clinical issue is to identify MCI patients who will progress from those who will not, as this would make it possible to implement strategies to prevent or delay dementia, and early therapeutical interventions are more likely to be effective.

Some believe that functional alterations antedate structural changes [7], so that functional imaging plays a key role in detecting the dysfunction that characterizes the earliest stage of the disease, and provides pathophysiological information which cannot currently be detected by structural imaging. We have used deficits in cerebral perfusion, which can be accurately measured and mapped onto medial and superficial cortical grey matter structures, as proxies of cortical dysfunction.

Reports in the literature agree on metabolic reduction and hypoperfusion in the posterior parietal, temporal cortex and limbic system, and on relative preservation in the sensorimotor cortex, pons and cerebellum in AD [8,9]. On the contrary, previous longitudinal studies on patients with MCI assessing perfusion and metabolic markers of future conversion to AD are sparse and yield discrepant findings. Some authors, using ROI based-techniques, found that left frontal [10], prefrontal and parietal areas [11], temporoparietal cortex [12], precunei [13], posterior cingulate gyrus [9,14], and hippocampus [13, 15, 16, 17] are sensitive early markers of progression to AD. More recently, Borroni et al [18], using the Principal Component Analysis technique, found a specific hypoperfusion pattern in converters involving the parietal and temporal lobes, precuneus and posterior cingulate cortex, confirming some of the previous findings. In order to reduce the sources of variability which could explain such discrepant findings, we considered only amnestic MCI and we used an advanced SPECT processing protocol.

Aim of this study was to use SPM voxel-based analysis to find cerebral perfusion correlates of conversion to dementia in patients with amnestic MCI.

Methods

MCI patients.

MCI patients were taken from a prospective project on MCI ("Mild Cognitive Impairment in Brescia - MCIBs"), aimed to study the natural history of non demented persons with apparently primary cognitive deficits, i.e. not due to psychic or physical conditions. The study protocol was approved by the local ethics committee and all participants signed an informed participation consent.

Inclusion criteria in the study were all of the following: (i) complaint of memory or other cognitive disturbances; (ii) mini mental state examination (MMSE) score of 24 to 27/30 or MMSE of 28 and higher plus low performance (score of 2/6 or higher) on the clock drawing test [19]; (iii) sparing of instrumental and basic activities of daily living or functional impairment stably due to causes other than cognitive impairment. Exclusion criteria were any one of the following: (i) age of 90 years and older; (ii) history of depression or psychosis of juvenile onset; (iii) history or neurological signs of major stroke; (iv) alcohol abuse; (v) craniocerebral trauma; (vi) heavy use of psychotropic drugs.

Based on these criteria, 139 patients were evaluated from April 2002 to March 2005. All of these underwent: (i) semi-structured interview with the patient and – whenever possible – with another informant (usually the patient's spouse or a child) by a geriatrician; (ii) physical and neurological examinations; (iii) performance-based tests of physical function, gait and balance; (iv) neuropsychological battery assessing verbal and non-verbal memory, attention and executive functions (Trail Making Test B-A [20]; Clock Drawing Test [19]), abstract thinking (Raven matrices [21]), frontal functions (Inverted Motor Learning [22]), language (Phonological and Semantic fluency [23]; Token test [22]), and apraxia and visuo-constructional abilities (Rey figure copy [24]); (v) assessment of depressive symptoms with the Center for Epidemiologic Studies Depression Scale (CES-D [25]). Of these, 17 scored within normal limits (above the 10th percentile of the age- gender- and education-specific distribution) on all neuropsychological tests and 18 did not have MR imaging of adequate quality.

Among the 104 remaining patients 56 agreed to undergo SPECT scan and were further considered. MCI patients who did and did not undergo a SPECT were similar for age (70±6 vs 71±8, p=0.230), gender (58% vs 69% females, p=0.271), physical health (hypertension: 51% vs 54%, p=0.768; diabetes: 23% vs 10%, p=0.062; heart

disease: 33% vs 31%, p=0.879), medial temporal lobe atrophy (1.6±1.3 vs 1.9±1.2, p=0.151) and white matter hyperintensities load (3.3±3.4 vs 4.0±3.9, p=0.354); they differed only for education (9.2±4.6 vs 6.5±3.3, p=0.002) and MMSE (27.6±1.6 vs 26.6±1.8, p=0.007).

We divided MCI patients into amnestic (N=28, age=71±6, 12 women) and non-amnestic (N=28, age=67±7, 20 women), according to the presence of memory deficit or cognitive disturbances other than memory deficit, based on neuropsychological assessment. Memory disturbance was defined as scoring below the 10th percentile, i.e. 1.28 standard deviations below the mean of the age- gender- and education-specific distribution, in at least one memory test of logical memory, Rey word list, immediate and delayed recall, and Rey figure recall. When Rey figure copy was too low for recall to be reliably assessed (under the 10th percentile) Rey figure recall was not taken into account to define memory disturbance. The presence of cognitive disturbances other than memory deficit was defined as performance below the 10th percentile of the age-gender- and education-specific distribution in any one of the single tests of 4 different neuropsychological domains (listed in table 2). In most cases memory impairment was associated with cognitive impairment in other neuropsychological domains. We accounted as amnestic all MCI patients with memory deficit, either single-domain (N=5) or multi-domain (2 domains: N=8, 3 domains: N=8, 4 domains: N=7).

Amnestic MCI patients underwent a yearly follow-up visit, consisting of complete clinical and neuropsychological examination, from 1 to 3 years after enrolment (mean observation time 19±10 months), and we ascertained conversion to dementia according to clinical diagnostic criteria for Alzheimer's disease [26], subcortical vascular dementia [27], dementia with Lewy bodies [28], and fronto-temporal dementia [29]. Four amnestic MCI patients refused to have any follow-up visit and dropped out, one patient converted to fronto-temporal dementia, while all other converters converted to Alzheimer's disease. Among non-converters, there were no improved MCI patients, with no longer evident neuropsychological deficits in any domain. We finally included in the study only amnestic MCI patients who converted to AD (N=9, age=69±3, 4 females) and those who did not convert (N=14, age=71±8, 6 females). The conversion rate was 25% per person year.

Normal controls.

We selected healthy subjects from those enrolled in a study on normal brain structure

with MR (ArchNor) aiming to capitalize on unnecessary scans in otherwise normal persons, as described in detail elsewhere [30]. Briefly, subjects were consecutive normal volunteers picked among those undergoing brain MR scan at the Neuroradiology Unit of the "Città di Brescia" Hospital, Brescia from October 2004 to June 2006 for reasons unrelated to cognition. The reasons for MR prescription were generally migraine and headache, auditory (hypoacusia, dizziness, tinnitus) or visual concerns (diplopia), sensory disturbances (paresthesias), suspected cerebrovascular disease or other rarer problems (dyslexia, orbit study, lipotimic episodes, etc.) in both samples. Exclusion criteria were based on information prior to MR and secondary to possible findings in MR. A priori exclusion criteria were: (1) MR scan for memory problems or cognitive impairment, (2) MR scan for clinical suspicion of neuro-degenerative diseases (Parkinson's disease, progressive supranuclear palsy, Huntington's disease, multiple system atrophy, etc), (3) MR scan for suspected stroke and (4) history of TIA or stroke, head trauma, alcohol and substance abuse, cortico-steroid therapy, and loss of weight greater than 5 kilograms in the last 6 months. A posteriori exclusion criteria included: MR scan showing (1) brain mass, (2) white matter hyperintensities in a subject undergoing MR for suspected multiple sclerosis, (3) aneurysm larger than 10 mm, (4) arteriovenous malformations (except for developmental venous anomaly), (5) malformations of the central nervous system and (6) cognitive impairment on neuropsychological testing. All scans of enrolled subjects were normal on visual assessment of a neuroradiologist. Subjects were intercepted in the waiting room of the neuroradiology units, explained the aims and methods of the study, and asked to take part to the study after signing the informed consent.

Subjects underwent multidimensional assessment including clinical, neurological and neuropsychological evaluations, and drawing of a blood sample.

For this study, we asked all subjects aged 65 years or older to undergo a SPECT scan, and we further considered only those with both MR and SPECT images (3 males and 4 females).

To enlarge the normal controls group, we asked other healthy volunteers aged 65 years or older, among patients' spouses, friends of them, and researchers' acquaintances, to undergo the same protocol as subjects taken from the ArchNorm study (SPECT scan included), using the same exclusion criteria as above (5 males and 5 females).

Table 1: Sociodemographic and clinical features of normal controls, amnestic MCI converters and non-converters to AD.

		Amnestic MCI			
	Normal controls	Converters to AD	Non converters		p
	n = 17	n = 9	n = 14		
Sociodemographic features					
Age, years	69±3	69±3	71±8		0.623
Gender, women	9 (53%)	4 (44%)	6 (42%)		0.837
Education, years	9.8±4.1	11.4±5.7	8.6±3.6		0.310
Cognitive and mental features					
Mini Mental State Exam	27.8±1.6	26.8±1.8	27.0±2.0		0.293
Disease duration (months)	---	30±17	34±33		0.707
Depression (CES-D)	---	16±8	15±6		0.776
Physical health					
Hypertension	7 (41%)	2 (22%)	11 (79%)	**	0.019
Diabetes	2 (12%)	1 (11%)	5 (35%)		0.190
Heart disease	2 (12%)	3 (33%)	6 (43%)		0.141
Brain structural features					
MTA score	0.6±0.5	2.4±1.2	1.7±1.1		0.001
ARWMC score	1.6±2.1	2.3±2.8	3.7±2.8		0.112
L Hippocampus (mm^3)	2770±274	2172±444	2347±598		0.013
R Hippocampus (mm^3)	2715±221	2359±404	2555±567		0.094
APOEε4, carriers	1/12 (8%)	5 (56%)	6 (43%)		0.040

CES-D: Center for Epidemiologic Studies Depression Scale; ARWMC: Age-Related White Matter Changes; MTA: Medial Temporal lobe Atrophy. Hippocampal volumes were normalized to mean total intracranial volume.
p denotes difference significance among all groups on X2 test (categorical variables, i.e. sex, hypertension, diabetes and heart disease), one-way ANOVA (continuous variables) or Kruskal-Wallis test (ordinal non-continuous variables, i.e. MTA and ARWMC scores).
(**) denotes a significant difference between the two amnestic MCI subgroups

SPECT scan

Both patients and normal controls underwent SPECT scan in the nuclear medicine department of the Ospedali Riuniti hospital, Bergamo. Each patient received an intravenous injection of 925 MBq of technetium-99m ethyl cysteinate dimer (99mTc-ECD) in resting conditions, lying supine with eyes closed in a quiet, dimly-lit room. Forty to 60 minutes after injection, brain SPECT was performed using a dual-head

rotating gamma camera (GE Elscint Helix) equipped with low energy-high resolution, parallel hole collimators. A 128x128 pixel matrix, zoom = 1.5, was used for image acquisition with 120 views over a 360° orbit (in 3° steps) with a pixel size and slice thickness of 2.94 mm. Butterworth filtered-back projection (order = 7, cut-off = 0.45 cycles/cm) was used for image reconstruction, and attenuation correction was performed using Chang's method (attenuation coefficient = 0.11/cm). Images were exported in DICOM format.

SPECT processing protocol.

To achieve a precise normalization, we generated a study-specific SPECT template using both SPECT and MR scans of all patients and normal controls under study, following a procedure described in detail elsewhere [31]. Briefly, we created a customised high-definition MR template, we converted SPECT scans to Analyze format using MRIcro [32], and we coregistered them to their respective MR scans with SPM2 [33]. We normalized each MR to the customized MR template through a nonlinear transformation (cutoff 25mm), and we applied the normalization parameters to the coregistered SPECT. We obtained the customized SPECT template as the mean of all the latter normalized SPECT images.

The creation of a study-specific template allows for better normalisation, since low uptake in ventricular structures and cortical hypoperfusion effects frequently present in elderly patients are accounted for.

For each coregistered SPECT scan, we set origin to the anterior commissure with SPM99, using the respective MR image as a reference, and we processed all scans with SPM2 according to an optimized processing protocol described in detail elsewhere [31]: (I) we smoothed each scan with a 10 mm full width at half maximum (FWHM) Gaussian, and spatially normalized it with an affine deformation to the customized SPECT template. We applied the same deformation to the unsmoothed images; (II) we masked the unsmoothed normalized images from I to remove scalp activity using SPM2's "brainmask". We smoothed with a 10 mm FWHM Gaussian, and warped them to the customized template with a nonlinear transformation (cutoff 25 mm). We applied the same transformation to the unsmoothed masked images; (III) we smoothed the normalized unsmoothed images from II with a 12 mm FWHM Gaussian.

MR imaging

Both patients and normal controls underwent brain T1-weighted magnetic resonance

imaging in the neuroradiology department of the Città di Brescia Hospital, Brescia, as previously discussed [31].

MR images were processed with SPM2 [33] following an optimized Voxel-Based Morphometry protocol, described in detail elsewhere [34, 35].

Manual tracings of hippocampal and total intracranial volumes were performed using DISPLAY [36]. Native hippocampal volumes were normalized to the individual intracranial volumes and rescaled to the mean total intracranial volume according to the following formula ([volume/individual total intracranial volume]*mean total intracranial volume).

Statistical Analysis

We investigated significance of the difference among groups in sociodemographic and clinical features and in neuropsychological tests scores using X2 test for categorical variables (sex, hypertension, diabetes and heart disease, ApoE), one-way ANOVA for continuous variables, and Kruskal-Wallis test for ordinal non-continuous variables (MTA and ARWMC scores). We then investigated significance of the difference between the two MCI subgroups on independent t-test. In all cases we set the significant threshold at $P<0.05$.

We used the "single subject: conditions and covariates" SPM2 model to assess differences in perfusion between groups on a voxel-by-voxel basis, and we compared either all amnestic MCI patients, amnestic MCI converted to AD, or amnestic MCI non-converted to dementia with normal controls. We used age as confounding variable. We set the significance threshold of the t-statistics at 0.001 uncorrected for multiple comparisons and the extent threshold at 100 voxels [37]. We used proportional scaling to remove inter-subject global variations in SPECT intensities, setting to 50 the mean count in all scalp-free brains.

To investigate whether grey matter hypoperfusion we found was either due to atrophy or not, we assessed grey matter atrophy in the same groups, using the same "single subject: conditions and covariates" SPM2 model on segmented GM images. We set the significance threshold at $P<0.001$ uncorrected for multiple comparisons, and we entered age and total intracranial volume as confounding variables.

Since native SPECT scans were coregistered to their respective MR images, and the study-specific SPECT template was coregistered to the high-definition MR template, all the normalised SPECT and MR images used for the statistical analysis were

coregistered to the SPM standard anatomical space.

We then compared significant hypoperfusion with significant atrophy on a voxel-by-voxel basis using a conjunction analysis, setting both hypoperfusion and atrophy significant thresholds at P<0.001 uncorrected for multiple comparisons.

Table 2: Neuropsychological tests scores corrected by age and education for normal controls, amnestic MCI converters and non-converters to AD.

		Amnestic MCI		
	Normal controls	**Converters to AD**	**Non converters**	**p**
	n = 17	n = 9	n = 14	
Memory				
Logical memory test (Spinnler and Tognoni, 1987)	13.1±3.5	7.9±3.8	9.5±3.3	0.001
Rey Auditory verbal learning test immediate recall (Carlesimo et al. 1996)	---	28.7±9.8	32.5±10.5	0.001
Rey Auditory verbal learning test delayed recall (Carlesimo et al. 1996)	---	3.7±2.3	6.4±3.5	<0.0005
Rey figure recall (Caffarra et al., 2002)	15.6±6.3	9.7±10.6	12.0±6.4	0.150
Executive and frontal functions				
TMT B-A (Giovagnoli et al., 1996)	43±108	83±67	74±57	0.463
CDT (Shulman et al., 1993)	---	3.0±1.1	2.4±1.1	0.238
Raven matrices (Basso et al., 1987)	31.8±4.1	29.6±4.1	27.7±4.6	0.038
Language				
COWAT, letter fluency (Novelli et al., 1986)	36.4±8.9	30.1±9.4	27.1±7.2	0.014
COWAT category fluency (Novelli et al., 1986)	41.9±9.2	30.1±9.4	31.1±8.7	<0.0005
Token test (Spinnler and Tognoni, 1987)	33.0±1.6	31.8±2.5	31.0±1.8	0.041
Apraxia				
Rey figure copy (Caffarra et al., 2002)	31.6±6.0	32.5±4.2	29.7±6.6	0.519

TMT: trail making test. CDT: clock drowing test. COWAT: controlled oral word association test.
All test scores are corrected by age and education
p denotes difference significance among all groups on one way ANOVA.

Results

Table 1 shows that the 3 groups differed significantly in medial temporal lobe atrophy, hypertension, left hippocampal volume and APOEε4 frequency. They did not differ for any other sociodemographic or physical health feature. Although Mini Mental State

Exam and Age-Related White Matter Changes were not significantly different among groups, MCI converters scored the lowest MMSE value, while non-converters scored the highest ARWMC value.

Restricting the comparison to amnestic MCI subgroups, using an independent t-test, we found a significant difference only in hypertension ($p=0.019$). Although hippocampal volumes, corrected by total intracranial volumes, were not significantly different, hippocampal volumes of amnestic MCI converters were smaller (about 8.5% less) than non-converters, in agreement with MTA scores. The analysis of the prevalence of the ε4 allele of apolipoprotein E (ApoE) shows a high prevalence of ε4 allele carriers in both amnestic MCI converters (56%) and non-converters (43%), but not in the normal control groups (just 1 carrier out of 12 normal controls with available data, 8%).

In neuropsychological test scores (table 2), the 3 groups differed significantly for all memory tests except for the Rey figure recall, for all language tests and for Raven matrices executive test. We had no differences for apraxia.

Restricting the comparison to amnestic MCI subgroups, we found a trend for significance only in the Rey Auditory verbal learning test delayed recall ($P=0.062$) [38].

Comparing the whole amnestic MCI group with the normal controls group, we found hypoperfusion in the left supramarginal, occipital, and inferior temporal gyri.

Table 3 and Figure 1 show the perfusion comparison between amnestic MCI converters and normal controls at $P<0.001$ uncorrected for multiple comparisons. The hypoperfusion peaks and clusters were located in the right parahippocampal gyrus and enthorinal cortex, and in the left inferior temporal and fusiform gyri.

Hypoperfusion in amnestic MCI patients non-converters, compared with normal controls at an uncorrected significance threshold of $P<0.001$, involved the retrosplenial cortex, precuneus and occipital gyri, mainly on the left side (Table 3 and Figure 2).

In comparison with normal controls, the whole amnestic MCI group showed GM atrophy in the bilateral inferior temporal gurus, in the right occipital gyrus, in the right orbital gyrus, in the left head of the hippocampus, and in the left cerebellum. MCI converters to AD showed GM atrophy in the inferior temporal gyrus bilaterally, in the hippocampus bilaterally, and in the right occipital gyrus, whereas amnestic MCI non-converters only showed small clusters of GM atrophy located bilaterally in the inferior and middle temporal gyri.

Comparing significant hypoperfusion with significant atrophy on a voxel-by-voxel basis, we found no overlap.

Figure 1: Areas of grey matter hypoperfusion in the 9 amnestic MCI patients who converted to AD vs 17 normal controls (p=0.001 uncorrected, extent threshold=100 voxels). Age was included as confounding variable. MCI patients who converted to AD showed hypoperfusion in the parahippocampal and inferior temporal gyri bilaterally. The figure shows the most significant cluster, located in the right parahippocampal gyrus (stereotactic coordinates 30,-20,-24).

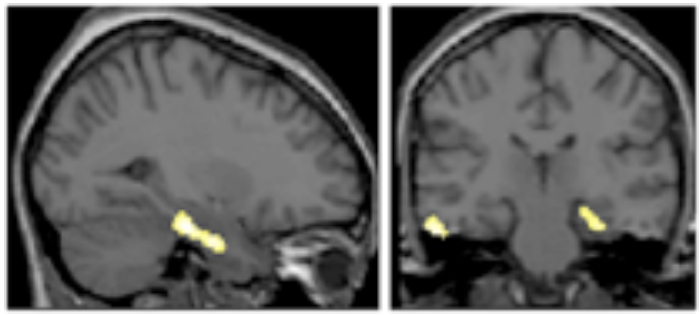

Table 3: Areas of grey matter hypoperfusion in amnestic MCI converters and non-converters to AD vs normal controls (p=0.001 uncorrected, extent threshold=100 voxels)

Cluster size	Regions	Stereotactic coordinates (mm)			Z score
		x	y	z	
Converters to AD vs normal controls					
291	R parahippocampal gyrus	30	-20	-24	3.87
	R parahippocampal gyrus	30	-4	-34	3.65
424	L inferior temporal gyrus	-64	-26	-26	3.65
	L inferior temporal gyrus	-60	-44	-20	3.47
	L fusiform gyrus	-54	-50	-14	3.47
Non converters vs normal controls					
375	L occipital gyrus	-48	-78	42	4.34
245	L precuneus	-6	-68	36	3.78

L = left, R = right.
Reading example: the first line denotes the presence of a 3D cluster made of 291 contiguous voxels of significant hypoperfusion . The most significant voxel of the cluster has stereotactic coordinates of (30, -20, -24) and is located in the right parahippocampal gyrus. Within the same cluster there is another peak of significance distant more than 8 mm from the former and located at (30, -4, -34).
Both comparisons were carried out using age as confounding variable.

Figure 2: Areas of grey matter hypoperfusion in 14 amnestic MCI patients who did not convert to dementia vs 17 normal controls (p=0.001 uncorrected, extent threshold=100 voxels). Age was included as confounding variable. MCI non-converters showed hypoperfusion in the retrosplenial cortex, mainly on the left side. The figure shows the most significant cluster, located in the left occipital gyrus (stereotactic coordinates -48,-78,42).

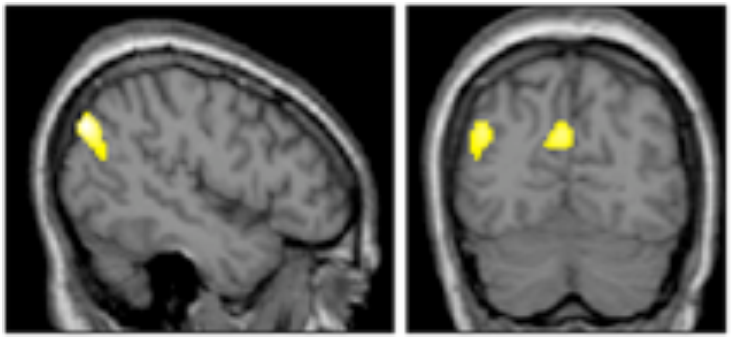

Figure 3: Areas of grey matter hypoperfusion (red) in comparison with areas of grey matter atrophy (green). A: as compared with normal controls, MCI converters to Alzheimer Disease showed GM atrophy in the hippocampus, in the inferior temporal gyri bilaterally, and in the right occipital gyrus, but not in any of the hypoperfusion areas. B: MCI non-converters showed a few small clusters of GM atrophy located bilaterally in the inferior and middle temporal gyri; none of them overlapped with the retrosplenial hypoperfusion areas. For both atrophy and hypoperfusion the uncorrected significance threshold was set at 0.001, and age was included as confounding variable. Total intracranial volume was included as further confounding variable in GM atrophy assessment.

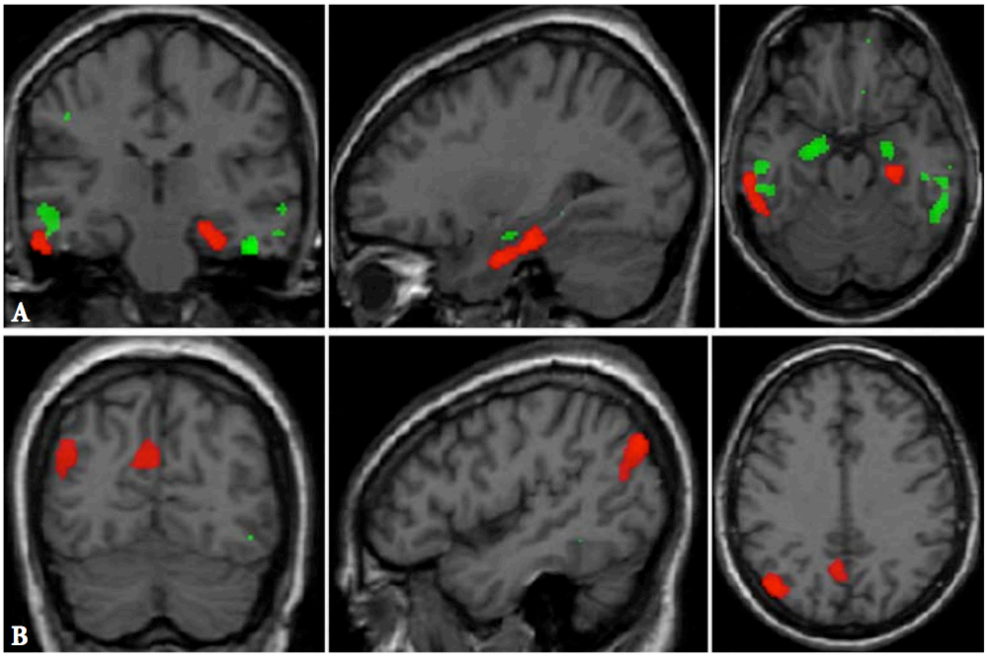

Discussion

Amnestic MCI converters to AD showed parahippocampal and inferior temporal hypoperfusion, whereas amnestic MCI patients non-converters showed hypoperfusion in the retrosplenial cortex. Hypoperfusion areas did not overlap with areas of grey matter atrophy.

In amnestic MCI converters to AD, memory impairment can be due to underlying Alzheimer Disease.

Comparing amnestic MCI converters to AD with normal controls, we found significantly reduced perfusion in the right enthorinal cortex and parahippocampal gyrus, and in the left inferior temporal and fusiform gyri. Our findings are in line with neurobiological knowledge about AD, with the enthorinal cortex being the earliest site to be compromised, even at a preclinical stage [39, 40], and with the right medial temporal lobe being affected earlier and to a greater extent by AD than the left medial temporal lobe [41, 42, 43]. Notably, we found no atrophy in the hypoperfusion areas. As it is well-known that functional alterations precede structural changes [7], cerebral perfusion analysis enables to show transentorinal and limbic dysfunction which cannot be detected by structural imaging, as atrophy has not yet occurred. The finding of parahippocampal hypoperfusion raises the question on why dysfunction in the medial temporal lobe has not been reported as an early correlate of conversion of MCI to AD in the SPECT/PET literature [11, 12, 14, 17, 18], despite it is largely expected on the basis of current knowledge on the pathophysiology of AD. This issue has been thoroughly discussed by a recent review [44], pointing to the problems of low spatial resolution of first-generation SPECT/PET equipments and to the smoothing procedure needed by the softwares performing voxel-based analysis. More recent reports, employing both SPECT [13, 15] and PET [16, 17] with last-generation equipments were able to find medial temporal hypoperfusion, in agreement with our findings.

We found hypoperfusion in amnestic MCI non-converters in the retrosplenial cortex, precuneus and occipital gyri, mainly on the left side. The ε4 allele of apoE is associated with cognitive decline among elderly people, being a risk factor for cognitive impairment in normal aging across a broad spectrum of domains, including memory decline, as well as a risk factor for late onset AD [45, 46, 47]. Since we found a high prevalence of the ε4 allele in both amnestic MCI converters to AD (56%) and non-

converters (43%) but not in the normal controls group (8%, in agreement with previous studies showing that ε4 allele frequency in a normal population of Italian elderly people is about 10% [48]), we investigated whether apoE could be in some way responsible for the hypoperfusion pattern in amnestic MCI non-converters. We considered only ε4 allele non-carrier amnestic MCI patients who did not convert to dementia, and we compared them with normal controls using SPM2. We found a hypoperfusion pattern similar to the one found for the whole group of amnestic MCI patients non-converters, so that we excluded the possibility that apoE affected the hypoperfusion pattern.

The retrosplenial cortex is typically involved in Alzheimer's disease, along with medial-temporal lobe and temporo-parietal regions. Although amnestic MCI non-converters did not develop AD during the observation time, they could do so in the future, and retrosplenial cortex deficit may be a correlate of later onset of AD. However, retrosplenial cortex is also reported to be involved in memory problems not depending on AD.

Using event-related functional magnetic resonance imaging, Ranganath et al. demonstrated that successful memory formation is associated with transient increases in a distributed network of limbic cortical areas – including perirhinal, orbitofrontal, and retrosplenial/posterior cingulate cortex – that are anatomically connected with the hippocampal formation, as well as in lateral temporal, medial parietal, and medial occipital cortex [49].

Comparing amnestic MCI non-converters to dementia with normal controls we found no grey matter atrophy except for some small clusters in the inferior and medial temporal gyri. We therefore excluded grey matter atrophy as a cause of hypoperfusion. We finally hypothesized that retrosplenial cortex dysfunction could be a cause of memory impairment without being a biomarker of conversion to dementia.

We believe that one of the strengths of this study lies in the prediction of conversion to dementia in amnestic MCI patients, rather than in an undifferentiated MCI group considered in most of the previous studies [10, 12, 11, 13, 17]. Restricting the analysis to a better defined subgroup limited heterogeneity, and yielded stronger results.

Another strength is the advanced SPECT processing protocol we used. Spatial normalisation was improved by using a study-specific SPECT template derived using deformations from companion MR images.

Voxel-based SPECT analysis indicated that the hypoperfusion pattern for amnestic MCI converters to AD was different to the pattern for non-converters, while neuropsychological test scores failed to distinguish between the two subgroups. Neuropsychological testing of the subgroups revealed a trend for significance (P=0.062) in the Rey Auditory verbal learning test delayed recall [38] only. Moreover, amnestic MCI non-converters to AD scored worse than converters in several neuropsychological tests (executive Raven matrices test [21], letter fluency and Token tests for language [22, 23], and Rey figure copy test for apraxia [24]).

To investigate whether grey matter atrophy was responsible for hypoperfusion or not, we compared significant hypoperfusion with significant atrophy on a voxel-by-voxel basis. As we found no overlap, we could state that the detected hypoperfusion was not due to volumetric loss. In both amnestic MCI converters to AD and non-converters atrophy patterns mainly involved temporal gyri, while hypoperfusion patterns were significantly different. SPECT analysis could show the dysfunction that characterizes the earliest stage of the disease, and provide pathophysiological information not available from structural imaging, because functional alterations precede structural changes [7].

In order to investigate whether the normal controls recruitment modality could have any influence on the results, as we had 7 subjects undergoing MR scan for reasons unrelated to cognition but to some extent possibly related to cerebral perfusion, we repeated all the analysis using only the 10 volunteers. The results we obtained were the same as those presented in the current paper, even if the significant clusters were smaller, probably due to the normal sample reduction.

Some limitations should also be considered in the interpretation of the results. Perfusion correlates of conversion to dementia were assessed using relatively small groups, and larger groups of patients would be needed to confirm our results. Physical health differences among groups, e.g. differences in hypertension, could have influenced the results, and physical health-matched groups would be needed. In all comparisons, we set the significant threshold at $P<0.001$ uncorrected for multiple comparisons. This unrestrictive threshold should be used only when any apriori hypothesis could be made, which was the case for converters to AD, for whom hypoperfusion in the medial temporal lobe was expected, but not for non-converters, for whom we had no apriori hypothesis. Amnestic MCI patients underwent yearly

follow-up visits, consisting of complete clinical and neuropsychological examination, from 1 to 3 years after enrolment (mean observation time 19±10 months). Since available data seem to suggest that the likelihood of an amnestic MCI patient to develop Alzheimer's dementia in the long term is around 50% [4], some of the amnestic MCI patients who did not convert to dementia during the observation time may develop dementia later and bias the segregation of converters and non-converters. It will be interesting to replicate this study with longer follow-up.

In this study we investigated only cerebral perfusion correlates of conversion. However, predicting conversion to dementia is a multimodal task, requiring the use of biomarkers from different fields of research. The combination of cerebral perfusion with other predictive markers, such as low hippocampal volume [50], and tau protein in the CSF [51], could enable to increase the overall sensitivity and therefore the diagnostic accuracy of predicting conversion to dementia [52, 53].

In conclusion, our results suggest that parahippocampal and inferior temporal hypoperfusion in amnestic MCI patients could be considered as a correlate of conversion to AD. Hypoperfusion in the retrosplenial cortex seems to be involved in memory impairment but does not seem the key prognostic indicator of conversion to dementia.

References

1. Petersen RC, Smith GE, Waring SC, Ivnik RJ, Tangalos EG, Kokmen E. Mild cognitive impairment: clinical characterization and outcome. Arch Neurol 1999; 56:303–308.
2. Petersen RC, Doody R, Kurz A, et al. Current concepts in mild cognitive impairment. Arch Neurol 2001; 58:1985–1992.
3. Flicker C, Ferris SH, Reisberg B. Mild cognitive impairment in the elderly: predictors of dementia. Neurology 1991; 41:1006–1009.
4. Visser PJ, Kester A, Jolles J, Verhey F. Ten-year risk of dementia in subjects with mild cognitive impairment. Neurology 2006; 67:1201-1207.
5. Bennett DA, Wilson RS, Schneider JA, et al. Natural history of mild cognitive impairment in older persons. Neurology 2002; 59:198–205.
6. Larrieu S, Letenneur L, Orgogozo JM, et al. Incidence and outcomes of mild cognitive impairment in a population-based prospective cohort. Neurology 2002; 59:1594-1599.
7. Small AS. Alzheimer disease, in living color. Nat Neurosci 2005; 8:404-405.
8. Benson DF, Kuhl DE, Hawkins RA, Phelps ME, Cummings JL, Tsai SY. The fluorodeoxyglucose 18F scan in Alzheimer's disease and multi-infarct dementia. Arch Neurol 1983; 40:711-714.
9. Minoshima S, Giordani B, Berent S, Frey KA, Foster NL, Kuhl DE. Metabolic reduction in the posterior cingulated cortex in very early Alzheimer's disease. Ann Neurol 1997; 42:85-94.
10. Cabranes JA, De Juan R, Encinas M, et al. Relevance of functional neuroimaging in the progression of mild cognitive impairment. Neurol Res 2004; 26:496-501.
11. Encinas M, De Juan R, Marcos A, et al. Regional cerebral blood flow assessed with 99mTc-ECD SPET as a marker of progression of mild cognitive impairment to Alzheimer's disease. Eur J Nucl Med Mol Imaging 2003; 30:1473-1480.
12. Chetelat G, Desgranges B, De La Sayette V, Viader F, Eustache F, Baron JC. Mild cognitive impairment: Can FDG-PET predict who is to rapidly convert to Alzheimer's disease? Neurology 2003; 60:1374-1377.
13. Hirao K, Ohnishi T, Hirata Y, et al. The prediction of rapid conversion to Alzheimer's disease in mild cognitive impairment using regional cerebral blood flow SPECT. Neuroimage 2005; 28:1014-1021.
14. Huang C, Wahlund LO, Svensson L, Winblad B. Cingulate cortex hypoperfusion predicts Alzheimer's disease in mild cognitive impairment. BMC Neurol 2002; 2:9-14.
15. Ishiwata A, Sakayori O, Minoshima S, Mizumura S, Kitamura S, Katayama Y. Preclinical evidence of Alzheimer changes in progressive mild cognitive impairment: a qualitative and quantitative SPECT study. Acta Neurol Scand 2006; 114:91–96
16. Anchisi D, Borroni B, Franceschi M, et al. Heterogeneity of Brain Glucose Metabolism in Mild Cognitive Impairment and Clinical Progression to Alzheimer Disease. Arch Neurol 2005; 62:1728-1733.
17. Drzezga A, Lautenschlager N, Siebner H, et al. Cerebral metabolic changes accompanying conversion of mild cognitive impairment into Alzheimer's disease: a PET follow-up study. Eur J Nucl Med Mol Imaging 2003; 30:1104–1113.
18. Borroni B, Anchisi D, Paghera B, et al. Combined 99mTc-ECD SPECT and neuropsychological studies in MCI for the assessment of conversion to AD. Neurobiol Aging 2006; 27:24-31.

19. Shulman KI. Clock-drawing: is it the ideal cognitive screening test? Int J Geriatr Psychiatry 2000; 15:548-561.
20. Giovagnoli AR, Del Pesce M, Mascheroni S, Simoncelli M, Laiacona M, Capitani E. Trail making test: normative values from 287 normal adult controls. Ital J Neurol Sci 1996; 17:305-309.
21. Basso A, Capitani E, Laiacona M. Raven's coloured progressive matrices: normative values on 305 adult normal controls. Funct Neurol 1987; 2:189-194.
22. Spinnler H, Tognoni G. Standardizzazione e taratura italiana di test neurologici. Ital J Neurol Sci 1987; 8:47-50.
23. Novelli G, Papagno C, Capitani E, Laiacona M, Cappa SF, Vallar G. Tre test clinici di ricerca e produzione lessicale. Taratura su soggetti normali. Arch Psicol Neurol Psichiatr 1986; 47:477-506.
24. Caffarra P, Vezzadini G, Dieci F, Zonato F, Venneri A. Rey-Osterrieth complex figure: normative values in an Italian population sample. Neurol Sci 2002; 22:443-447.
25. Radloff LS. The CES-D scale: A self-report depression scale for research in the general population. Appl Psychol Measure 1997; 1:385-401.
26. McKhann G, Drachman D, Folstein M, Katzman R, Price D, Stadlan EM. Clinical diagnosis of Alzheimer's disease: report of the NINCDS-ADRDA Work Group under the auspices of Department of Health and Human Services Task Force on Alzheimer's Disease. Neurology 1984; 34:939-944.
27. Erkinjuntti T, Inzitari D, Pantoni L, et al. Research criteria for subcortical vascular dementia in clinical trials. J Neural Transm Suppl 2000; 59:23-30.
28. McKeith IG, Ballard CG, Perry RH, et al. Prospective validation of consensus criteria for the diagnosis of dementia with Lewy bodies. Neurology 2000; 54:1050-1058.
29. Knopman DS, Boeve BF, Parisi JE, et al. Antemortem Diagnosis of Frontotemporal Lobar Degeneration. Ann Neurol 2005; 57:480-488.
30. Riello R, Sabattoli F, Beltramello A, et al. Brain volumes in healthy adults aged 40 years and over: a voxel based morphometry study. Aging Clin Exp Res 2005; 17:329-336.
31. Caroli A, Testa C, Geroldi C, et al. Brain perfusion correlates of medial temporal lobe atrophy and white matter hyperintensities in mild cognitive impairment. J Neurol 2007; 254:1000-1008.
32. Rorden C, Brett M. Stereotaxic display of brain lesions. Behav Neurol 2000; 12:191-200.
33. SPM, Statistical Parametric Mapping, version 2 (2002). London: Functional Imaging Laboratory. Available at: http://www.fil.ion.ucl.ac.uk/spm/software/spm2
34. Frisoni GB, Testa C, Sabattoli F, Beltramello A, Soininen H, Laakso MP. Structural correlates of early and late onset Alzheimer's disease: voxel based morphometric study. J Neurol Neurosurg Psychiatry 2005; 76:112-114.
35. Filippini N, Scassellati C, Boccardi M, et al. Influence of serotonin receptor 2A His452Tyr polymorphism on brain temporal structures: a volumetric MR study. Eur J Hum Genet 2006; 14:443-449.
36. DISPLAY. Brain Imaging Center - Montreal Neurological Institute. Available at: http:// www.bic.mni.mcgill.ca/software
37. Friston KJ, Worsley KJ, Frackowiak RSJ, Mazziotta JC, Evans AC. Assessing the significance of focal activations using their spatial extent. Hum Brain Mapp 1994; 1:214-220.

38. Carlesimo GA, Marfia GA, Loasses A, Caltagirone C. Recency effect in anterograde amnesia: evidence for distinct memory stores underlying enhanced retrieval of terminal items in immediate and delayed recall paradigms. Neuropsychologia 1996; 34:177-184.
39. Braak H, Braak E. Evolution of neuronal changes in the course of Alzheimer's disease. J Neural Transm Suppl 1998; 53:127-140.
40. Pennanen C, Kivipelto M, Tuomainen S, et al. Hippocampus and enthorinal cortex in mild cognitive impairment and early AD. Neurobiol Aging 2004; 25:303-310.
41. Baron JC, Chetelat G, Desgranges B, et al. In vivo mapping of grey matter loss with voxel-based morphometry in mild Alzheimer's disease. Neuroimage 2001; 14:298–309.
42. Rombouts SA, Barkhof F, Witter MP, Scheltens P. Unbiased whole-brain analysis of grey matter loss in Alzheimer's disease. Neurosci Lett 2000; 285:231–233.
43. Ohnishi T, Matsuda H, Tabira T, Asada T, Uno M. Changes in brain morphology in Alzheimer disease and normal ageing: is Alzheimer disease an exaggerated aging process? Am J Neuroradiol 2001; 22:1680–1685.
44. Mosconi L. Brain glucose metabolism in the early and specific diagnosis of Alzheimer's disease. Eur J Nucl Med Mol Imaging 2005; 32:486-510.
45. Dik MG, Jonker C, Bouter LM, Geerlings MI, van Kamp GJ, Deeg DJ. APOE-epsilon4 is associated with memory decline in cognitively impaired elderly. Neurology 2000; 54:1492-1497.
46. Bretsky P, Guralnik JM, Launer L, Albert M, Seeman TE; MacArthur Studies of Successful Aging. The role of APOE-epsilon4 in longitudinal cognitive decline: MacArthur Studies of Successful Aging. Neurology 2003; 60:1077-1081.
47. Ye S, Huang Y, Mullendorff K, et al. Apolipoprotein (apo) E4 enhances amyloid β peptide production in cultured neuronal cells: ApoE structure as a potential therapeutic target. PNAS 2005; 102:18700-18705.
48. Corbo RM, Scacchi R. Apolipoprotein E (APOE) allele distribution in the world. Is APOE*4 a 'thrifty' allele? Ann Hum Genet 1999; 63:301-310.
49. Ranganath C, Heller A, Cohen MX, Brozinsky CJ, Rissman J. Functional connectivity with the hippocampus during successful memory formation. Hippocampus 2005; 15:997-1005.
50. Jack CR Jr, Petersen RC, Xu YC, et al. Prediction of AD with MRI-based hippocampal volume in mild cognitive impairment. Neurology 1999; 52:1397-1403.
51. Riemenschneider M, Lautenschlager N, Wagenpfeil S, Diehl J, Drzezga A, Kurz A. Cerebrospinal fluid tau and beta-amyloid 42 proteins identify Alzheimer disease in subjects with mild cognitive impairment. Arch Neurol 2002; 59:1729-1734.
52. Okamura N, Arai H, Maruyama M, et al. Combined analysis of CSF Tau levels and [123I]Iodoamphetamine SPECT in mild cognitive impairment: implications for a novel predictor of Alzheimer's disease. Am J Psychiatry 2002; 159:474-476.
53. Modrego PJ. Predictors of conversion to dementia of probable Alzheimer type in patients with mild cognitive impairment. Curr Alzheimer Res 2006; 3:161-170.

Chapter 4

Brain perfusion correlates of medial temporal lobe atrophy and white matter hyperintensities in mild cognitive impairment

Caroli A, Testa C, Geroldi C, Nobili F, Guerra UP, Bonetti M, Frisoni GB

Journal of Neurology 2007; 254:1000-1008

Abstract

Objective: To assess the association of Medial Temporal lobe Atrophy (MTA) and White Matter Hyperintensities (WMHs) with grey matter perfusion in Mild Cognitive Impairment (MCI). Methods: 56 MCI patients (age=69.3±7.0, 32 females) underwent brain MR scan and 99mTc ECD SPECT. We evaluated MTA according to Scheltens' five-point scale on T1 MR images, and assessed WMHs using the rating scale for age-related white matter changes on T2-weighted and FLAIR MR images. We divided MCI into age-matched subgroups with high and low MTA and high and low WMHs load. We processed SPECT images with SPM2 following an optimized protocol and performed a voxel-based statistical analysis comparing high vs low MTA and high vs low WMHs, setting p-value at 0.001 uncorrected, thresholding cluster extent at 100 voxels, using proportional scaling and entering age and WMHs or MTA respectively as nuisance covariates. Results: MCI with high compared with low MTA showed hypoperfusion in the left hippocampus and in the left parahippocampal gyrus. MCI with high compared with low WMHs showed a hypoperfusion area in the left insular region and superior temporal gyrus. Conclusions: MTA in MCI is associated with hippocampal grey matter hypoperfusion while WMHs is associated with grey matter hypoperfusion in areas of the insula and temporal neocortex. These results confirm that MTA is associated with local functional changes and suggest that WMHs may be associated with remote brain cortical dysfunction.

Introduction

Mild cognitive impairment (MCI) is a clinical syndrome characterized by cognitive deficits without functional impact on daily living, and thus not severe enough to allow a diagnosis of dementia [1]. Clinical studies of elderly individuals with MCI suggest that this is often a transition state between normal cognition and dementia.

The most frequent causes of the MCI phenotype are neuropathological damage in the medial temporal lobe (MTL) due to Alzheimer's disease [1-3], denoted by medial temporal lobe atrophy (MTA) on T1-weighted MR imaging [4], and white matter damage due to hypertensive or diabetic small vessel disease [5,6], denoted by white matter hyperintensities (WMHs) in T2-weighted images. Unfortunately, in older patients the two lesions often occur together and the estimate of the contribution of Alzheimer's and small vessel disease lesions to cortical dysfunction has so far eluded investigation.

The relevant clinical issue in MCI patients consists in distinguishing MCI patients who will shortly develop AD from those who will never develop dementia. This is a multimodal task requiring the use of a number of biomarkers for AD. Okamura and colleagues showed that the combination of CSF tau levels and measures of cerebral blood flow enables to increase the sensitivity and specificity of each marker [7].

Alzheimer disease progresses through different stages: the cell sickness stage, during which it causes neurons to malfunction; the histological stage, during which AD causes insoluble protein aggregation, typified by amyloid plaques and neurofibrillary tangles; and finally the cell death stage, during which the disease kills off neurons, resulting in volumetric loss [8]. As functional alterations antedate structural changes, functional imaging plays a key role to visualize the dysfunction that characterizes the earliest stage of the disease, and provide pathophysiological information which cannot yet be detected by structural imaging.

We have used defects of cerebral perfusion as proxies of cortical dysfunction. The advantage of using defects of cerebral perfusion is that they can be accurately measured and mapped onto medial temporal and cortical grey matter structures. We have thus assessed the effect of MTA and WMHs on perfusion of grey matter structures.

Literature data allowed us to expect finding an effect of MTA on medial temporal grey matter perfusion [9]. On the contrary, there are just a few studies about the effect of

WMHs on grey matter structures in dementia, with contrasting findings [10-12]. We hypothesied that if WMHs have an effect on cortical function, we would find a relationship between WMHs and cortical perfusion.

Methods

Subjects

Patients were taken from a prospective project on MCI ("Mild Cognitive Impairment in Brescia - MCIBs"), aimed to study the natural history of non demented persons with apparently primary cognitive deficits, i.e. not due to psychic or physical conditions. The study protocol was approved by the local ethics committee and all participants signed an informed participation consent.

Inclusion criteria in the study were all of the following: (i) memory or other cognitive disturbances; (ii) mini mental state examination score of 24 to 27/30 or MMSE of 28 and higher plus low performance (score of 2/6 or higher) on the clock drawing test [13]; (iii) sparing of instrumental and basic activities of daily living or functional impairment stably due to causes other than cognitive impairment. Exclusion criteria were any one of the following: (i) age of 90 years and older; (ii) history of depression or psychosis of juvenile onset; (iii) history or neurological signs of major stroke; (iv) alcohol abuse; (v) craniocerebral trauma; (vi) heavy use of psychotropic drugs.

Based on these criteria, 139 patients were evaluated from April 2002 to March 2005. All of these underwent: (i) semi-structured interview with the patient and – whenever possible – with another informant (usually the patient's spouse or a child) by a geriatrician; (ii) physical and neurological examinations; (iii) performance-based tests of physical function, gait and balance; (iv) neuropsychological battery assessing verbal and non-verbal memory, attention and executive functions (Trail Making Test B-A [14]; Clock Drawing Test [13]), abstract thinking (Raven matrices [15]), frontal functions (Inverted Motor Learning [16]), language (Phonological and Semantic fluency [17]; Token test [16]), and apraxia and visuo-constructional abilities (Rey figure copy [18]); (v) assessment of depressive symptoms with the Center for Epidemiologic Studies Depression Scale (CES-D [19]). Of these, 17 scored within normal limits (above the 10th percentile of the age- gender- and education-specific distribution) on all neuropsychological tests and 18 did not have MR imaging of adequate quality for the scoring of MTA (see later). Among the 104 remaining patients, 56 agreed to undergo

SPECT scan and were included in the present study. MCI patients who did and did not undergo a SPECT were similar for age (70±6 vs 71±8, p=0.230), gender (58% vs 69% females, p=0.271), physical health (hypertension: 51% vs 54%, p=0.768; diabetes: 23% vs 10%, p=0.062; heart disease: 33% vs 31%, p=0.879), MTA (1.6±1.3 vs 1.9±1.2, p=0.151) and WMH load (3.3±3.4 vs 4.0±3.9, p=0.354); they differed only for education (9.2±4.6 vs 6.5±3.3, p=0.002) and MMSE (27.6±1.6 vs 26.6±1.8, p=0.007).

Table 1: Sociodemographic and clinical features of MCI patients with high medial temporal lobe atrophy (MTA) and white matter hyperintensity (WMHs) scores and age-matched peers with low scores.

	MTA			WMHs		
	Low n = 12	High n = 12	p	Low n = 15	High n = 15	p
Sociodemographic features						
Age, years	71±4	75±6	0.106	68±4	70±6	0.119
Gender, women	8 (67%)	4 (33%)	0.102	5 (53%)	9 (60%)	0.705
Education, years	7.5±4.3	11.9±4.9	0.004	11.2±4.3	7.8±4.4	0.026
Cognitive and mental features						
Mini Mental State Exam	27.7±1.4	27.4±0.8	0.504	27.3±1.9	27.9±1.4	0.199
Disease duration (months)	54±34	42±39	0.265	56±58	38±31	0.119
Depression (CES-D)	19±10	14±7	0.322	13±10	18±9	0.153
Verbal learning (delayed recall test)	7.7±2.6	4.7±2.3	0.010	6.8±3.8	8.9±4.2	0.016
Trail making test B-A	140±292	64±52	0.394	95±99	115±243	0.771
Attention matrix	43.4±7.6	44.1±9.4	0.876	41.5±7.9	43.4±9.7	0.483
Non-verbal learning (Rey figure recall)	17.0±6.3	10.2±6.1	0.037	15.0±9.4	15.7±7.6	0.904
Physical health						
Hypertension	8 (67%)	6 (50%)	0.480	3 (20%)	10 (67%)	0.008
Diabetes	0 (0%)	2 (17%)	0.157	3 (20%)	4 (27%)	0.705
Heart disease	5 (42%)	4 (33%)	0.655	3 (20%)	7 (47%)	0.157
Brain structural features						
MTA rating scale	0.7±0.5	3.3±0.5	<0.001	1.1±1.3	1.7±1.1	0.040
ARWMC scale	4.3±4.0	3.5±2.5	0.546	0.0±0.0	7.1±1.6	<0.001

CES-D: Center for Epidemiologic Studies Depression Scale; MTA: Medial Temporal lobe Atrophy; ARWMC: Age-Related White Matter Changes.
Neuropsychological test scores are corrected for age, gender, and education.
p denotes difference significance between MCI subgroups on paired t-test (independent t-test for age only) or nonparametric Wilcoxon test for dependent samples.

MR scan

MCI patients underwent brain magnetic resonance imaging in the neuroradiology department of the Città di Brescia Hospital, Brescia, with a 1.0 Tesla Philips Gyroscan scanner. A T1-weighted scan was acquired in the sagittal plane with a gradient echo 3D technique as follows: TR = 20 ms, TE = 5 ms, flip angle = 30°, field of view = 220 mm, acquisition matrix 256x256, slice thickness = 1.3 mm, number of slices = 115. Dual echo T2-DP images were acquired in the axial plane as follows: TR = 2000 ms, TE = 8.8/110 ms, flip angle = 90°, field of view = 230 mm, acquisition matrix 256x256, distance factor = 1.0, slice thickness = 5 mm. FLAIR images were acquired in the axial plane as follows: TR = 5000 ms, TE = 100 ms, flip angle = 90°, field of view = 230 mm, acquisition matrix 256x256, distance factor = 1.0, slice thickness = 5 mm, space between slices = 6 mm, with 1 mm gap. T1-weighted 3D images were used to score MTA, and double echo and FLAIR images to score WMHs.

White matter assessment. We assessed WMHs using the rating scale for Age-Related White Matter Changes (ARWMC) [20] on T2-weighted and FLAIR MR images. A single observer (R.R.) rated WMHs in the right and left hemispheres separately in frontal, parieto-occipital, temporal, infratentorial areas and basal ganglia on a 4 point scale. Scores of 0, 1, 2, and 3 were assigned in frontal, parieto-occipital, temporal, infratentorial areas for: no WMHs, focal lesions, beginning confluence of lesion, and diffuse involvement of the entire region, respectively. Scores of 0, 1, 2, and 3 were assigned in basal ganglia for: no WMHs, 1 focal lesion, more than 1 focal lesion, and confluent lesions, respectively. For each area, a score was given by the sum of the right and left subscores, and WMH score was computed as the sum of all subscores. Intra-rater reliability was assessed on a random sample of 20 subjects. The intraclass correlation coefficient was 0.989, indicating a very high reliability [21].

Visual rating scale of MTA. A single operator (L.B.) visually assessed MTA on digital 3D-T1 MR images blind to clinical data. The images were first tilted to 2 mm thick coronal slices oriented perpendicular to the intercommissural axis, and for each subject six contiguous coronal sections were selected in which medial temporal lobe structures could be best evaluated. The rater evaluated MTA for each image and separately for the right and the left sides according to a five-point scale developed and validated by Scheltens et al. [22], considering both the shrinkage of hippocampal formation (the

hippocampus and the parahippocampal gyrus) and the enlargement of the surrounding cerebrospinal fluid spaces (the width of choroid fissure and the width of temporal horn). MTA score was computed as the maximum between right and left scores. A single operator (L.B.) assessed the test-retest reliability of the visual MTA scale in 10 patients and 10 controls randomly selected. The Cohen's k coefficient for intrarater reliability was 0.72, indicating satisfactory reliability [23].

SPECT scan

MCI patients underwent a SPECT scan in the Nuclear Medicine Department of the Ospedali Riuniti hospital, Bergamo. Each patient received an intravenous injection of 925 MBq of technetium-99m ethyl cysteinate dimer (99mTc-ECD) in resting conditions, lying supine with eyes closed in a quiet, dimly-lit room. Fourty to 60 minutes after injection, brain SPECT scan was performed using a dual-head rotating gamma camera (GE Elscint Helix) equipped with low energy-high resolution, parallel hole collimators. A 128x128 pixel matrix, zoom = 1.5, was used for image acquisition with 120 views over a 360° orbit (in 3° steps) with a pixel size and slice thickness of 2.94 mm. Butterworth filtered-back projection (order = 7, cut-off = 0.45 cycles/cm) was used for image reconstruction, and attenuation correction was performed using Chang method [24] (attenuation coefficient = 0.11/cm). Images were exported in DICOM format.

Customized SPECT template. To achieve a precise normalization, we generated a study-specific SPECT template using both the SPECT and MR scans of MCI patients under study [25].

We firstly created a sixth (VI) generation MR template as follows: we matched 3D T1 MR scans from 30 healthy people using linear transformations to the MNI T1 weighted template in SPM2 [26], and computed the mean of the linearly transformed images; we used the mean image as template, and spatially normalized the original MR images to it using nonlinear transformations; we computed a new mean, and used it as template (generation I) for a further nonlinear normalization. We iteratively repeated six times the process to create a high resolution sixth (VI) generation MR template.

We converted SPECT scans to Analyze format using MRIcro [27], and we coregistered them to their respective MR scans with SPM2. We normalized each MR to the sixth (VI) generation MR template created with a nonlinear transformation (cutoff 25mm), and we applied the normalization parameters to the coregistered SPECT. We obtained the study-specific SPECT template from the mean of these normalized SPECT images. All

templates and normalised scans had a voxel size of 2x2x2 mm. More detailed information are available at http://www.centroalzheimer.it/public/SPECT_template_JoN.doc.

The creation of a study-specific template allows for better normalisation, since the central and cortical hypoperfusion effects frequently present in elderly patients are accounted for.

SPECT processing protocol. For each coregistered SPECT scan, we set the origin to the anterior commissure with SPM99, using the respective MR image as a reference and processed them with SPM2 according to an optimized processing protocol [28,29]: (I) we smoothed each scan with a 10 mm FWHM Gaussian, and spatially normalized it with an affine deformation to the customized SPECT template. We applied the same deformation to the unsmoothed images; (II) we masked the unsmoothed normalized images from I to remove scalp activity using SPM2's "brainmask". We smoothed with a 10 mm FWHM Gaussian, and warped them to the customized template with a nonlinear transformation (cutoff 25 mm). We applied the same transformation to the unsmoothed masked images; (III) we smoothed the normalized unsmoothed images from II with a 12 mm FWHM Gaussian. The whole SPECT processing protocol is summarized in a flow chart available at http://www.centroalzheimer.it/public/SPECT_processing_JoN.doc.

MCI subgroups.

We divided MCI patients into those with high and low MTA and high and low WMH load according to the following procedure. Of the 56 MCI patients, 29 had normal MTA (score=0-1, age=65±7, 19 females), 9 had mild to moderate MTA (score=2, age=72±4, 4 females), and 12 had moderate to severe MTA (score=3-4, age=75±6, 5 females). Since age was significantly different between extreme groups and age is a potential confounder being a strong correlate of both predictor (MTA) and outcome (brain perfusion), for each of the 12 patients with moderate to severe MTA we selected one patient with normal MTA whose age matched as closely as possible and in any case within ±5 years. This way, we came out with a group of 12 patients with normal MTA with age=71±4, 8 of whom were females.

Similarly, in order to select patients of extreme WMH load, we divided the whole MCI group into tertiles based on WMH score (WMH score=0, N=17, age=72±7, 10 females; 1≤WMH score≤5, N=20, age=70±7, 10 females; WMH score≥6, N=17, age=66±6, 11

females). Since age was significantly different between the extreme groups and, again, age is a strong correlate of both WMHs and brain perfusion, we sought to select for each of the 17 patients in the highest tertile one patient in the lowest tertile whose age matched as closely as possible and in any case within ±5 years. We excluded the two oldest patients of the highest tertile due to lack of suitable matches and came out with 15 patients with high WMHs (age=70±6, 9 females), and 15 low WMHs (age=68±4, 5 females).

Statistical Analysis

We investigated significance of the difference in sociodemographic and clinical features between age-matched groups with paired t-test (for continuous variables) or nonparametric Wilcoxon test for dependent samples (for discrete variables). We used an independent t-test for age only, as this was the matching variable. In all cases we set the significant threshold at $P<0.05$.

We used the SPM2 ANCOVA model (Compare populations: 1 scan/subject) to assess differences in perfusion between groups on a voxel-by-voxel basis. We ran two separate experiments: 1) patients with high vs those with low MTA; 2) patients with high vs those with low WMHs. We used age as nuisance covariate in both experiments and WMHs as a nuisance covariate in the MTA experiment and viceversa. We set the significance threshold of the t-statistics at 0.001 uncorrected for multiple comparisons and the extent threshold at 100 voxels (0.8 cc). We used proportional scaling to remove inter-subject global variations in SPECT intensities, setting to 50 the mean count in all scalp-free brains. We repeated the same analysis setting significance at the most restrictive threshold of $P=0.05$, Family-Wise Error (FWE) corrected for multiple comparisons.

We assessed grey matter atrophy in MCI with high MTA vs. low MTA with SPM2 using an optimized Voxel-Based Morphometry protocol described in detail elsewhere [30,31], setting the significant threshold first at $P<0.001$ uncorrected for multiple comparisons, and then at a less restrictive value of $P<0.05$ uncorrected. We compared significant hypoperfusion ($P<0.001$) with significant atrophy ($P<0.05$) on a voxel-by-voxel basis. A detailed description of the procedure is available at http://www.centroalzheimer.it/public/GM_atrophy_JoN.doc.

Results

Table 1 shows that MCI patients with low MTA had lower education than patients with high MTA, while patients with low WMHs had higher education than those with high WMHs. MCI patients with low MTA were not different from those with high MTA for age, sex, physical health, cognitive and mental features except learning (both auditory verbal learning test delayed recall and Rey figure recall). MCI patients with low WMHs were not different from those with high WMHs for all variables except hypertension, as MCI with high WMHs had higher prevalence of the disease, verbal learning and MTA. All white matter lesions found in patients with high WMHs were located in the frontal and parieto-occipital lobes and basal ganglia; no lesions were found in the temporal and infratentorial areas.

Table 2 and figure 1 show the perfusion comparison between MCI patients with high and low MTA scores at P<0.001 uncorrected for multiple comparisons. The hypoperfusion peaks and clusters were located in the left hippocampus (both head and tail), in the left parahippocampal gyrus, and in the cerebellum bilaterally.

Table 2: Areas of grey matter hypoperfusion in MCI patients with high vs. those with low medial temporal lobe atrophy (MTA) scores, and with high vs. low white matter hyperintensities (WMHs) scores (p=0.001 uncorrected, extent threshold = 100 voxels).

Cluster size	Regions	Stereotactic coordinates (mm)			Uncorrected p value	Z score
		x	y	z		
High vs low MTA score						
572	L hippocampus, tail	-30	-46	2	<0.0005	4.43
	L hippocampus, tail	-38	-54	-2	<0.0005	4.09
	L parahippocampal gyrus	-40	-44	4	<0.0005	3.31
113	R cerebellum	14	-40	-40	<0.0005	3.97
134	L cerebellum	-10	-50	-30	<0.0005	3.68
110	L hippocampus, head	-26	-18	-20	<0.0005	3.62
High vs low WMH score						
112	L Superior Temporal Gyrus	-44	20	-18	<0.0005	3.78

L = left, R = right.

Reading example: the first line denotes the presence of a 3D cluster made of 572 contiguous voxels of significant hypoperfusion . The most significant voxel of the cluster has stereotactic coordinates of (-30, -46, 2) and is located in the left parahippocampal gyrus. Within the same cluster there are two other peaks of significance distant more than 8 mm from the former and located at (-38, -54, -2) and (-40, -44, 4) respectively.

Both comparisons were carried out using age as nuisance covariate; WMHs and MTA scores were used as further nuisance covariates in the first and second experiment respectively.

Figure 1: Areas of grey matter hypoperfusion in 12 MCI patients with high vs. those 12 with low medial temporal lobe atrophy (MTA) scores (p=0.001 uncorrected, extent threshold=100 voxels). Age and white matter hyperintensity scores were included as nuisance covariates. MCI with high MTA showed large hypoperfusion in the left hippocampus and in the left parahippocampal gyrus. Figure (A) shows the main significant cluster, located in the tail of the hippocampus (stereotactic coordinates -30, -46, 2), and figure (B) shows the cluster located in the head of the hippocampus (-26, -18, -20).

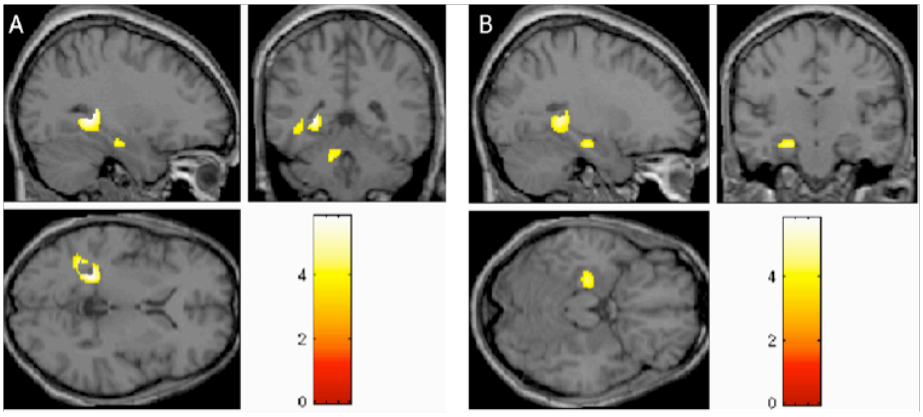

We found no clusters of relative hyperperfusion. Using the more restrictive threshold of 0.05 corrected, the cluster located in the tail of the left hippocampus showed a trend to significance (corrected P-value=0.077, peak coordinates: -30 -46 2), while all the others were not significant.

Hypoperfusion in MCI patients with high WMHs, as compared with those with low WMHs at a significance threshold of P<0.001 uncorrected, involved the left insular and superior temporal regions (table 2 and figure 2).

Figure 2: Areas of grey matter hypoperfusion in 15 MCI patients with high vs. those 15 with low white matter hyperintensities (WMHs) scores (p=0.001 uncorrected, extent threshold=100 voxels). Age and medial temporal lobe atrophy scores were included as nuisance covariates. MCI with high WMHs showed a hypoperfusion cluster in the left insular region and superior temporal gyrus (stereotactic coordinates -44, 20, -18).

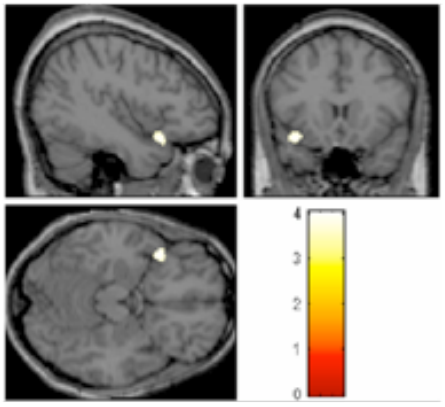

We found no clusters of relative hyperperfusion. Using the more restrictive threshold of

P<0.05 corrected, we had no suprathreshold clusters.

Setting the significance threshold at P<0.001 uncorrected, we found only a small significant cluster of GM atrophy in MCI with high MTA vs. low MTA, located in the medial temporal lobe. Setting the threshold at a less restrictive P-value (P<0.05 uncorrected) we found significant clusters of atrophy in the medial temporal lobe and in the hippocampus. Comparing significant hypoperfusion (P<0.001) with significant atrophy (P<0.05) on a voxel-by-voxel basis, we found just a few overlapping voxels. Explanatory figures are available at http://www.centroalzheimer.it/public/GM_atrophy_JoN.doc.

Discussion

Our findings suggest that MTA in MCI is associated with hippocampal and medial temporal grey matter hypoperfusion while WMHs are associated with grey matter hypoperfusion in areas of the left insula and temporal neocortex.

Hippocampal atrophy is currently one of the most sensitive markers to discriminate patients with AD from controls and to predict development of AD in patients with MCI. Previous studies in AD found a significant correlation between hippocampal atrophy and both decreased glucose metabolism [32,33] and brain perfusion [9]. Our findings are in line with previous results, and seem to show that not only in AD but also in MCI there is a significant correlation between biological severity of the disease (assessed by MTA rating) and hippocampal hypoperfusion. Furthermore, these findings have an effect of validity on the non-standard method of postprocessing SPECT analysis proposed herein.

As hippocampal hypoperfusion could be an artifact associated with grey matter atrophy in the medial temporal lobe, we checked partial volume effects in the regions of decreased perfusion. We assessed grey matter atrophy in MCI with high MTA vs. low MTA with SPM2, using an optimized Voxel-Based Morphometry protocol described in detail elsewhere [30,31]. As expected, we found significant clusters of atrophy in the medial temporal lobe and in the hippocampus (P=0.05 uncorrected). Notably, just a few voxels of significant atrophy was overlapping with the voxels of significant hypoperfusion, in line with previous results [34].

It is well-known that in AD functional alterations antedate structural changes [8]. SPECT imaging in MCI enables to visualize the dysfunction that characterizes the

earliest stage of the disease and provides pathophysiological information which cannot yet be detected by structural imaging. It can enable early diagnosis even before clinical or structural evidence, and it can suggest an early therapeutical intervention, more likely to be effective than at more progressed stages of the disease.

We found that MTA was also associated with reduced perfusion in the cerebellum. Even though the cerebellum has often been considered one of the most spared brain regions in AD, there are both neuropathological and functional studies suggesting cerebellar involvement in AD, even at early stages. Sjobeck and colleagues found that the main structural cerebellar changes in AD patients, as compared with healthy age-matched controls, were neuronal loss, atrophy and gliosis, which might be reflected in some of the symptoms and signs seen in AD that are generally overlooked or judged to be of noncerebellar origin [35]. A functional study in AD by Newberg and colleagues showed significant correlations between glucose metabolic deficits in the cerebellum and neuropsychological function (MMSE, memory and clock drawing) [36]. Alternatively, the findings of cerebellar hypoperfusion in relation to high MTA could be due to a completely different etiology such as hypoxia, which selectively affects CA1 and Purkinje cell neurons.

Comparing MCI patients with low and high WMHs, we found that WMHs were associated with reduced grey matter perfusion in MCI in restricted areas of the insular and temporal neocortex. These results might be the functional analogue of the structural findings of a previous study on an independent group of healthy subjects [21], where Rossi and colleagues found an association between WMHs and GM atrophy in the insular cortex. It should be underlined that the distribution of WMHs in our MCI population is in agreement with current knowledge that frontal and parieto-occipital regions are the most common sites of WMHs [37-39]: 89% of patients with WMHs showed frontal, and 70% parieto-occipital lesions; we found no WMHs in the temporal and infratentorial areas.

A possible explanation for the involvement of the insular region is that it has efferent and afferent connections with many areas of the brain (frontal, parietal, and temporal cortex, limbic areas) [40]. The frontal operculum, lateral and posterior orbital cortex, the orbitofrontal cortex, and the prefrontal cortex have reciprocal connections with the insular lobe [41]. The insula is also connected with the cortex in the parietal lobe with efferent and afferent fibers to and arising from cortex adjoining the somatosensory

area, anterior inferior parietal cortex and the parietal operculum [41]. Insular efferents reach the cortex of the temporal lobe including the temporal pole and the supratemporal plane [41]. Fibers destined for the insular lobe arise from the temporal pole, auditory cortex, superior temporal cortex and temporal operculum [41]. The insula is also connected with limbic areas. In particular, the insula sends fibers to the amygdala, to the anterior hippocampus, to the anterior enthorinal cortex and to the piriform cortex [40].

The findings of reduced grey matter perfusion in the superior temporal lobe in relation to high WMH is in agreement with a study by Yang et al of patients with subcortical vascular dementia. The authors found significant hypoperfusion in the bilateral superior temporal gyri in patients compared to normal controls, and showed that only the deep white matter hyperintensity was associated with a cerebral blood flow reduction in the left superior temporal gyrus [42].

The most relevant technical issue deserving discussion regards the normalization of cerebral perfusion. In view of the variability of tracer uptake, measured brain activity counts (i.e. raw data values) cannot be used directly for quantification of SPECT images, and must be scaled to a reference region. The best reference region to be used for scaling is still a controversial issue, the most used being the wholebrain [43-45] and the cerebellum [25,46-48]. Scaling to wholebrain, which is the method at the base of SPM2 proportional scaling, all brain counts are divided by the overall mean perfusion. This method is preferred when dealing with a diagnostically heterogeneous group of subjects or whenever the hypoperfusion pattern is unknown (hypoperfusion areas involved in the disease are included in the average, but the effect is minimized as the average is computed on a wide area). On the other hand, when scaling to cerebellum all brain counts are divided by the mean perfusion computed on the cerebellum only. This method is preferred when dealing with pathologies where the cerebellum is known to be spared. As the patients of the present study are affected by MCI, which comprises heterogeneous diseases, we chose to scale raw data values to the wholebrain, using SPM2 proportional scaling (mean global activity of each scan was adjusted to a grand mean of 50mL/100mL/min).

We believe that one of the strengths of this study lies in the accurate control of potential confounders. One of the most relevant correlates of brain perfusion is age [29,45]. Our groups with high MTA and high WMH scores were age-matched to peers

with low scores, so there is no reason to hypothesize an effect of age in one group but not in the other. Moreover, voxel-based comparisons were carried out correcting for age in order to exclude the effect of the small residual difference of age between groups. WMH score was used as further nuisance covariate in the comparison between high and low MTA in order to remove the effect of hypoperfusion due to WMHs and viceversa. Spatial normalisation was improved by using a study-specific SPECT template derived using deformations from companion MR images.

Some limitations should also be considered in the interpretation of the results.

We assessed both MTA and WMHs by visual rating. Although the visual rating scale of MTA has shown good agreement with hippocampal volume assessment [23], and the rating scale for age-related white matter changes has shown a good sensitivity in the detection of WMHs [20] and a good correlation with WMH volume [49], more sensitive volumetric measurements made with advanced quantitative tools could be useful to confirm the present findings. The influence of MTA and WMHs on cerebral perfusion was assessed using relatively small groups. Larger groups of patients would be needed to confirm our results. We showed that both the neuropathological damage of AD in the medial temporal lobe and small vessel damage in the white matter led to reduced cerebral perfusion. It needs to be stressed that although perfusion deficits might underlie cognitive impairment, this is not necessarily the case. In order to test whether perfusion defects indeed have an effect on cognitive performance, one should investigate the correlation between the presence of hypoperfusion and the progression of cognitive impairment. Lastly, MCI theoretically includes neurodegenerative diseases featuring little hippocampal atrophy, such as Lewy Body Dementia and FrontoTemporal Dementia. However, the low prevalence of these conditions makes significant contamination of our study group unlikely.

In conclusion, our results confirm that a strong structural damage such as MTA is associated with relevant local functional changes and suggest that WMHs may be associated with remote cortical brain dysfunction.

References

1. Petersen RC, Smith GE, Waring SC, Ivnik RJ, Tangalos EG, Kokmen E. Mild cognitive impairment: clinical characterization and outcome. Arch Neurol 1999; 56:303-308.
2. Morris JC, Storandt M, Miller JP, et al. Mild cognitive impairment represents early-stage Alzheimer disease. Arch Neurol 2001; 58:397–405.
3. Petersen RC, Doody R, Kurz A, et al. Current concepts in mild cognitive impairment. Arch Neurol 2001; 58:1985–1992.
4. Jack CR Jr, Petersen RC, Xu YC, et al. Prediction of AD with MRI-based hippocampal volume in mild cognitive impairment. Neurology 1999; 52:1397-1403.
5. De Carli C, Miller BL, Swan GE, Reed T, Wolf PA, Carmeli D. Cerebrovascular and brain morphologic correlates of mild cognitive impairment in the National Heart, Lung, and Blood Institute Twin Study. Arch Neurol 2001; 58:643-647.
6. De Groot K, Schmidt DK, Arlt AC, Gross WL, ReinHold-Keller E. Standardized neurologic evaluations of 128 patients with Wegener granulomatosis. Arch Neurol 2001; 58:1215-1221.
7. Okamura N, Arai H, Maruyama M, et al. Combined analysis of CSF Tau levels and [123I]Iodoamphetamine SPECT in mild cognitive impairment: implications for a novel predictor of Alzheimer's disease. Am J Psychiatry 2002; 159:474-476.
8. Small AS. Alzheimer disease, in living color. Nat Neurosci 2005; 8:404-405.
9. Garrido GE, Furuie SS, Buchpiguel CA, et al. Relation between medial temporal atrophy and functional brain activity during memory processing in Alzheimer's disease: a combined MRI and SPECT study. J Neurol Neurosurg Psychiatry 2002; 73:508-516.
10. Waldemar G, Christiansen P, Larsson HB, et al. White matter magnetic resonance hyperintensities in dementia of the Alzheimer type: morphological and regional cerebral blood flow correlates. J Neurol Neurosurg Psychiatry 1994; 57:1458-1465.
11. Ott BR, Faberman RS, Noto RB, et al. A SPECT imaging study of MRI white matter hyperintensity in patients with degenerative dementia. Dement Geriatr Cogn Disord 1997; 8:348-354.
12. Ebmeier KP, Prentice N, Ryman A, et al. Temporal lobe abnormalities in dementia and depression: a study using high resolution single photon emission tomography and magnetic resonance imaging. J Neurol Neurosurg Psychiatry 1997; 63:597-604.
13. Shulman KI. Clock-drawing: is it the ideal cognitive screening test? Int J Geriatr Psychiatry 2000; 15:548-561.
14. Giovagnoli AR, Del Pesce M, Mascheroni S, Simoncelli M, Laiacona M, Capitani E. Trail making test: normative values from 287 normal adult controls. Ital J Neurol Sci 1996; 17:305-309.
15. Basso A, Capitani E, Laiacona M. Raven's coloured progressive matrices: normative values on 305 adult normal controls. Funct Neurol 1987; 2:189-194.
16. Spinnler H, Tognoni G. Standardizzazione e taratura italiana di test neurologici. Ital J Neurol Sci 1987; 8:47-50.
17. Novelli G, Papagno C, Capitani E, Laiacona M, Cappa SF, Vallar G. Tre test clinici di ricerca e produzione lessicale. Taratura su soggetti normali. Arch Psicol Neurol Psichiatr 1986; 47:477-506.

18. Caffarra P, Vezzadini G, Dieci F, Zonato F, Venneri A. Rey-Osterrieth complex figure: normative values in an Italian population sample. Neurol Sci 2002; 22:443-447.
19. Radloff LS. The CES-D scale: A self-report depression scale for research in the general population. Applied Psychological Measurement 1977; 1:385-401.
20. Wahlund LO, Barkhof F, Fazekas F, et al.; European Task Force on Age-Related White Matter Changes. A new rating scale for age-related white matter changes applicable to MRI and CT. Stroke 2001; 32:1318-1322.
21. Rossi R, Boccardi M, Sabattoli F, et al. Topographic correspondence between white matter hyperintensities and brain atrophy. J Neurol 2006; 253:919-927.
22. Scheltens P, Leys D, Barkhof F, et al. Atrophy of medial temporal lobes on MRI in "probable" Alzheimer's disease and normal ageing: diagnostic value and neuropsychological correlates. J Neurol Neurosurg Psychiatry 1992; 55:967-972.
23. Bresciani L, Rossi R, Testa C, et al. Visual assessment of medial temporal atrophy on MR films in Alzheimer's disease: comparison with volumetry. Aging Clin Exp Res 2005; 17:8-13.
24. Chang LT. A method for attenuation correction in radionuclide computed tomography. IEEE Trans Nucl Sci 1978; 25:638–643.
25. Firbank MJ, Colloby SJ, Burn DJ, McKeith IG, O'Brien JT. Regional cerebral blood flow in Parkinson's disease with and without dementia. Neuroimage 2003; 20:1309-1319.
26. SPM, Statistical Parametric Mapping, version 2 (2002). London: Functional Imaging Laboratory. Available at: http://www.fil.ion.ucl.ac.uk/spm/software/spm2
27. Rorden C, Brett M. Stereotaxic display of brain lesions. Behavioural Neurology 2000; 12:191-200.
28. Barnden LR, Behin-Ain S. Data Based Optimization of Brain SPECT Processing for Voxel-based Statistical Analysis. NSS–MIC Conference Record 2004.
29. Barnden LR, Behin-Ain S, Kwiatek R, Casse R, Yelland L. Age related preservation and loss in optimized brain SPECT. Nucl Med Commun 2005; 26:497-503.
30. Frisoni GB, Testa C, Sabattoli F, Beltramello A, Soininen H, Laakso MP. Structural correlates of early and late onset Alzheimer's disease: voxel based morphometric study. J Neurol Neurosurg Psychiatry 2005; 76:112-114.
31. Filippini N, Scassellati C, Boccardi M, et al. Influence of serotonin receptor 2A His452Tyr polymorphism on brain temporal structures: a volumetric MR study. Eur J Hum Genet 2006; 14:443-449.
32. Yamaguchi S, Meguro K, Itoh M, et al. Decreased cortical glucose metabolism correlates with hippocampal atrophy in Alzheimer's disease as shown by MRI and PET. J Neurol Neurosurg Psychiatry 1997; 62:596-600.
33. Mosconi L, Tsui WH, De Santi S, et al. Reduced hippocampal metabolism in MCI and AD: automated FDG-PET image analysis. Neurology 2005; 64:1860-1867.
34. Matsuda H, Kitayama N, Ohnishi T, et al. Longitudinal evaluation of both morphological and functional changes in the same individuals with Alzheimer's disease. J Nucl Med 2002; 43:304-311.
35. Sjobeck M, Englund E. Alzheimer's disease and the cerebellum: a morphological study on neuronal and glial changes. Dement Geriatr Cogn Disord 2001; 12:211-218.

36. Newberg A, Cotter A, Udeshi M, et al. Brain metabolism in the cerebellum and visual cortex correlates with neuropsychological testing in patients with Alzheimer's disease. Nucl Med Commun 2003; 24:785-790.
37. Gootjes L, Teipel SJ, Zebuhr Y, et al. Regional Distribution of White Matter Hyperintensities in Vascular Dementia, Alzheimer's Disease and Healthy Aging. Dement Geriatr Cogn Disord 2004; 18:180-188.
38. Tullberg M, Fletcher E, DeCarli C, et al. White matter lesions impair frontal lobe function regardless of their location. Neurology 2004; 63:246-253.
39. Wen W, Sachdev P, Shnier R, Brodaty H. Effect of white matter hyperintensities on cortical cerebral blood volume using perfusion MRI. Neuroimage 2004; 21:1350-1356.
40. Augustine JR. Circuitry and functional aspects of the insular lobe in primates including humans. Brain Res Brain Res Rev 1996; 22:229-244.
41. Augustine JR. The insular lobe in primates including humans. Neurol Res 1985; 7:2-10.
42. Yang DW, Kim BS, Park JK, Kim SY, Kim EN, Sohn HS. Analysis of cerebral blood flow of subcortical vascular dementia with single photon emission computed tomography: adaptation of statistical parametric mapping. J Neurol Sci 2002; 203-204:199-205.
43. Benoit M, Koulibaly PM, Migneco O, Darcourt J, Pringuey DJ, Robert DH. Brain perfusion in Alzheimer's disease with and without apathy: a SPECT study with statistical parametric mapping analysis. Psychiatry Res 2002; 114:103-111.
44. Kogure D, Matsuda H, Ohnishi T, et al. Longitudinal evaluation of early Alzheimer's disease using brain perfusion SPECT. J Nucl Med 2000; 41:1155-1162.
45. Van Laere K, Versijpt J, Audenaert K, et al. 99mTc-ECD brain perfusion SPET: variability, asymmetry and effects of age and gender in healthy adults. Eur J Nucl Med 2001; 28:873-887.
46. Kemp PM, Holmes C, Hoffmann SM, et al. Alzheimer's disease: differences in technetium-99m HMPAO SPECT scan findings between early onset and late onset dementia. J Neurol Neurosurg Psychiatry 2003; 74:715-719.
47. Soonawala D, Amin T, Ebmeier KP, et al. Statistical parametric mapping of (99m)Tc-HMPAO-SPECT images for the diagnosis of Alzheimer's disease: normalizing to cerebellar tracer uptake. Neuroimage 2002; 17:1193-1202.
48. Lee YC, Liu RS, Liao YC, et al. Statistical parametric mapping of brain SPECT perfusion abnormalities in patients with Alzheimer's disease. Eur Neurol 2003; 49:142-145.
49. Kapeller P, Barber R, Vermeulen RJ, et al; European Task Force of Age Related White Matter Changes. Visual rating of age-related white matter changes on magnetic resonance imaging: scale comparison, interrater agreement, and correlations with quantitative measurements. Stroke 2003; 34:441-445.

Chapter 5

In vivo mapping of amyloid toxicity in Alzheimer's disease

Frisoni GB, Lorenzi M, Caroli A, Kemppainen N, Någren K, Rinne JO

Neurology 2009; 72:1504-1511

Abstract

Objective. To study the relationship between grey matter atrophy and amyloid deposition in Alzheimer's disease. Methods. Volumetric MR and [11C]-PIB-PET were acquired of 23 AD patients and 17 healthy older persons. Standardized [11C]-PIB uptake values were coregistered to MR scans in a standard space. Decreased density of and increased [11C]-PIB uptake in the grey matter of AD patients versus controls were assessed with both voxel-based ($p<.05$ corrected) and region-of-interest (ROI) analyses. The relationship between decreased density of and increased [11C]-PIB uptake in the grey matter was investigated with voxel-based Pearson's r maps (thresholded at $p<.05$) and ROI linear regression plots. Results. Atrophy mapped to a restricted region corresponding to the hippocampus while increased [11C]-PIB uptake to large frontal, parietal, and posterior cingulate cortical areas. ROI analysis showed the largest effect size for atrophy in hippocampus (2.01) and amygdala (1.27) and the highest effect size for [11C]-PIB uptake in frontal (2.66), posterior cingulate/retrosplenial (2.43), insular (2.41), and temporal (2.23) regions. In the hippocampus, [11C]-PIB uptake was significantly increased, but effect size was milder (1.72). Significant correlations between atrophy and increased [11C]-PIB uptake were found in the hippocampal ($r =-.54$) and amygdalar ROIs ($r =-.40$) but not in the frontal, temporal, posterior cingulate/retrosplenial, insular, and caudate ROIs (r between .04 and .25). Conclusion. The medial temporal lobe might be highly susceptible to amyloid toxicity while neocortical areas might be more resilient.

Introduction

The relationship between brain atrophy and amyloid deposition in Alzheimer's disease has implications on current clinical trials with antiamyloid drugs. Atrophy is a valid disease marker in AD and brain atrophy is currently a widely used surrogate outcome in current phase III clinical trials of drugs that might delay or arrest AD progression [1]. Most current disease-modifying drugs for AD have been developed under the assumption that cognitive deterioration is due to amyloid deposition and that slowing or arresting amyloid deposition will lead to slowing or arresting cognitive deterioration [2].

The recent availability of in vivo PET ligands for amyloid such as [11C]-PIB, i.e. 2-[4´-(methylamino)phenyl]-6-hydroxybenzothiazole, has led to the possibility of studying the relationship between brain atrophy and amyloid deposition directly and in vivo, the prediction being that regions with greater atrophy would also be those with greater amyloid deposition. This has been found not to be the case, as the first AD patients scanned with [11C]-PIB showed the largest amount of uptake in the frontal cortex [3], an area where the disease is believed to strike relatively later in the course, and, as consequently, atrophy is believed to appear relatively late. A later study investigating the relationship of prospective percentage tissue loss with tracer uptake seemed to somehow reconcile the contrasting findings in that faster tissue loss before amyloid imaging was reportedly associated with greater amyloid burden [4]. Recently, the toxicity of brain amyloid deposition was again questioned by showing that faster rates of tissue loss were not correlated with pathologically confirmed greater amyloid burden but rather with more severe Braak neurofibrillary tangle stage [5].

The aim of the present study is to assess the relationship between grey matter atrophy and amyloid deposition in AD by mapping the match and mismatch of the two phenomena. MR-based structural images were collected at the time of [11C]-PIB-PET images in 23 patients and 17 controls, coregistered, and studied with voxel-based methods.

Methods.

Subjects

The [11C]-PIB uptake results of the majority of the subjects of this study have been previously described [6]. Patients (Table 1) were diagnosed with probable AD

according to NINCDS-ADRDA criteria, had progressive disease with impairment of memory and at least one additional cognitive domain, and were assessed using a comprehensive neuropsychological test battery that included CERAD, Wechsler Memory Scale–Revised, parts of WAIS–Revised, Trail Making Test, Stroop, ADAS-Cog, clock drawing, Rey's figure copy, digit span forward, Boston Naming Test, and word fluency. The tests showed typical impairment in memory functions and in at least one separate cognitive function compared with age-appropriate norms and estimated premorbid levels (data not shown).

Seventeen healthy volunteers with no history of neurologic or psychiatric disease, with no medications affecting the central nervous system, and with normal brain MR scans were studied as a control group. The study was approved by the Ethical Committee of Southwest Finland Health Care District and both patients and healthy volunteers gave informed consent to perform the study.

Table 1: Socio-demographic and cognitive features of the study groups.

	AD **n = 23**	**Controls** **n = 17**	**p value**
Age, years	72.0 (7.5)	65.1 (7.6)	0.24
Sex, n (%) of females	12 (53%)	13 (76%)	0.002
Mini Mental State Exam	23.4 (2.9)	28.4 (1.3)	<0.001
[range]	[16 to 27]	[26 to 30]	
Disease duration, years	2.4 (1.6)	---	---
Cholinesterase inhibitors	16 (70%)	---	---
Memantine	2 (9%)	---	---

Values denote mean (SD) or n (percentage). P values are based on t or $\chi 2$ tests.

Image acquisition

[11C]-PIB-PET scanning protocol. Radiochemistry details have been previously provided [6]. All subjects underwent a 90-minute dynamic PET scan with a GE Advance PET scanner (GE Medical Systems, Milwaukee, WI) in the three-dimensional scanning mode (septa retracted) providing 35 slices of 4.25-mm thickness covering the whole brain. The spatial resolution (full width at half maximum) of the camera is 4.3 mm transaxially and 4.3 mm axially. Laser light beams were used in head positioning

according to the orbitomeatal and sagittal lines. Before the injection of the radiotracer, an 8-minute transmission scan with 68Ge rod sources was done for attenuation correction. [11C]-PIB was then injected into an antecubital vein as a bolus with a mean dose of 414 MBq (SD 103) and flushed with saline. The frame sequence of the scan consisted of four 30-second frames, nine 1-minute frames, three 3-minute frames, ten 5-minute frames, and two 10-minute frames. No blood sampling was performed during the scan. Imaging data were reconstructed into a 128 x 128 matrix using a transaxial Hann filter with a 4.6-mm cut-off and an axial ramp filter with an 8.5-mm cut-off.

MR imaging acquisition protocol. At the time of PET scanning, all subjects also underwent magnetic resonance imaging scan with a Philips Gyroscan Intera 1.5-T CV Nova Dual scanner (Philips Medical Systems, Best, the Netherlands). This included axial T2-weighted spin-echo images, coronal fluid-attenuated inversion recovery images, and axial T1-weighted 3D (repetition time 25 msec, echo time 5 msec, slice thickness 1 mm) with a 512x512 or 256x256 matrix and 1 excitation.

Image processing

PIB voxel-based imaging. We flipped parametric [11C]-PIB images to neurological convention using MRIcro software [7] (MRIcro; http://www.sph.sc.edu/comd/rorden/mricro.html), and we resampled voxel size to 2x2x2 with SPM2 (Statistical Parametric Mapping, version 2; http://www.fil.ion.ucl.ac.uk/spm/software/spm2). We coregistered [11C]-PIB to the pertinent MR images after BET [8] scalp removal. We then created a [11C]-PIB customized template through: (i) coregistration and affine normalization of the [11C]-PIB images to the respective MR images; (ii) linear plus non linear spatial normalization of images from i) using parameters determined from the normalization of MR images to the MR template; (iii) creation of the mean image from ii) and averaging with its mirror copy to ensure the symmetry. We processed all coregistered [11C]-PIB scans with SPM2 according to an optimized processing protocol previously developed and validated for SPECT and FDG-PET images, and described in detail elsewhere [9].

MR voxel-based imaging. Due to differences in acquisition matrix size (either 512x512 or 256x256), we first resampled all MR images to 256x256 size using a specific tool developed at the Montreal Neurological Institute (MNI) (mincresample; http://www.bic.mni.mcgill.ca/software). We then scaled all images to the same

intensity range ([0,100]), flipped them in neurological convention using MRIcro, and processed them with SPM2 following a standard Voxel Based Morphometry procedure described in detail elsewhere [10,11].

We computed a customized template and customized prior probability maps for grey matter (GM), white matter and cerebrospinal fluid from the whole sample [12]. MR images were then normalized to the customized template through affine and nonlinear transformations, were segmented into GM, white matter and cerebrospinal fluid using the customized priors masked to remove non-brain tissue voxels, were modulated, and finally smoothed with a 12 mm isotropic Gaussian kernel [10,11]. Only GM images were further used in the statistical analysis.

Region-of-interest (ROI) analyses. We chose several ROIs relevant to AD, located in the frontal and temporal lobes, posterior cingulate/retrosplenial region, insula, caudate, and amygdala, from the Wake Forest University (WFU) Pickatlas, available as a SPM2 toolbox [13]. As these regions relate to the SPM2 MNI_T1 template, we normalized the latter to our customized template, and we applied the transformation parameters to all ROIs in order to make these suitable to our maps. The hippocampal mask was defined according to a procedure derived by Mosconi and colleagues [14]. All ROIs used in this study are available at www.centroalzheimer.it/public/ROIs_paper.doc.

Statistical Analysis

Group difference analysis. We used "single subject: conditions and covariates" SPM2 model to assess, on a voxel-by-voxel basis, where [11C]-PIB uptake in AD is greater than in normal controls. Statistical comparison was performed setting the one tailed significance threshold at .05 corrected for FWE. We also tested also the opposite comparison, but with no significant finding.

We then used the same "single subject: conditions and covariates" SPM2 model on segmented GM images to assess whether grey matter density in normal controls is greater than in AD patients. Total intracranial volume was entered as a confounding variable.

Again, the opposite comparison was also tested with no significant finding.

Correlation analysis. Two different approaches were used to investigate the correlation between atrophy and PIB uptake. Since native [11C]-PIB scans were coregistered to their respective MR images, and the study-specific [11C]-PIB template

was coregistered to the high-definition MR template, all the normalised [11C]-PIB and MR images used for the statistical analysis were coregistered to the SPM standard anatomical space, so that [11C]-PIB uptake and atrophy patterns could be compared on a voxel-by-voxel basis.

Pearson's r coefficient was computed voxel-wise, and a whole brain correlation map was created, using a Matlab script written specifically for this purpose. Linear relationship between variables was assumed, and intensity normal distribution was checked on ROI mean values. Voxel-by-voxel significance of Pearson's r correlation map was computed using Matlab and significance threshold was set at $p<.001$ uncorrected.

We computed mean GM intensities and PIB uptake region-to-cerebellar ratio values within each ROI for all AD patients and normal controls, and we then compared these values between the two groups through a t-test. We finally investigated the correlation between atrophy and PIB uptake and the related significance in each ROI using the SPSS software (SPSS version 12; SPSS Inc, Chicago, Ill).

Results.

The voxel-based analyses show that significant grey matter atrophy was confined to the medial temporal lobe while increased [11C]-PIB uptake was widespread to frontal, temporal, parietal, and posterior cingulate cortical areas (Figure 1). The failure to detect atrophy in the temporoparietal junction and the posterior cingulate cortex should be interpreted in view of the restrictive significance criterion used in both comparisons ($p<.05$ corrected for FWE). Indeed, when the threshold was set at the lower threshold of $p<.001$ uncorrected, significant atrophy emerged also in the temporal, posterior cingulate/retrosplenial, insular, and parietal cortical regions. A figure showing grey matter atrophy at the two thresholds is available on www.centroalzheimer.it/public/AD_Ctrls_GM_comparison.png.

A ROI-based analysis confirmed that the grey matter density of AD patients was not significantly different from controls in all but the medial temporal (hippocampal and amygdalar) ROIs (Table 2), while [11C]-PIB uptake was significantly increased in all areas, with different effect sizes ranging between 1.51 in the caudate ROIs and 2.66 in the frontal ROIs (Table 2). Effect size was highest in the frontal and lowest in the caudate and hippocampal ROIs.

Table 2: Effect size of the difference of signal intensity (arbitrary units) of grey matter density and PIB uptake in 23 AD patients and 17 controls.

	AD mean (SD)	Controls mean (SD)	p value	effect size
Grey matter density				
Frontal	.211 (.027)	.216 (.018)	0.52	0.21
Temporal	.144 (.144)	.147 (.147)	0.59	0.17
Posterior cingulate/retrosplenial	.233 (.036)	.243 (.021)	0.29	0.34
Insula	.269 (.020)	.284 (.032)	0.09	0.54
Caudate	.183 (.028)	.193 (.021)	0.21	0.4
Amygdala	.350 (.045)	.401 (.033)	<.001	1.27
Hippocampus	.340 (.040)	.414 (.033)	<.001	2.01
PiB uptake				
Frontal	1.569 (.297)	.996 (.063)	<.001	2.66
Temporal	1.142 (.199)	.819(.045)	<.001	2.23
Posterior cingulate/retrosplenial	1.653 (.358)	1.028 (.057)	<.001	2.43
Insula	1.607 (.297)	1.094 (.044)	<.001	2.41
Caudate	1.166 (.261)	.871 (.089)	<.001	1.51
Amygdala	1.361 (.220)	1.080 (.033)	<.001	1.67
Hippocampus	1.307 (.187)	1.068 (.055)	<.001	1.72

Signal intensities are averaged between right and left ROIs.
Effect size is computed as: Cohen's d: (Mean1-Mean2)/sqrt((SD12+SD22)/2)).

Figure 2 shows that the areas with significant lower grey matter density corresponding to greater [11C]-PIB uptake were located in the medial temporal regions, a few small scattered spots being present also in neocortical areas. These included the lateral temporal, parietal, posterior cingulate, and frontal cortex. Figure 3 shows the same effect at the ROI level: despite [11C]-PIB uptake in the hippocampus is lower (between 1.0 and 1.6) than in most other regions of the brain (up to 2.25 in the posterior cingulate/retrosplenial cortex), here the reduction in grey matter density ties in with the amount of [11C]-PIB uptake ($r=-.54$, $p<.001$). In the other areas this result is significant only in the amygdala ($r=-.40$), while it is not significant in the frontal, temporal, posterior cingulate/retrosplenial, insular, and caudate ROIs.

Figure 1: Topography of (a) significant grey matter loss and [11C]-PiB uptake in the grey matter of 23 AD patients compared to 17 normal controls. Grey matter loss is confined to amygdala and hippocampus while (b) increased [11C]-PiB uptake involves widespread areas in the frontal, parietal, temporal, and posterior cingulate cortices. To study the grey matter only, t-maps of both atrophy and low [11C]-PiB uptake were masked with the same customized binary grey matter mask, obtained by thresholding at .1 the 5 mm full width at half maximum (FWHM) smoothed grey matter map of the normal control with the highest quality MR scan. The color bars denote Student's t with 37 (a) and 38 (b) degrees of freedom (significance threshold set at p<.05 corrected for family-wise error).

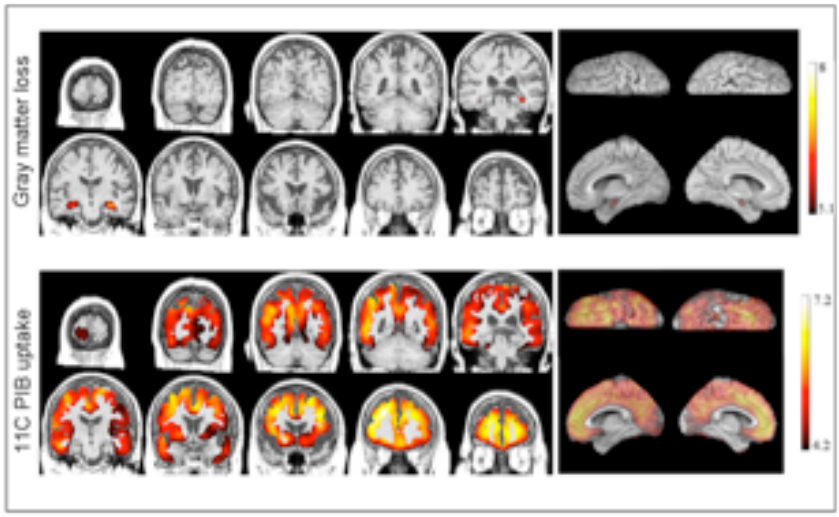

Figure 2: Pearson's correlation between grey matter and [11C]-PIB uptake in 23 AD patients and 17 normal controls and associated significance map. Correlation is highest and most significant in the medial temporal region region and few scattered spots in the neocortex including the posterior cingulate cortex. The color bars denote Pearson's r and Student's t with 32 degrees of freedom (significance threshold set at p<.001 uncorrected).

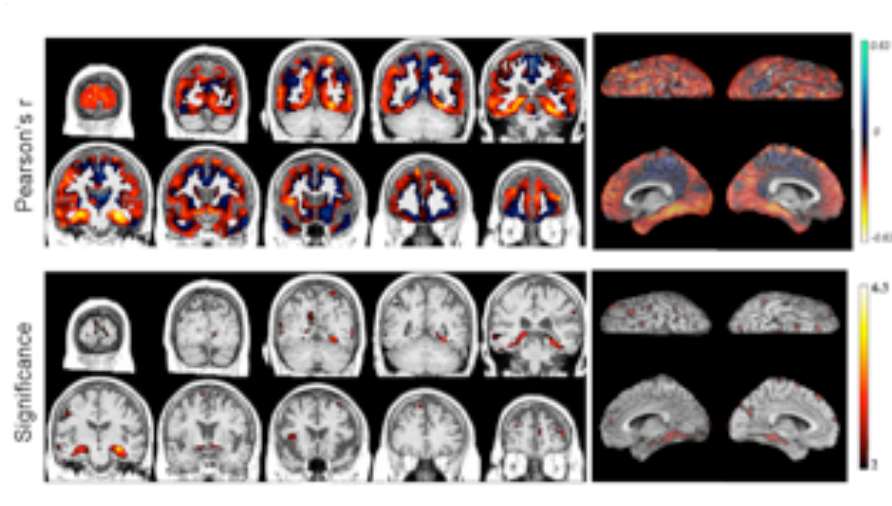

The point estimate of the slope of the relationship between hippocampal grey matter density and [11C]-PIB uptake is significantly different from zero (B=-.15, 95% Confidence Interval -.23 to -.07; Figure 3, Hippocampus). When the relationship was assessed in the smaller group of AD patients alone, the point estimate of the slope was still negative although not significantly different from zero (B=-.05, 95% Confidence Interval -.14 to .05).

Figure 3: Relationship between grey matter density and [11C]-PIB uptake in the grey matter. Lower grey matter density is associated with greater [11C]-PIB uptake only in the hippocampus. Full circles denote AD and open circles healthy controls.

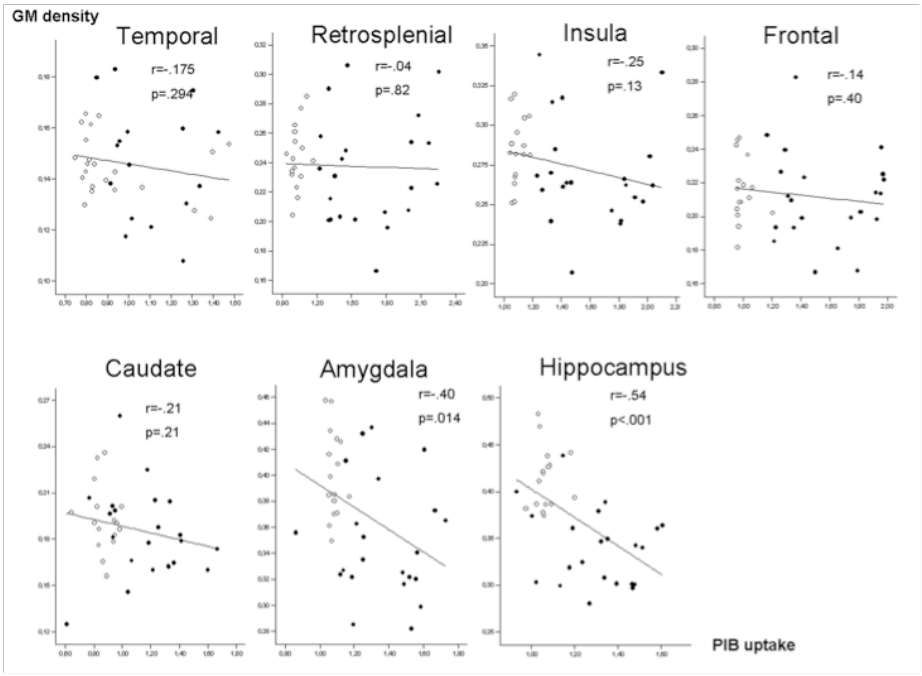

Discussion.

In this study we have studied in vivo the local toxicity on the grey matter of amyloid deposition, toxicity being indexed by atrophy on MR imaging and amyloid deposition by [11C]-PIB uptake on PET. We have found that greater amyloid deposition was generally not associated with more severe grey matter atrophy except in the medial temporal lobes (amygdalae and hippocampi), where greater amyloid deposition was associated with lower grey matter density. The medial temporal lobe was among the

regions with the lowest amount of amyloid deposition, indicating that different types of amyloid may deposit in the brain, different brain regions may be differentially susceptible to its toxic effects, or that amyloid is peripheral to neurodegeneration.

The relative amount and topography of [11C]-PIB uptake that we found in the present study as well as the topography of brain atrophy are consistent with available literature. [11C]-PIB uptake is highest in the frontal lobe and milder in the medial temporal lobe [15] possibly due to greater deposition of tangles relative to amyloid [16,17]. In late onset AD brain atrophy is more severe in the medial temporal and posterior cingulate/retrosplenial region and relatively milder in neocortical frontal, temporal, parietal, and occipital regions [18,19]. A recent study has found that atrophy and [11C]-PIB uptake independently contribute to discriminating has AD, amnestic MCI patients, and healthy elders [20]. Although these results are in agreement with those of the present study, the topographic relationship of the two phenomena was not explicitly addressed, which we did in the present study.

The local association of amyloid load and atrophy in the medial temporal lobe is in agreement with pathological data indicating that amyloid load in the medial temporal lobe correlates with cognitive performance. Although the largest body of literature indicates that the strongest correlates of cognitive impairment are neuronal counts and neurofibrillary tangles in the medial temporal lobe and neocortex [21], accurate estimates of amyloid burden have shown that the assessment of the total volume occupied by the amyloid deposits in the entorhinal cortex and subiculum can be considered an effective predictor of dementia severity [22]. Others, however, claim that the effect of fibrillar amyloid deposits on cognition is indirect as it disappears when adjusting for total tangle numbers in this area [23], which we could not control for in the present study. Findings of a post mortem study that a decrease in spinophilin-immunoreactivity (a marker of synaptic integrity) was significantly related to both Braak neurofibrillary tangle staging and clinical severity but not amyloid deposition staging is in agreement with the dissociation found between neuronal loss (atrophy) and amyloid load ([11C]-PIB uptake) in our study [24]. At least two hypotheses can be proposed to explain the topographic mismatch between [11C]-PIB uptake and atrophy.

The hypothesis of differential susceptibility to amyloid is supported by findings of a pathological study of 17 subjects in the severe stage of AD where numerical densities

of neurons with neurofibrillary tangles correlated with the densities of thioflavin-S-positive fibrillar plaques with neurofibrillary changes, indicating that neurofibrillary pathology in neocortical plaques reflects the topography of neurofibrillary changes in neocortical neurons [25]. In line with in vitro evidence that tau is essential to beta amyloid-induced neurotoxicity [26], the authors conclude that fibrillar beta amyloid affects neurofibrillary changes only in neurons already involved in neurofibrillary degeneration. Seeing as neurofibrillary degeneration occurs early in the disease course and is particularly severe in the medial temporal structures and relatively milder in the neocortex, this observation might represent the pathophysiological basis of the greater susceptibility of medial temporal structures to the toxic effects of beta amyloid.

Regional differences of the toxic effect of amyloid load have been recently reported by two combined [11C]-PIB and [18F]-FDG-PET studies [27,28] in patients with probable AD and healthy controls showing that increased amyloid load in temporo-parietal regions and the cingulate gyrus was associated with lower glucose use in these same areas, whereas larger loads of amyloid in the frontal lobes, striatum, and thalamus were not coupled with similar metabolic decreases [27,28]. These data support the idea that amyloid plaques exert non-uniform effects across different brain areas. Alternatively insoluble beta amyloid might be a downstream marker of local cell death, but amyloid imaging cannot test which hypothesis is correct.

The differential susceptibility hypothesis invokes the old question of what molecular mechanisms are behind the selective vulnerability (pathoklisis) of different brain areas in neurodegenerative diseases [29,30]. It has been suggested that brain areas with lower basal or default activity on fMRI and greater task-specific activity are more resistant, whereas brain regions with high basal activity, such as the posterior cingulate/retrosplenial, temporoparietal, and cingulate cortex are more prone to beta amyloid deposition [31].

Whether [11C]-PIB binds to different types of amyloid with different toxicity is a more speculative argument. Evidence is accumulating that [11C]-PIB binds to extracellular plaques as well as vascular amyloid [32,33], and biochemical differences have been described between plaque and vascular amyloid regarding associated hydrophobic amyloid variants [34] that might differentially bind to [11C]-PIB. However, the molecular features of the binding of [11C]-PIB to different beta amyloid types such as Abeta40 and Abeta42 that are differentially distributed in parenchymal plaques and

vascular amyloid are only partly known [35].

Of course, it is also possible to regard the modest relationship between brain atrophy and brain amyloidosis that we found as indicative that neither of the previous two hypotheses are true, but rather that PIB positive amyloidosis is peripheral to brain degeneration. Indeed, the so far dominant amyloid hypothesis of AD has lately been shaken by a number of observations coming from failed clinical trials of antiamyloid drugs [36,37] and pathological data from the original AN1792 vaccine trial [38]. Moreover, a recent [11C]-PIB PET imaging study has found that about one fifth of cognitively unimpaired older persons can be categorized as PIB positive in at least one brain region [39]. However, we feel that the overwhelming evidence on familial AD cases due to mutations of enzymes involved in amyloid metabolism provide still unfalsified backing to the amyloid hypothesis of AD. Any purely non-amyloid hypothesis is therefore at least as incomplete.

Some limitations should be taken into account in the interpretation of the present results. First, our controls were about 7 years younger than patients. While this might have inflated the structural and functional image differences between the two groups, it can hardly account for the differential topography of the relationship between atrophy and [11C]-PIB uptake. Second, we did not perform partial volume effect correction for our data. In small atrophied structures such as the hippocampus, partial volume effect could result in weaker signal because of inclusion of surrounding CSF in the ROI. Last, in the present study we have studied the correlation between [11C]-PIB and atrophy by pooling healthy persons and AD patients and we cannot exclude that intergroup differences in both hippocampal volume and [11C]-PIB uptake might have driven the correlation results. Future work with larger study groups will need to confirm the relationships we found in AD patients only.

References

1. Frisoni GB, Caroli A. Neuroimaging outcomes for clinical trials. J Nutr Health Aging 2007; 11:348-352.
2. Hardy JA, Higgins GA. Alzheimer's disease: The amyloid cascade hypothesis. Science 1992; 256:184-185.
3. Klunk WE, Engler H, Nordberg A, et al. Imaging brain amyloid in Alzheimer's disease with Pittsburgh Compound-B. Ann Neurol 2004; 55:306-319.
4. Archer HA, Edison P, Brooks DJ, et al. Amyloid load and cerebral atrophy in Alzheimer's disease: An 11C-PIB positron emission tomography study. Ann Neurol 2006; 60:145-147.
5. Josephs KA, Whitwell JL, Ahmed Z, et al. Beta-amyloid burden is not associated with rates of brain atrophy. Ann Neurol 2008; 63:204-212.
6. Kemppainen NM, Aalto S, Wilson IA, et al. Voxel-based analysis of PET amyloid ligand [11C]PIB uptake in Alzheimer disease. Neurology 2006; 67:1575-1580.
7. Rorden C, Brett M. Stereotaxic display of brain lesions. Behav Neurol 2000; 12:191-200.
8. Jenkinson M, Pechaud M, Smith S. BET2: MR-based estimation of brain, skull and scalp surfaces. In Eleventh Annual Meeting of the Organization for Human Brain Mapping, 2005.
9. Caroli A, Testa C, Geroldi C, et al. Brain perfusion correlates of medial temporal lobe atrophy and white matter hyperintensities in mild cognitive impairment. J Neurol 2007; 254:1000-1008.
10. Frisoni GB, Testa C, Sabattoli F, Beltramello A, Soininen H, Laakso MP. Structural correlates of early and late onset Alzheimer's disease: Voxel based morphometric study. Neurol Neurosurg Psychiatry 2005; 76:112-114.
11. Filippini N, Scassellati C, Boccardi M, et al. Influence of serotonin receptor 2A His452Tyr polymorphism on brain temporal structures: A volumetric MR study. Eur J Hum Genet 2006; 14:443-449.
12. Good CD, Johnsrude IS, Ashburner J, Henson RNA, Friston KJ, Frackowiak RSJ. A voxel-based morphometric study of ageing in 465 normal adult human brains. NeuroImage 2001; 14:21–36.
13. Maldjian JA, Laurienti PJ, Kraft RA, Burdette JH. An automated method for neuroanatomic and cytoarchitectonic atlas-based interrogation of fMRI data sets. Neuroimage 2003; 19:1233-1239.
14. Mosconi L, Tsui WH, De Santi S, et al. Reduced hippocampal metabolism in MCI and AD: Automated FDG-PET image analysis. Neurology 2005; 64:1860-1867.
15. Lopresti BJ, Klunk WE, Mathis CA, et al. Simplified quantification of pittsburgh compound B amyloid imaging PET studies: A comparative analysis. J Nucl Med 2005; 46:1959-1972.
16. Kemppainen NM, Aalto S, Wilson IA, et al. PET amyloid ligand [11C]PIB uptake is increased in mild cognitive impairment. Neurology 2007; 68:1603-1606.
17. Thal DR, Rub U, Orantes M, Braak H. Phases of A beta-deposition in the human brain and its relevance for the development of AD. Neurology 2002; 58:1791-1800.
18. Smith AD. Imaging the progression of Alzheimer pathology through the brain. Natl Acad Sci USA 2002; 99:4135-4137.
19. Frisoni GB, Pievani M, Testa C, et al. The topography of grey matter involvement in early and late onset Alzheimer's disease. Brain 2007; 130:720-730.
20. Jack CR Jr, Lowe VJ, Senjem ML, et al. 11C PiB and structural MRI provide complementary information

in imaging of Alzheimer's disease and amnestic mild cognitive impairment. Brain 2008; 131:665-680.

21. Giannakopoulos P, Herrmann FR, Bussiere T, et al. Tangle and neuron numbers, but not amyloid load, predict cognitive status in Alzheimer's disease. Neurology 2003; 60:1495-1500.
22. Bussiere T, Friend PD, Sadeghi N, et al. Stereologic assessment of the total cortical volume occupied by amyloid deposits and its relationship with cognitive status in aging and Alzheimer's disease. Neuroscience 2002; 112:75-91.
23. von Gunten A, Kovari E, Bussiere T, et al. Cognitive impact of neuronal pathology in the entorhinal cortex and CA1 field in Alzheimer's disease. Neurobiol Aging 2006; 27:270-277.
24. Akram A, Christoffel D, Rocher AB, et al. Stereologic estimates of total spinophilin-immunoreactive spine number in area 9 and the CA1 field: Relationship with the progression of Alzheimer's disease. Neurobiol Aging 2008; 29:1296-1307.
25. Wegiel J, Bobinski M, Tarnawski M, et al. Shift from fibrillar to nonfibrillar abeta deposits in the neocortex of subjects with Alzheimer disease. J Alzheimers Dis 2001; 3:49.
26. Rapoport M, Dawson HN, Binder LI, Vitek MP, Ferreira A. Tau is essential to beta -amyloid-induced neurotoxicity. Proc Natl Acad Sci USA 2002; 99:6364-6369.
27. Edison P, Archer HA, Hinz R, et al. Amyloid, hypometabolism, and cognition in Alzheimer disease: An [11C]PIB and [18F]FDG PET study. Neurology 2007; 68:501-508.
28. Furst AJ, Mormino EC, Lal RA, et al. The local and global impact of amyloid burden on glucose metabolism in Alzheimer's disease: evidence from [11C]PIB and [18F]FDG PET imaging. Human Amyloid Imaging: April 11, 2008; Chicago, Illinois.
29. Schmitt HP. Neuro-modulation, aminergic neuro-disinhibition and neuro-degeneration. Draft of a comprehensive theory for Alzheimer disease. Med Hypotheses 2005; 65:1106-1119.
30. Del Tredici K, Rub U, De Vos RA, Bohl JR, Braak H. Where does parkinson disease pathology begin in the brain? J Neuropathol Exp Neurol 2002; 61:413-426.
31. Buckner RL, Snyder AZ, Shannon BJ, et al. Molecular, structural, and functional characterization of Alzheimer's disease: Evidence for a relationship between default activity, amyloid, and memory. J Neurosci 2005; 25:7709-7717.
32. Bacskai BJ, Frosch MP, Freeman SH, et al. Molecular imaging with pittsburgh compound B confirmed at autopsy: A case report. Arch Neurol 2007; 64:431-434.
33. Remes AM, Laru L, Tuominen H, et al. Carbon 11-labeled pittsburgh compound B positron emission tomographic amyloid imaging in patients with APP locus duplication. Arch Neurol 2008; 65:540-544.
34. Kuo YM, Emmerling MR, Woods AS, Cotter RJ, Roher AE. Isolation, chemical characterization, and quantitation of A beta 3-pyroglutamyl peptide from neuritic plaques and vascular amyloid deposits. Biochem Biophys Res Commun 1997; 237:188-191.
35. Ikonomovic MD, Klunk WE, Abrahamson EE, et al. Post-mortem correlates of in vivo PiB-PET amyloid imaging in a typical case of Alzheimer's disease. Brain 2008; 131:1630-1645.
36. Wilcock GK, Black SE, Hendrix SB, Zavitz KH, Swabb EA, Laughlin MA. Tarenflurbil Phase II Study investigators. Efficacy and safety of tarenflurbil in mild to moderate Alzheimer's disease: a randomised phase II trial. Lancet Neurol 2008; 7:483-493.

37. Wong GT. FDA Deems U.S. Alzhemed Trial Results Inconclusive. In: Alzforum News [online]. Available at http://www.alzforum.org/new/detail.asp?id=1647. Accessed August 28, 2007.
38. Holmes C, Boche D, Wilkinson D, et al. Long-term effects of Abeta42 immunisation in Alzheimer's disease: follow-up of a randomised, placebo-controlled phase I trial. Lancet 2008; 372:216-223.
39. Aizenstein HJ, Nebes RD, Saxton JA, et al. Frequent amyloid deposition without significant cognitive impairment among the elderly. Arch Neurol 2008; 65:1509-1517.

Chapter 6

Functional compensation in incipient Alzheimer's disease

Caroli A, Geroldi C, Nobili F, Barnden LR, Guerra UP, Bonetti M, Frisoni GB

Neurobiol of Aging 2010; 31(3):387-397
(epub June, 12 2008)

Abstract

Aim of this study was to investigate the functional compensation mechanism in incipient Alzheimer's Disease. 17 elderly healthy subjects and 9 amnestic MCI patients with incipient AD underwent brain MR scan and 99mTc ECD SPECT. We processed all images with SPM2, we created t maps, showing the wholebrain GM atrophy and functional changes, and we properly masked them with each other in order to assess relatively preserved perfusion or depression. Incipient AD showed GM atrophy in the medial-temporal and temporoparietal lobes, in the insula and in the retrosplenial cortex, and GM hypoperfusion in the medial-temporal and temporoparietal lobes. Relatively preserved perfusion, we could hypothesize to be compensatory in the setting of neuronal loss, was found in the posterior cingulate, in the head of the hippocampus, in the amigdala, and in the insula bilaterally, while functional depression occurred in bilateral parahippocampal gyri. In AD, a perfusional compensatory mechanism takes place in the neocortex, while perfusional depression occurs in the medial temporal lobe. These results help understand the reactive phenomena induced by the brain to try and counteract the pathological changes of AD.

Introduction

Mild cognitive impairment (MCI) is a clinical syndrome characterized by cognitive deficits without functional impact on daily living, and thus not severe enough to allow a diagnosis of dementia [1]. MCI has often been considered a preclinical stage of Alzheimer Dementia, converting to dementia in the frequency of 10–15% per year [2] vs. 2% per year of cognitively intact persons [1, 3]. The relevant clinical issue is to identify MCI patients who will progress to AD from those who will not. An accurate study of MCI patients with preclinical AD could help in better understanding AD pathology, and would make it possible to implement strategies to prevent or delay dementia, given that early therapeutical interventions are more likely to be effective.

Alzheimer's disease is associated with widespread structural and functional brain alterations. Both profiles of alterations have been well documented, with consistent regional distribution of atrophy [4-8] and hypoperfusion/hypometabolism [9-13] across studies.

As in AD, already at the early stage, the atrophy and functional alteration patterns partially overlap and partially do not [7], it would be interesting to investigate the existing relationship between the two processes with a special focus on the regions affected by AD neuropathology, in order to see whether the GM tissue loss is the only responsible for functional reduction, and whether the partial divergence between the two patterns either is due to coregistration and partial volume effect problems of SPECT/PET techniques or rather it reflects an existing difference between the two processes. Several SPECT/PET studies have already investigated atrophy and hypoperfusion or hypometabolism. Some PET or SPECT studies, after applying partial volume effect (PVE) correction, concluded that grey matter loss did not entirely explain the observed hypometabolism [14-18], and few studies assessed both the structural and functional wholebrain alteration profiles in the same patients [7,15,19-22]. However, none of the previous studies assessed the relative degree of wholebrain GM atrophy and functional changes.

Aim of this study was thus to compare on a voxel-by-voxel basis GM atrophy and functional reduction (assessed in terms of cerebral perfusion deficits) in incipient AD, using a method specifically designed for this purpose, in order to investigate the functional compensation mechanism in the regions affected by AD neuropathology.

Methods

MCI patients.

MCI patients were taken from a prospective project on MCI ("Mild Cognitive Impairment in Brescia - MCIBs"), aimed to study the natural history of non demented persons with apparently primary cognitive deficits, i.e. not due to psychic or physical conditions. The study protocol was approved by the local ethics committee and all participants signed an informed participation consent.

Inclusion criteria in the study were all of the following: (i) complaint of memory or other cognitive disturbances; (ii) mini mental state examination (MMSE) score of 24 to 27/30 or MMSE of 28 and higher plus low performance (score of 2/6 or higher) on the clock drawing test [23]; (iii) sparing of instrumental and basic activities of daily living or functional impairment stably due to causes other than cognitive impairment. Exclusion criteria were any one of the following: (i) age of 90 years and older; (ii) history of depression or psychosis of juvenile onset; (iii) history or neurological signs of major stroke; (iv) alcohol abuse; (v) craniocerebral trauma; (vi) heavy use of psychotropic drugs.

Based on these criteria, 139 patients were evaluated from April 2002 to March 2005. All of these underwent: (i) semi-structured interview with the patient and – whenever possible – with another informant (usually the patient's spouse or a child) by a geriatrician; (ii) physical and neurological examinations; (iii) performance-based tests of physical function, gait and balance; (iv) neuropsychological battery assessing verbal and non-verbal memory, attention and executive functions (Trail Making Test B-A [24]; Clock Drawing Test [23]), abstract thinking (Raven matrices [25]), frontal functions (Inverted Motor Learning [26]), language (Phonological and Semantic fluency [27]; Token test [26]), and apraxia and visuo-constructional abilities (Rey figure copy [28]); (v) assessment of depressive symptoms with the Center for Epidemiologic Studies Depression Scale (CES-D [29]). Of these 139 patients, 17 scored within normal limits (above the 10th percentile of the age- gender- and education-specific distribution) on all neuropsychological tests and 18 did not have MR imaging of adequate quality.

Among the 104 remaining patients 56 agreed to undergo SPECT scan and were further considered. MCI patients who did and did not undergo SPECT were similar for age (70±6 vs 71±8, p=0.230), gender (58% vs 69% females, p=0.271), physical health (hypertension: 51% vs 54%, p=0.768; diabetes: 23% vs 10%, p=0.062; heart

disease: 33% vs 31%, p=0.879), MTA (1.6±1.3 vs 1.9±1.2, p=0.151) and white matter hyperintensities load (3.3±3.4 vs 4.0±3.9, p=0.354); they differed only for education (9.2±4.6 vs 6.5±3.3, p=0.002) and MMSE (27.6±1.6 vs 26.6±1.8, p=0.007).

Table 1: Sociodemographic and clinical features of normal controls and incipient AD.

	Normal controls N=17	Incipient AD N=9	p
Sociodemographic features			
Age, years	69±3	69±3	0.976
Gender, women	9 (53%)	4 (44%)	0.680
Education, years	9.8±4.1	11.4±5.7	0.393
Cognitive and mental features			
Mini Mental State Exam	28±2	27±2	0.145
Disease duration (months)	---	30±17	---
Depression (CES-D)	---	16±8	---
Physical health			
Hypertension	7 (41%)	2 (22%)	0.334
Diabetes	2 (12%)	1 (11%)	0.960
Heart disease	2 (12%)	3 (33%)	0.184
Brain structural features			
MTA score	0.6±0.5	2.4±1.2	0.001
ARWMC score	1.6±2.1	2.3±2.8	0.634
L Hippocampus (mm3)	2770±274	2172±444	0.001
R Hippocampus (mm3)	2715±221	2359±404	0.008
APOEε4, carriers	1/12 (8%)	5 (56%)	0.056

CES-D: Center for Epidemiologic Studies Depression Scale; ARWMC: Age-Related White Matter Changes; MTA: Medial Temporal lobe Atrophy. Hippocampal volumes were normalized to mean total intracranial volume.
p denotes difference significance on X2 test (categorical variables, i.e. sex, hypertension, diabetes and heart disease), independent t-test (continuous variables) or Kruskal-Wallis test (ordinal non-continuous variables, i.e. MTA and ARWMC scores).

We divided MCI patients into amnestic (N=28, age=71±6, 12 women) and non-amnestic (N=28, age=67±7, 20 women), according to the presence of memory deficit or cognitive disturbances other than memory deficit, based on neuropsychological assessment. Memory disturbance was defined as scoring below the 10th percentile, i.e.

1.28 standard deviations below the mean of the age- gender- and education-specific distribution, in at least one memory test of logical memory, Rey word list, immediate and delayed recall, and Rey figure recall. When Rey figure copy was too low for recall to be reliably assessed (under the 10th percentile) Rey figure recall was not taken into account to define memory disturbance. The presence of cognitive disturbances other than memory deficit was defined as performance below the 10th percentile of the age-gender- and education-specific distribution in any one of the single tests of 4 different neuropsychological domains (listed in table 2). In most cases memory impairment was associated with cognitive impairment in other neuropsychological domains. We accounted as amnestic all MCI patients with memory deficit, either single-domain (N=5) or multi-domain (2 domains: N=8, 3 domains: N=8, 4 domains: N=7).

Table 2: Neuropsychological tests scores corrected by age and education for normal controls and incipient AD.

		Normal controls	Incipient AD	p
		N=17	N=9	
Memory				
Logical memory test [26]		13.1±3.5	7.9±3.8	0.002
Rey Auditory verbal learning test recall [56]	Immediate	---	28.7±9.8	---
	Delayed	---	3.7±2.3	---
Rey figure recall [28]		15.6±6.3	9.7±10.6	0.088
Executive and frontal functions				
TMT B-A [24]		43±108	83±67	0.333
Raven matrices [25]		31.8±4.1	29.6±4.1	0.195
Language				
Verbal fluency [27]	Letter	36.4±8.9	30.1±9.4	0.107
	Category	41.9±9.2	26.7±6.1	0.000
Token test [26]		33.0±1.6	31.8±2.5	0.182
Apraxia				
Rey-Osterrieth Complex Figure, Copy [28]		31.6±6.0	32.5±4.2	0.716

TMT: trail making test. CDT: clock drawing test. COWAT: controlled oral word association test.
All test scores are corrected by age and education
p denotes difference significance between the two groups on independent t-test.

Amnestic MCI patients underwent a yearly follow-up visit, consisting of complete clinical and neuropsychological examination, from 1 to 3 years after enrolment (mean observation time 19±10 months), and we ascertained conversion to dementia according to clinical diagnostic criteria for Alzheimer's disease [30], subcortical vascular dementia [31], dementia with Lewy bodies [32], and fronto-temporal dementia [33]. Four amnestic MCI patients refused to have any follow-up visit and dropped out, one patient converted to fronto-temporal dementia, while all other converters converted to Alzheimer's disease. Among non-converters, there were no improved MCI patients, with no longer evident neuropsychological deficits in any domain. For the purpose of the present study, aimed at investigating exceeding atrophy or hypoperfusion in predementia AD, we finally included in the study only amnestic MCI patients who converted to AD (N=9, age=69±3, 4 females). The conversion rate was 25% per person year.

Normal controls.

We selected healthy subjects from those enrolled in a study on normal brain structure with MR (ArchNor) aiming to capitalize on unnecessary scans in otherwise normal persons, as described in detail elsewhere [34]. Briefly, subjects were consecutive normal volunteers picked among those undergoing brain MR scan at the Neuroradiology Unit of the "Città di Brescia" Hospital, Brescia from October 2004 to June 2006 for reasons unrelated to cognition. The reasons for MR prescription were generally migraine and headache, auditory (hypoacusia, dizziness, tinnitus) or visual concerns (diplopia), sensory disturbances (paresthesias), suspected cerebrovascular disease or other rarer problems (dyslexia, orbit study, lipotimic episodes, etc.) in both samples. Exclusion criteria were based on information prior to MR and secondary to possible findings in MR. A priori exclusion criteria were: (1) MR scan for memory problems or cognitive impairment, (2) MR scan for clinical suspicion of neuro-degenerative diseases (Parkinson's disease, progressive supranuclear palsy, Huntington's disease, multiple system atrophy, etc), (3) MR scan for suspected stroke and (4) history of TIA or stroke, head trauma, alcohol and substance abuse, cortico-steroid therapy, and loss of weight greater than 5 kilograms in the last 6 months. A posteriori exclusion criteria included: MR scan showing (1) brain mass, (2) white matter hyperintensities in a subject undergoing MR for suspected multiple sclerosis, (3) aneurysm larger than 10 mm, (4) arteriovenous malformations (except for

developmental venous anomaly), (5) malformations of the central nervous system and (6) cognitive impairment on neuropsychological testing. All scans of enrolled subjects were normal on visual assessment of a neuroradiologist. Subjects were intercepted in the waiting room of the neuroradiology units, explained the aims and methods of the study, and asked to take part to the study after signing the informed consent.

Subjects underwent multidimensional assessment including clinical, neurological and neuropsychological evaluations, and drawing of a blood sample.

For this study, we asked all subjects aged 65 years or older to undergo a SPECT scan, and we further considered only those with both MR and SPECT images (3 males and 4 females).

To enlarge the normal controls group, we asked other healthy volunteers aged 65 years or older, among patients' spouses, friends of them, and researchers' acquaintances, to undergo the same protocol as subjects taken from the ArchNorm study (SPECT scan included), using the same exclusion criteria as above (5 males and 5 females).

SPECT scan

Both patients with incipient AD and normal controls underwent SPECT scan in the nuclear medicine department of the Ospedali Riuniti hospital, Bergamo. Each patient received an intravenous injection of 925 MBq of technetium-99m ethyl cysteinate dimer (99mTc-ECD) in resting conditions, lying supine with eyes closed in a quiet, dimly-lit room. Forty to sixty minutes after injection, brain SPECT was performed using a dual-head rotating gamma camera (GE Elscint Helix) equipped with low energy-high resolution, parallel hole collimators. A 128x128 pixel matrix, zoom = 1.5, was used for image acquisition with 120 views over a 360° orbit (in 3° steps) with a pixel size and slice thickness of 2.94 mm. At least 5 million counts were acquired for each scan, according to the guidelines of the European Association of Nuclear Medicine [35]. Butterworth filtered-back projection (order = 7, cut-off = 0.45 cycles/cm) was used for image reconstruction, and attenuation correction was performed using Chang's method (attenuation coefficient = 0.11/cm). Images were exported in DICOM format.

SPECT processing protocol.

To achieve a precise normalization, we generated a study-specific SPECT template using both SPECT and MR scans of all patients and normal controls under study, following a procedure described in detail elsewhere [36]. The creation of a study-

specific template allows for better normalisation, since low uptake in ventricular structures and cortical hypoperfusion effects frequently present in elderly patients are accounted for.

For each coregistered SPECT scan, we set origin to the anterior commissure with SPM99, using the respective MR image as a reference, and we processed all scans with SPM2 according to an optimized SPECT processing protocol described in detail elsewhere [36] and schematically represented in Figure 1. Briefly, we normalised SPECT data through a double-stage spatial normalisation, we masked to remove scalp-facial activity and we smoothed them at 12mm FWHM.

Figure 1: Flow chart summarizing the whole MRI-SPECT processing protocol and the steps for the creation of the functional compensation or depression maps.

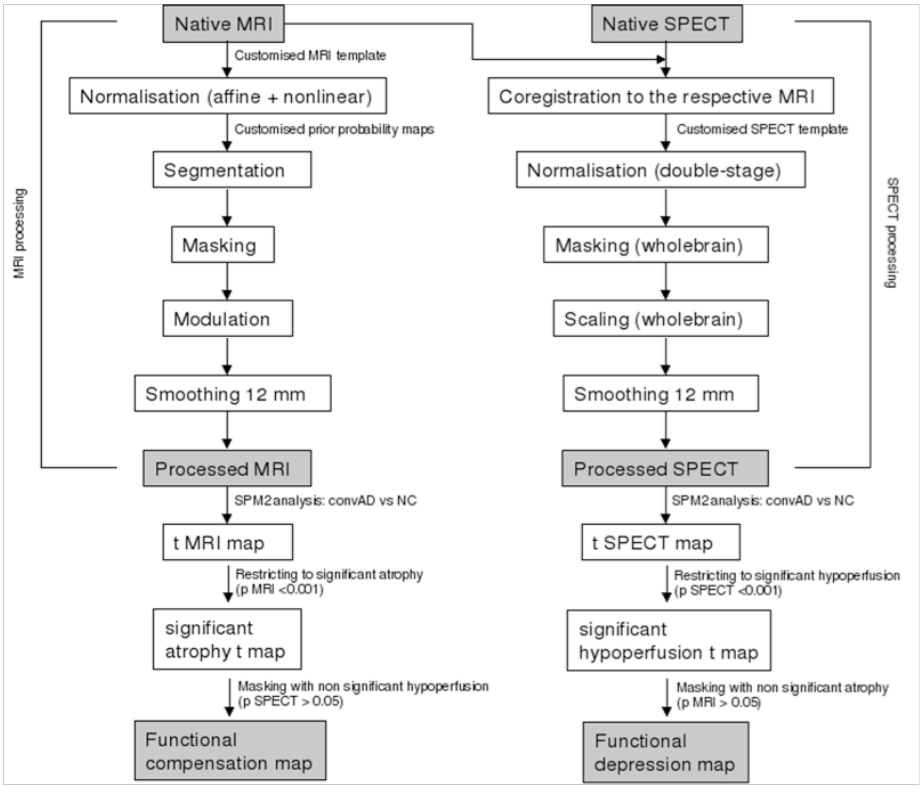

MR imaging

Both patients and normal controls underwent brain T1-weighted magnetic resonance

imaging in the neuroradiology department of the Città di Brescia Hospital, Brescia, as previously discussed [36].

MR images were processed with SPM2 [37] following an optimized Voxel-Based Morphometry protocol, described in detail elsewhere [38,39] and schematically represented in Figure 1.

Briefly, customised prior probability maps were computed for GM, WM and CSF [6]. The original MR images were normalised to a customised high resolution MR template [36] through affine and nonlinear transformations, they were segmented into GM, WM and CSF using the customised priors, masked to remove non-brain tissue voxels, modulated, and finally smoothed with a 12mm isotropic Gaussian kernel [40]. Only GM images were further used in the statistical analysis.

Manual tracings of hippocampal and total intracranial volumes were performed using DISPLAY [41]. Native hippocampal volumes were normalized to the individual intracranial volumes and rescaled to the mean total intracranial volume according to the following formula ([volume/individual total intracranial volume]*mean total intracranial volume).

Statistical Analysis

We investigated the significance of the difference among groups in sociodemographic and clinical features and in neuropsychological tests scores using X2 test for categorical variables (sex, hypertension, diabetes, and heart disease, ApoE), independent t-test for continuous variables, and Kruskal-Wallis test for ordinal non-continuous variables (MTA and ARWMC scores). In all cases we set the significant threshold at $P<0.05$.

We used the "single subject: conditions and covariates" SPM2 model to assess differences in perfusion between incipient AD and normal controls, on a voxel-by-voxel basis. We used age as confounding variable, and we used proportional scaling to remove inter-subject global variations in SPECT intensities, setting to 50 the mean count in all scalp-free brains.

We used the same "single subject: conditions and covariates" SPM2 model on segmented GM images to assess grey matter atrophy in incipient AD compared to normal controls. We entered age and total intracranial volume as confounding variables.

Functional compensation and depression visualisation

In order to visualise functional compensation and depression we used the t-values maps resulting from the SPM2 analysis above, showing the wholebrain atrophy and hypoperfusion in incipient AD as compared to normal controls.

In order to direct attention to grey matter and include in the further analysis only GM voxels, we masked both the atrophy and hypoperfusion t maps with the same customised binary GM mask, obtained by thresholding the GM customised prior probability map at 0.2.

Since native SPECT scans were coregistered to their respective MR images, and the study-specific SPECT template was coregistered to the high-definition MR template, all the normalised SPECT and MR images used for the statistical analysis were coregistered to the SPM standard anatomical space, so that hypoperfusion and atrophy patterns (i.e. hypoperfusion and atrophy t maps) could be compared on a voxel-by-voxel level.

Since the regions of functional compensation are denoted by significant atrophy but non significant functional deficit, we specifically created a map of non significant hypoperfusion by restricting the hypoperfusion t map to non significant voxels (scoring t-value>-1.688, which is the significance threshold corresponding to $p>0.05$ in a one-tail t-test with 36 degrees of freedom, as for our case) and we used it to mask the significant atrophy t map (obtained thresholding the atrophy t map at $t<-3.3$, corresponding to $p<0.001$ in a two-tails t test). As a result of this masking procedure we got a t map displaying regions of functional compensation.

Similarly, since the regions of functional depression are denoted by significant hypoperfusion but non significant atrophy, we specifically created a map of non significant atrophy (voxels with t-value>-1.69, corresponding to $p>0.05$ in a one-tail t-test with 35 degrees of freedom), we used it to mask the hypoperfusion t map (obtained thresholding the hypoperfusion t map at $t<-3.3$, i.e. $p<0.001$), and we got a t map displaying regions of functional depression.

Results

Table 1 shows that incipient AD differed significantly from normal controls in medial temporal lobe atrophy and in both left and right hippocampal volumes. They did not differ for any other sociodemographic or physical health feature. Although Mini Mental State Exam was not significantly different between the two groups, incipient AD scored

a mean MMSE value lower than normal controls, as expected. The analysis of the prevalence of the ε4 allele of ApoE showed an almost significantly (p=0.056) higher prevalence of ε4 allele carriers in incipient AD (56%) as compared to normal controls (just 1 carrier out of 12 normal controls with available data, 8%).

As far as neuropsychological test (table 2), incipient AD showed significantly lower scores than normal controls on the logical memory and category fluency tests, and a trend for lower scores on the Rey figure recall test (p=0.082). Although we had no significant difference in the other tests, incipient AD had worse performance than normal controls in all neuropsychological domains except for apraxia, evaluated by the Rey figure copy test [28].

Figure 2 shows the atrophy t map, that is the pattern of GM atrophy in incipient AD as compared with normal controls, expressed in terms of negative t values: the higher is the negative t value, the more significant is the GM volume reduction, i.e. GM atrophy. The pattern of GM atrophy involved the temporoparietal and medial temporal lobes, the insula and the retrosplenial cortex bilaterally, as expected, with the main peak of atrophy located in the right entorinhal cortex. Only regions of significant atrophy (with t value < -3.3) are shown in the figure.

Figure 3 shows the hypoperfusion t map, that is the pattern of significant GM hypoperfusion in incipient AD as compared with normal controls, expressed in terms of negative t values as for the atrophy t map. Significant hypoperfusion was mainly located in the medial temporal lobe and, to a smaller extent, in the temporoparietal lobe and in the caudate. Only regions of significant hypoperfusion (with t value < -3.3) are shown in the figure.

In order to study the relationship between atrophy and hypoperfusion, in particular the functionality of the regions affected by AD neuropathology, we looked at the atrophy map and masked it with the regions of non significant hypoperfusion. We found significant atrophy but no functional deficit, denoting the presence of a compensatory mechanism, in the head of the hippocampus and in the amigdala bilaterally, in the posterior cingulate and in both the left and right insular regions (Figure 4). Similarly, we looked at the hypoperfusion map and masked it with the regions of non significant atrophy and we found perfusional deficit in both the left and right parahippocampal gyri (Figure 5).

Figure 2: t MRI map, showing the pattern of GM atrophy in incipient AD as compared with normal controls, expressed in terms of negative t-scores: the higher is the negative t-score, the more significant is the GM volume reduction, i.e. GM atrophy. The pattern of GM atrophy involved the temporoparietal and medial temporal lobes, the insula and the retrosplenial cortex bilaterally, with the main peak of atrophy located in the right entorinhal cortex. Only regions of significant atrophy (with MRI t-value < -3.3, corresponding to $p<0.001$ uncorrected for multiple comparisons) are shown in the figure.

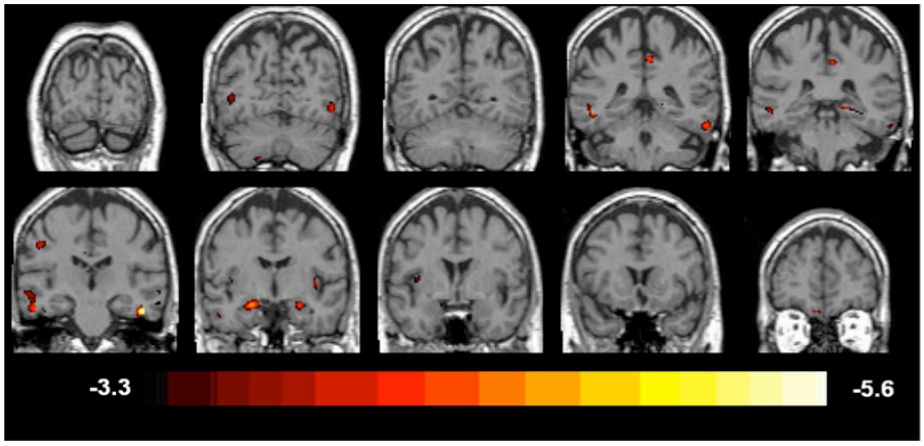

Figure 3: t SPECT map, showing the pattern of significant GM hypoperfusion in incipient AD as compared with normal controls, expressed in terms of negative t-scores as for the t MRI map. Significant hypoperfusion was mainly located in the medial temporal lobe and, to a smaller extent, in the temporoparietal lobe and in the caudate. Only regions of significant hypoperfusion (with SPECT t-value < -3.3, corresponding to $p<0.001$ uncorrected for multiple comparisons) are shown in the figure.

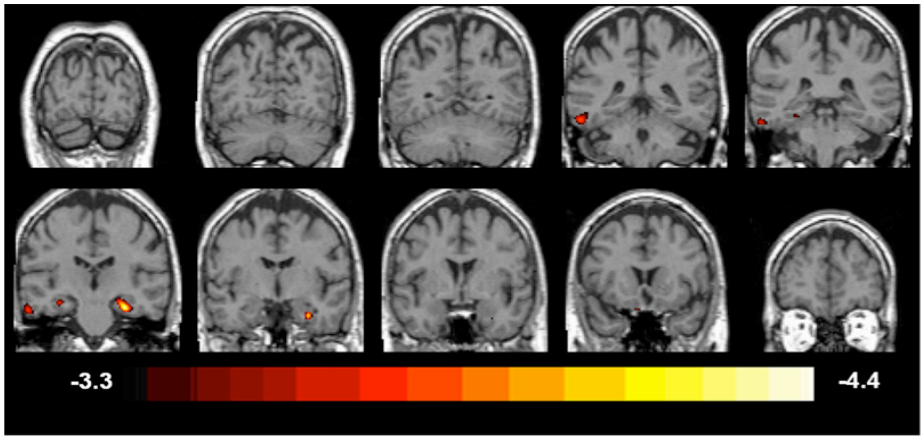

Figure 4: Functional compensation map, obtained by masking the significant atrophy t map (displaying MRI t-scores for all significant voxels with p<0.001 uncorrected for multiple comparisons, i.e. all voxels with t-MRI<-3.3) with the non significant hypoperfusion t map (displaying SPECT t-scores in all significant voxels with p>0.05 uncorrected for multiple comparisons, i.e. all voxels with t-SPECT>-1.688). Relatively preserved perfusion was found to occur in the head of the hippocampus and in the amigdala bilaterally, in the posterior cingulate and in both the left and right insular regions

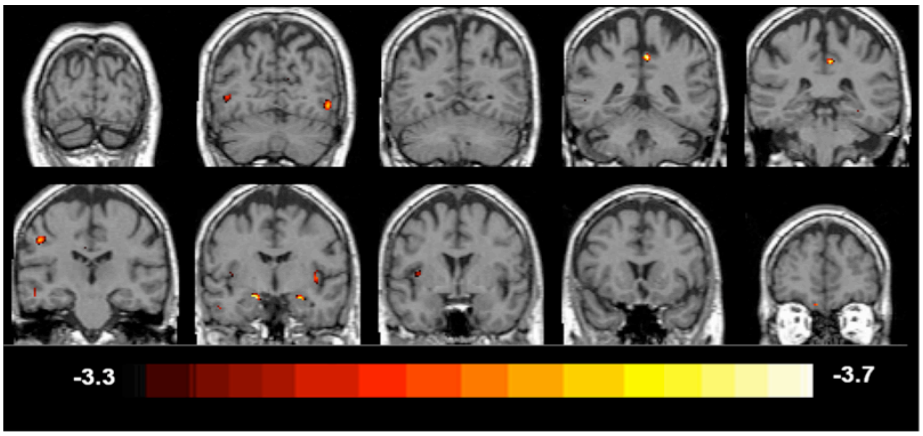

Figure 5: Functional depression map, obtained by masking the significant hypoperfusion t map (displaying SPECT t-scores for all significant voxels with p<0.001 uncorrected for multiple comparisons, i.e. all voxels with t-SPECT<-3.3) with the non significant atrophy t map (displaying MRI t-scores in all significant voxels with p>0.05 uncorrected for multiple comparisons, i.e. all voxels with t-MRI>-1.69). Functional depression was found to occur in both the left and right parahippocampal gyri.

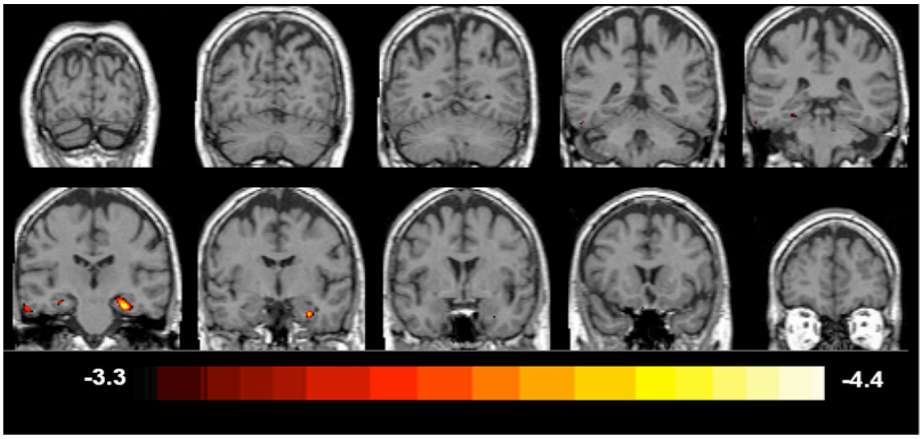

Discussion

The pattern of GM atrophy in incipient AD as compared with normal controls involved the temporoparietal and medial temporal lobes, the insula and the retrosplenial cortex

bilaterally, in line with current knowledge about AD neuropathology and previous VBM findings [4-8]. Furthermore, the main peak of atrophy was located in the entorinhal cortex, which is known to be the earliest site to be affected by AD, even at a preclinical stage [42,43].

Significant hypoperfusion in incipient AD was located in the medial temporal and temporoparietal lobes, in agreement with previous findings. Metabolic and perfusion reductions in the parietotemporal association cortex bilaterally have long been recognised as a relatively specific pattern of AD [44-47]. Furthermore, more recent reports, employing both SPECT and PET with last-generation equipments, and using a detailed anatomical sampling guided by coregistered MRI, demonstrated functional reductions in the medial temporal lobe in AD patients, even at an early stage [15,16,48,49].

As atrophy and hypoperfusion patterns only partially overlapped, we set out to study the relationship between the two processes, with a special focus on the regions affected by AD neuropathology.

Several SPECT/PET studies have already investigated atrophy and hypoperfusion or hypometabolism in order to see whether the GM tissue loss is the only responsible for functional reduction or not. Some PET or SPECT studies, after applying partial volume effect correction, concluded that grey matter loss did not entirely explain the observed hypometabolism [14-18], and few studies assessed both the structural and functional wholebrain alteration profiles in the same patients [7,15,19-22].

However, none of the previous studies assessed and quantified the relative degree of wholebrain GM atrophy and hypoperfusion.

Several fMRI reports found increased activation in patients with mild cognitive impairment, mainly located in the hippocampus, in the posterior medial temporal and closely connected fusiform regions [50-52] and, moreover, a recent SPECT paper [53] found evidence of hyperperfusion in the rostral anterior cingulate, specific for MCI subjects who converted to AD, beyond the expected regional perfusional deficit. Both fMRI activation and hyperperfusion could reflect a compensatory response to the beginning of AD pathology.

To investigate the relationship between GM atrophy and hypoperfusion and to go more deep into the comprehension of the compensatory mechanism, we masked the atrophy map with the regions of non significant hypoperfusion in order to have the pattern of

functional compensation, and we masked the hypoperfusion map with the regions of non significant atrophy in order to have the pattern of perfusional depression. If functional reduction were directly related to atrophy, we would have found hypoperfusion in all and only the regions of atrophy. On the contrary, we found high regional variability, suggesting that additional processes affect the perfusion-GM volume relationship. Functional compensation occured in the posterior cingulate, in both the heads of the hippocampi (which were exactly the regions previously found to be hyperperfused [53] or activated [50-52] in MCI), in both the amigdalae, and in the insula bilaterally, while functional depression occurred in both the left and right parahippocampal gyri.

Most of the regions of atrophy, in particular throughout the neocortex, seem to yield preserved ability to relatively preserve perfusion despite tissue loss due to AD neuropathology. Beyond volume reduction, which surely affects the blood flow, perfusion is also influenced by vasodilation, stimulated by the physiological metabolism: the neuropathologically damaged tissue releases vasodilator agents (such as nitric oxid, NO) which alter the normal regulation of the perfusion in the metabolism behalf. As AD firstly affects neuron cells and only later blood vessels, the latter might be relatively spared early in the disease process and thus, when NO diffuses, small vessels can respond with hyperperfusion, causing the compensatory mechanism. NO diffuses quite quickly so that, once produced, it spread to regions wider than those indeed affected, causing artificial hyperperfusion in the close regions. Due to this problem and considering the low resolution of SPECT scans, the regions of relatively preserved perfusion we found should be slightly downsized; however, this does not affect the main results of the study.

Another possible mechanism underlying the increased perfusion in brain regions affected by AD neuropathology could be a vasodilative response induced by cholinergic neurons. In a recent study [54] Ionov described a two-stage mechanism that could intensify blood supply to a specifically brain area prone to AD, comprising amygdala, hippocampus, olfactory bulb, enthorinal cortex, and neocortex (AHBC area): cholinergic neurons from the nuclei of basal forebrain induce vasodilatory effect through release of acetylcholine. When the efficacy of this neuronal system declines, intensive formation of amyloidogenic peptides starts, causing the alpha7 nicotinic acetylcholine receptors activation, thus enhancing angiogenesis and restoring blood

supply to the AHBC area [54].

On the contrary, in both the left and the right parahippocampal gyri the compensatory capacity seems to be exhausted, resulting in perfusional depression significantly more severe than atrophy. This is in line with the findings of a previous study [22], where we reported hypoperfusion in the parahippocampal gyrus to be a correlate of conversion to AD. The medial temporal lobe is exceptionally vulnerable to AD pathology, even at a preclinical stage, the functional reserve of microcirculation might be already exhausted, and vessels could have lost vasodilatory capacity, allowing perfusional depression.

Since native SPECT scans were coregistered to their respective MR images, and the study-specific SPECT template was coregistered to the high-definition MR template, all the normalised SPECT and MR images used for the statistical analysis were coregistered to the SPM standard anatomical space, so that the atrophy and hypoperfusion t maps themselves were coregistered. Furthermore, despite the difference in resolution between MR and SPECT images, which is one of the main limits of comparing images from different modalities, after the optimised processing all normalised scans of both modalities, as well as t maps, had a voxel size of 2 x 2 x 2 mm, so that the atrophy and hypoperfusion t maps could be compared on a voxel-by-voxel level and used to mask each other in order to have relatively preserved perfusion and depression maps.

Despite the normal controls group was not homogeneous relatively to the recruitment modality, as we had 7 subjects undergoing MR scan for reasons unrelated to cognition but to some extent possibly related to cerebral perfusion, it is unlikely that this affected the results of the study in any way because it was proved in a previous study involving the same 17 normal controls [22].

We believe that the main limitation to be considered in the interpretation of the results is the small number of the samples: the compensatory mechanism was investigated using relatively small groups, and larger groups would be needed to confirm our results.

The procedure presented in this paper to investigate the relative degree of wholebrain GM atrophy and hypoperfusion has several others potential applications of interest. It could be used to assess functional compensation at different stages of the Alzheimer's disease, in order to map the time course of functional brain failure in persons

developing AD, hopefully opening the way to a more accurate disease marker than atrophy or perfusion alone. Moreover, it could be used to investigate functional compensation in other neurodegenerative diseases with a different pathogenesis, such as Fronto-Temporal Dementia. It would be interesting to use the methodology described in this paper to study the AD functional compensatory capacity even in terms of metabolism. In a recent PET study [55], Chetelat and collegues found that in patients with probable AD the hypometabolism significantly exceeds atrophy in most altered structures, particularly in the posterior cingulate-precuneus, orbitofrontal, inferior temporo-parietal, parahippocampal, angular and fusiform areas, while a few hypometabolic structures among which the hippocampus exhibit similar degrees of atrophy and hypoperfusion. The metabolism is expected to be affected by the disease earlier than the perfusion, as the biochemical mechanism that leads up to progressive neuronal loss inducing local hypometabolism preceeds the vessels damage, and the metabolism could probably not compensate the neuropathological deficit.

In conclusion, in predementia AD a perfusional relative compensatory mechanism appears to take place in the neocortex against atrophy and neuropathological damage, while a perfusional depression exceeding atrophy appears to occur in the parahippocampal gyri, as if in this areas, primarily affected by the disease, the microcircle functional reserve was over.

References

1. Petersen RC, Smith GE, Waring SC, Ivnik RJ, Tangalos EG, Kokmen E. Mild cognitive impairment: clinical characterization and outcome. Arch Neurol 1999; 56:303–308.
2. Petersen RC, Doody R, Kurz A, et al. Current concepts in mild cognitive impairment. Arch Neurol 2001; 58:1985–1992.
3. Flicker C, Ferris SH, Reisberg B. Mild cognitive impairment in the elderly: predictors of dementia. Neurology 1991; 41:1006–1009.
4. Baron JC, Chételat G, Desgranges B, et al. In vivo mapping of grey matter loss with voxel-based morphometry in mild Alzheimer's disease. Neuroimage 2001; 14:298-309.
5. Frisoni GB, Testa C, Zorzan A, et al. Detection of grey matter loss in mild Alzheimer's disease with voxel based morphometry. J Neurol Neurosurg Psychiatry 2002; 73:657-664.
6. Good CD, Scahill RI, Fox NC, et al. Automatic differentiation of anatomical patterns in the human brain: validation with studies of degenerative dementias. Neuroimage 2002; 17:29-46.
7. Matsuda H, Kitayama N, Ohnishi T, et al. Longitudinal evaluation of both morphologic and functional changes in the same individuals with Alzheimer's disease. J Nucl Med 2002; 43:304-311.
8. Karas GB, Burton EJ, Rombouts SA, et al. A comprehensive study of grey matter loss in patients with Alzheimer's disease using optimized voxel-based morphometry. Neuroimage 2003; 18:895-907.
9. Minoshima S, Giordani B, Berent S, Frey KA, Foster NL, Kuhl DE. Metabolic reduction in the posterior cingulate cortex in very early Alzheimer's disease. Ann Neurol 1997; 42:85-94.
10. Anchisi D, Borroni B, Franceschi M, et al. Heterogeneity of Brain Glucose Metabolism in Mild Cognitive Impairment and Clinical Progression to Alzheimer Disease. Arch Neurol 2005; 62:1728–1733.
11. Drzezga A, Lautenschlager N, Siebner H, et al. Cerebral metabolic changes accompanying conversion of mild cognitive impairment into Alzheimer's disease: a PET follow-up study. Eur J Nucl Med Mol Imaging 2003; 30:1104–1113.
12. Drzezga A, Grimmer T, Riemenschneider M, et al. Prediction of Individual Clinical Outcome in MCI by Means of Genetic Assessment and 18F-FDG PET. J Nucl Med 2005; 46:1625-1632.
13. Chételat G, Desgranges B, de la Sayette V, Viader F, Eustache F, Baron JC. Mild cognitive impairment: Can FDG-PET predict who is to rapidly convert to Alzheimer's disease? Neurology 2003; 60: 1374-1377.
14. Ibanez V, Pietrini P, Alexander GE, et al. Regional glucose metabolic abnormalities are not the result of atrophy in Alzheimer's disease. Neurology 1998; 50:1585-1593.
15. De Santi S, de Leon MJ, Rusinek H, et al. Hippocampal formation glucose metabolism and volume losses in MCI and AD. Neurobiol Aging 2001; 22:529-539.
16. Nestor PJ, Fryer TD, Smielewski P, Hodges JR. Limbic hypometabolism in Alzheimer's disease and mild cognitive impairment. Ann Neurol 2003; 54:343–351.
17. Mosconi L, Tsui WH, De Santi S, et al. Reduced hippocampal metabolism in MCI and AD. Neurology 2005; 64:1860-1867.
18. Matsuda H, Kanetaka H, Ohnishi T, et al. Brain SPET abnormalities in Alzheimer's disease before and after atrophy correction. Eur J Nucl Med Mol Imaging 2002; 29:1502-1505.
19. Ishii K, Sasaki H, Kono AK, Miyamoto N, Fukuda T, Mori E. Comparison of grey matter and metabolic

reduction in mild Alzheimer's disease using FDG-PET and voxel-based morphometric MR studies. Eur J Nucl Med Mol Imaging 2005; 32:959-963.

20. Mosconi L, Sorbi S, de Leon MJ, et al. Hypometabolism exceeds atrophy in presymptomatic early-onset familial Alzheimer's disease. J Nucl Med 2006; 47:1778-1786.
21. Kawachi T, Ishii K, Sakamoto S, et al. Comparison of the diagnostic performance of FDG-PET and VBM-MRI in very mild Alzheimer's disease. Eur J Nucl Med Mol Imaging 2006; 33:801-809.
22. Caroli A, Testa C, Geroldi C, et al. Cerebral perfusion correlates of conversion to Alzheimer's disease in amnestic mild cognitive impairment. J Neurol 2007; 254:1698-1707.
23. Shulman KI. Clock-drawing: is it the ideal cognitive screening test? Int J Geriatr Psychiatry 2000; 15:548-561.
24. Giovagnoli AR, Del Pesce M, Mascheroni S, Simoncelli M, Laiacona M, Capitani E. Trail making test: normative values from 287 normal adult controls. Ital J Neurol Sci 1996; 17:305-309.
25. Basso A, Capitani E, Laiacona M. Raven's coloured progressive matrices: normative values on 305 adult normal controls. Funct Neurol 1987; 2:189-194.
26. Spinnler H, Tognoni G. Standardizzazione e taratura italiana di test neurologici. Ital J Neurol Sci 1987; 8:47-50.
27. Novelli G, Papagno C, Capitani E, Laiacona M, Cappa SF, Vallar G. Tre test clinici di ricerca e produzione lessicale. Taratura su soggetti normali. Arch Psicol Neurol Psichiatr 1986; 47:477-506.
28. Caffarra P, Vezzadini G, Dieci F, Zonato F, Venneri A. Rey-Osterrieth complex figure: normative values in an Italian population sample. Neurol Sci 2002; 22:443-447.
29. Radloff LS. The CES-D scale: A self-report depression scale for research in the general population. Appl Psychol Measure 1997; 1:385-401.
30. McKhann G, Drachman D, Folstein M, Katzman R, Price D, Stadlan EM. Clinical diagnosis of Alzheimer's disease: report of the NINCDS-ADRDA Work Group under the auspices of Department of Health and Human Services Task Force on Alzheimer's Disease. Neurology 1984; 34:939-944.
31. Erkinjuntti T, Inzitari D, Pantoni L, et al. Research criteria for subcortical vascular dementia in clinical trials. J Neural Transm Suppl 2000; 59:23-30.
32. McKeith IG, Ballard CG, Perry RH, et al. Prospective validation of consensus criteria for the diagnosis of dementia with Lewy bodies. Neurology 2000; 54:1050-1058.
33. Knopman DS, Boeve BF, Parisi JE, et al. Antemortem Diagnosis of Frontotemporal Lobar Degeneration. Ann Neurol 2005; 57:480-488.
34. Riello R, Sabattoli F, Beltramello A, et al. Brain volumes in healthy adults aged 40 years and over: a voxel based morphometry study. Aging Clin Exp Res 2005; 17:329-336.
35. Tatsch K, Asenbaum S, Bartenstein P, et al.; European Association of Nuclear Medicine. European Association of Nuclear Medicine procedure guidelines for brain perfusion SPECT using 99mTc-labelled radiopharmaceuticals. Eur J Nucl Med 2002; 29:BP36–BP42.
36. Caroli A, Testa C, Geroldi C, et al. Brain perfusion correlates of medial temporal lobe atrophy and white matter hyperintensities in mild cognitive impairment. J Neurol 2007; 254:1000-1008.
37. SPM, Statistical Parametric Mapping (computer program). Version 2. London: Functional Imaging

Laboratory, 2002. Available at: http://www.fil.ion.ucl.ac.uk/spm/software/spm2

38. Frisoni GB, Testa C, Sabattoli F, Beltramello A, Soininen H, Laakso MP. Structural correlates of early and late onset Alzheimer's disease: voxel based morphometric study. J Neurol Neurosurg Psychiatry 2005; 76:112-114.
39. Filippini N, Scassellati C, Boccardi M, et al. Influence of serotonin receptor 2A His452Tyr polymorphism on brain temporal structures: a volumetric MR study. Eur J Hum Genet 2006; 14:443-449.
40. Ashburner J, Friston KJ. Why voxel-based morphometry should be used. Neuroimage 2001; 14: 1238–1243.
41. DISPLAY (computer program). Brain Imaging Center - Montreal Neurological Institute. Available at: http://www.bic.mni.mcgill.ca/software
42. Braak H, Braak E. Evolution of neuronal changes in the course of Alzheimer's disease. J Neural Transm Suppl 1998; 53:127-140.
43. Pennanen C, Kivipelto M, Tuomainen S, et al. Hippocampus and entohrinal cortex in mild cognitive impairment and early AD. Neurobiol Aging 2004; 25:303-310.
44. Foster NL, Chase TN, Mansi L, et al. Cortical abnormalities in Alzheimer's disease. Ann Neurol 1984; 16:649–654.
45. Friedland RP, Brun A, Budinger TF. Pathological and positron emission tomographic correlations in Alzheimer's disease. Lancet 1985; 26:228.
46. Holman BL, Johnson KA, Gerada B, Carvalho PA, Satlin A. The scintigraphic appearance of Alzheimer's disease: a prospective study using technetium-99m-HMPAO SPECT. J Nucl Med 1992; 33:181–185 (published erratum appears in J Nucl Med 33,484).
47. Sharp P, Gemmell H, Cherryman G, Besson J, Crawford J, Smith F. Application of iodine-123-labeled isopropylamphetamine imaging to the study of dementia. J Nucl Med 1986; 27:761–768.
48. Callen DJ, Black SE, Caldwell CB. Limbic system perfusion in Alzheimer's disease measured by MRI-coregistered HMPAO SPET. Eur J Nucl Med Mol Imaging 2002; 29:899-906.
49. Kemp PM, Hoffmann SA, Holmes C, et al. The contribution of statistical parametric mapping in the assessment of precuneal and medial temporal lobe perfusion by 99mTc-HMPAO SPECT in mild Alzheimer's and Lewy body dementia. Nucl Med Commun 2005; 26:1099-1106.
50. Dickerson BC, Salat DH, Greve DN, et al. Increased hippocampal activation in mild cognitive impairment compared to normal aging and AD. Neurology 2005; 65: 404-411.
51. Hamalainen A, Pihlajamaki M, Tanila H, et al. Increased fMRI responses during encoding in mild cognitive impairment. Neurobiol Aging 2007; 28:1889-1903.
52. Kircher TT, Weis S, Freymann, K et al. Hippocampal activation in patients with mild cognitive impairment is necessary for successful memory encoding. J Neurol Neurosurg Psychiatry 2007; 78: 812-818.
53. Johnson KA, Moran EK, Becker JA, Blacker D, Fischman AJ, Albert MS. Single photon emission computed tomography perfusion differences in mild cognitive impairment. J Neurol Neurosurg Psychiatry 2007; 78:240-247.
54. Ionov ID. Specific mechanism for blood inflow stimulation in brain area proe to Alzheimer's disease

lesions. Int J Neurosci 2007; 117:1425-1442.

55. Chetelat G, Desgranges B, Landeau B, et al. Direct voxel-based comparison between grey matter hypometabolism and atrophy in Alzheimer's disease. Brain 2008; 131:60-71.
56. Carlesimo GA, Sabbadini M, Fadda L, Caltagirone C. Word-list forgetting in young and elderly subjects: evidence for age-related decline in transferring information from transitory to permanent memory condition. Cortex 1997; 33:155-166.

Chapter 7

Metabolic compensation and depression in Alzheimer's Disease

Caroli A, Lorenzi M, Geroldi C, Nobili F, Paghera B, Bonetti M, Cotelli M, Frisoni GB

Dement Geriatr Cogn Disord 2010;29:37-45

Abstract

Background/Aims: Aim of this study was to map metabolic compensation and depression in Alzheimer's Disease on a voxel-by-voxel basis. Methods: Twenty-one healthy elderly subjects and 25 AD patients underwent cerebral MR and FDG-PET imaging. All images were processed with SPM2, and wholebrain GM atrophy and hypometabolism maps were computed. Metabolic compensation and depression were assessed using Biological Parametric Mapping software. Results: GM atrophy and hypometabolism mapped to similar regions, with variable degrees of severity. Significant metabolic compensation was found in the amygdala, while exceeding hypometabolism was mainly located in the posterior cingulate cortex. Conclusion: Metabolic depression can be due both to distant effects of atrophy and to additional hypometabolism-inducing factors, such as amyloid deposition. Conversely, metabolic compensation could reflect spared synaptic plasticity of the surviving neurons. The investigation of metabolic compensation mechanism could help in the comprehension of the AD underlying pathology.

Introduction

Alzheimer's disease is associated with widespread structural and functional brain alterations. Both profiles of alterations have been well documented, with consistent regional distribution of atrophy [1-4] and hypometabolism [5-8] across studies. As atrophy and functional alteration patterns only partly overlap [4], in the last years there has been growing interest towards the study of the relationship between the two processes, in terms of functional depression and compensation. A better understanding of such mechanisms, taking into account the overall cerebral alteration rather than any specific structural or functional damage, could help to go more deep into the comprehension of the AD underlying pathology, hopefully opening the way to a more accurate disease marker than atrophy or metabolism alone or suggesting novel therapeutic strategies to improve the resilience of the brain to neurodegenerative damage.

In a recent paper [9] we have investigated the functional compensation mechanism in AD in terms of perfusion. As FDG-PET imaging has higher resolution, provides better accuracy, and has been proved to have more diagnostic value than SPECT, especially at earliest stages [10], it is worthwile to investigate atrophy-functional loss mismatch in terms of metabolism. Up to now, there is only one PET study investigating the metabolic compensation mechanism in AD [6], finding hypometabolism significantly exceeding atrophy in most altered structures, mainly in the posterior cingulate, while atrophy exceeding hypometabolism in the amygdala.

Aim of this study is then to investigate metabolic compensation and depression in AD, providing evidence for previous findings based on an independent sample and using a novel image analysis approach.

Materials and Methods

AD patients.

AD patients were taken from the Outpatient Memory Clinic of the IRCCS S. Giovanni di Dio Fatebenefratelli among those coming to observation for the differential diagnosis of cognitive impairment and enrolled in a longitudinal project ("Longitudinal Cognitive Project in Brescia, PCLBs"). The study protocol was approved by the local ethics committee and the study was performed in accordance with the ethical standards laid down in the 1964 Declaration of Helsinki. All partecipants signed an informed

participation consent prior to their inclusion in the study. None of the patients had: (i) age of 90 years and older; (ii) history of depression or psychosis of juvenile onset; (iii) history or neurological signs of major stroke; (iv) alcohol abuse; (v) craniocerebral trauma; (vi) heavy use of psychotropic drugs.

All patients underwent: (i) semi-structured interview with the patient and – whenever possible – with another informant (usually the patient's spouse or a child) by a geriatrician; (ii) general medical and neurological examinations; (iii) performance-based tests of physical function, gait and balance; (iv) cognitive assessment including neuropsychological tests for short and long term memory; Digit Span; Spatial Span; Story Recall; Rey-Osterrieth Complex Figure Recall; attention and executive functions (Trail Making Test B-A); Clock Drawing Test; abstract reasoning (Raven Colored Progressive Matrices); language (Phonological and Semantic fluency; Token test), and apraxia and visuo-constructional abilities (Rey-Osterrieth Complex Figure, Copy) [11]; (v) assessment of depressive symptoms with the Center for Epidemiologic Studies Depression Scale (CES-D [12]); (v) routine blood drawing, aimed to exclude somatic or dysmetabolic diseases which could explain, at least in part, the cognitive impairment; (vi) electrocardiogram (ECG), aimed to cardiac conduction and rhythm disorder; (vii) high resolution MRI; (viii) FDG-PET scan; and (ix) lumbar puncture, aimed to assess beta-amyloid and tau levels in the cerebrospinal fluid (CSF). This comprehensive set of diagnostic was aimed to accurate diagnosis.

Among all outpatients, we considered those diagnosed as AD according to clinical diagnostic criteria [13]. As some could not undergo MR scan due to pacemaker or metallic prosthesis or did not have MR imaging of adequate quality, and others did not agree to undergo PET scan, we included in the current study just AD patients with both PET and good quality MR scans (n=25, age=73±6, 22 females).

Control subjects.

We recruited volunteers among patients' spouses, friends of them, and researchers' acquaintances aged 60 years or older. We explained the aims and methods of the study, approved by the local ethics committee, and asked them to take part to the study after signing an informed consent. Control subjects underwent multidimensional assessment including clinical, neurological and neuropsychological evaluations (investigating memory, executive functions, language and apraxia), and drawing of a blood sample. They also underwent both high resolution MRI and FDG-PET scan. A

priori exclusion criteria were any of the following: history of TIA or stroke, head trauma, alcohol and substance abuse, cortico-steroid therapy, and loss of weight greater than 5 kilograms in the last 6 months. A posteriori exclusion criteria included: MR scan showing brain mass, high white matter hyperintensities load, aneurysm larger than 10 mm, arteriovenous malformations (except for developmental venous anomaly), malformations of the central nervous system, and cognitive impairment on neuropsychological testing.

All MRI and FDG-PET scans of enrolled subjects were rated as normal on visual assessment by a neuroradiologist and a nuclear physician, respectively. Only subjects with both MR and PET images of adequate quality were further considered (n=21, age=67±5, 11 females).

Table 1: Sociodemographic and clinical features of control subjects and AD patients

	Control subjects N=21	AD patients N=25	p
Sociodemographic features			
Age, years	67±5	74±6	0.002
Gender, women	11 (52%)	22 (88%)	0.003
Education, years	11±6	5±3	<0.005
Cognitive and mental features			
Mini Mental State Exam	28.4±2.4	17.7±5.4	<0.005
Disease duration (months)	---	37±26	---
Physical health			
Hypertension	6 (29%)	10 (40%)	0.360
Diabetes	0 (0%)	3 (12%)	0.094
Heart disease	3 (14%)	4 (16%)	0.826
Brain structural features			
Medial temporal atrophy	0.7±0.7	2.6±0.6	<0.005
Subcortical cerebrovascular disease	1.2±1.7	4.6±5.2	0.019

Medial Temporal Atrophy (MTA) was estimated with Scheltens rating scale [35] and subcortical cerebrovascular disease with the Age-Related White Matter Changes (ARWMC) scale [36].
p denotes difference significance among all groups on $\chi 2$ test (categorical variables, i.e. sex, hypertension, diabetes and heart disease), independent t-test (continuous variables) or Kruskal-Wallis test (ordinal non-continuous variables, i.e. MTA and ARWMC scores).

Table 2: Neuropsychological tests scores corrected by age and education for control subjects and AD patients.

		Control subjects N=21	AD patients N=25	p
Memory				
Story Recall		14.7±3.6	5.0±4.0	<0.005
Rey-Osterrieth Complex Figure, Recall		18.7±6.4	5.1±4.7	<0.005
Digit span		5.8±0.9	4.8±1.6	0.021
Spatial span		5.7±1.0	4.0±1.1	<0.005
Executive and frontal functions				
Trail-Making Test B-A		27±50	210±44	<0.005
Raven Colored Progressive Matrices		33.4±2.8	21.0±6.0	<0.005
Language				
Verbal Fluency	phonemic	37.8±10.5	24.6±10.7	<0.005
	semantic	45.8±8.7	26.0±8.9	<0.005
Token test		32.6±1.1	26.2±5.1	<0.005
Apraxia				
Rey-Osterrieth Complex Figure, Copy		32.6±5.9	18.6±10.4	<0.005

All test scores are corrected by age and education
p denotes difference significance among all groups on independent t-test.

PET scan

Both AD patients and control subjects underwent PET scan in the nuclear medicine department of the Spedali Civili hospital, Brescia. [18F] FDG-PET scan was acquired using a 24 rings General Electric 3D PET/CT device (GE Discovery ST PET with GE Light Speed CT; isotropic resolution of 5.99 mm; 15.7 cm axial FOV; 70 cm transaxial FOV). Subjects had been fasting for at least 4 hours before scanning, and blood glucose level was checked to be lower than 120 mg/dl. To minimise anxiety, the PET procedure was explained in detail beforehand.

A catheter was introduced in an antecubital vein, and 10 minutes later the patient received intravenously 150-185 MBq of [18F]FDG, according to the guidelines of the European Association of Nuclear Medicine [14], while sitting in an armchair in a dimly lit room with eyes opened. After 30-45 minutes in the resting condition the subject was positioned on the scanner bed with her head immobilized by a customized head holder.

[18F]FDG uptake was measured in the resting condition with closed eyes and PET images were acquired over 8-12 min (200 mil counts). CT-based attenuation correction was performed (CTAC). Images were reconstructed using the FORE-Iterative algorithm (48 subsets, 5 iterations) with xy and z filter cut off of 4 mm, yielding 128x128 matrix with a pixel size of 2.34 mm. PET image was exported in DICOM format using Xeleris software.

PET processing protocol.

To achieve a precise normalization, we generated a study-specific PET template using both PET and MR scans of all patients and control subjects under study, following a procedure described in detail elsewhere [15,16]. The creation of a study-specific template allows for better normalisation, since low uptake in ventricular structures and cortical hypometabolism effects frequently present in elderly patients are accounted for.

For each coregistered PET scan, we set origin to the anterior commissure with SPM2 [17], using the pertinent MR image as a reference, and we processed all scans with SPM2 according to an optimized processing protocol originally developed for SPECT and described in detail elsewhere [9,15,16]. Briefly, we normalised PET data through a double-stage spatial normalisation, we masked to remove scalp-facial activity and we smoothed them at 12mm FWHM.

MR imaging

Both AD patients and control subjects underwent brain T1-weighted magnetic resonance imaging in the neuroradiology department of the Città di Brescia Hospital, Brescia, as previously discussed [15,16]. MR images were processed with SPM2 following an optimized Voxel-Based Morphometry protocol, described in detail elsewhere [18]. Briefly, customised prior probability maps were computed for GM, WM and CSF [2]. The original MR images were normalised to a customised high resolution MR template [15] through affine and nonlinear transformations, they were segmented into GM, WM and CSF using the customised priors, masked to remove non-brain tissue voxels, modulated, and finally smoothed with a 12mm isotropic Gaussian kernel [19]. Only GM images were further used in the statistical analysis.

Statistical Analysis

Atrophy and hypometabolism. We investigated the significance of the difference between AD patients and control subjects in sociodemographic and clinical features

and in neuropsychological tests scores using X2 test for categorical variables (sex, hypertension, diabetes, and heart disease), unpaired t-test for continuous variables, and Kruskal-Wallis test for ordinal non-continuous variables (medial temporal atrophy andwhite matter hyperintensity scores). In all cases we set the significant threshold at $P<0.05$.

We assessed differences in glucose metabolism between AD patients and control subjects voxel-wise using SPM2, setting the significant threshold at $p<0.05$ corrected for false discovery rate (FDR). We used age as confounding variable, and we scaled all preprocessed PET scans to the cerebellum to remove inter-subject global variations in PET intensities, setting to 50 the mean count in all cerebellums.

Similarly, we assessed grey matter atrophy in AD patients as compared to control subjects, setting the significant threshold at $p<0.05$ FDR corrected, and entering age and total intracranial volume (TIV) as confounding variables.

Metabolic compensation and depression. To investigate the relationship between GM atrophy and hypometabolism we used the Biological Parametric Mapping (BPM) software [20] for multimodality brain image analysis.

We compared AD patients with control subject PET scans using ANCOVA, including age as scalar regressor and the pertinent GM images as imaging regressor, and we obtained a map of metabolic depression (hypometabolism exceeding atrophy). Similarly, we compared GM images using ANCOVA, including age and TIV as scalar and PET scans as imaging regressors, and we obtained a map of metabolic compensation (atrophy exceeding functional deficit).

As BPM relies on SPM for visualisation and statistical inference, we used SPM2 to restrict the two maps to significant values ($p<0.05$ FDR corrected). We further masked the results with a customised binary GM mask, obtained by thresholding at 0.1 the 5 mm FWHM smoothed GM map of the control subject with the highest quality MRI.

We finally repeated all the analysis using a different method, based on masking procedures, specifically developed for visualising functional compensation and depression, and published recently [9]. Despite BPM is statistically more reliable, this other method is still valid for the visualisation of the results, thus enabling to double-check the findings.

Results

Table 1 shows that AD patients significantly differed from control subjects in age, gender (AD patients were seven years older than control subjects, on average, and women were the great majority) and education, in Mini Mental State Exam, medial temporal lobe atrophy and age-related white matter changes. They did not differ for any physical health feature.

As far as neuropsychological test (Table 2), AD significantly differed from control subjects in all neuropsychological domains, on all administered tests.

Figure 1: AD atrophy map, expressed in terms of t-scores: the higher is the t-score, the more significant is the GM volume reduction, i.e. GM atrophy. The pattern of GM atrophy involved the temporoparietal and medial temporal lobes, insular regions and retrosplenial cortex bilaterally. Only regions of significant atrophy ($p<0.05$ FDR corrected) are shown in the figure

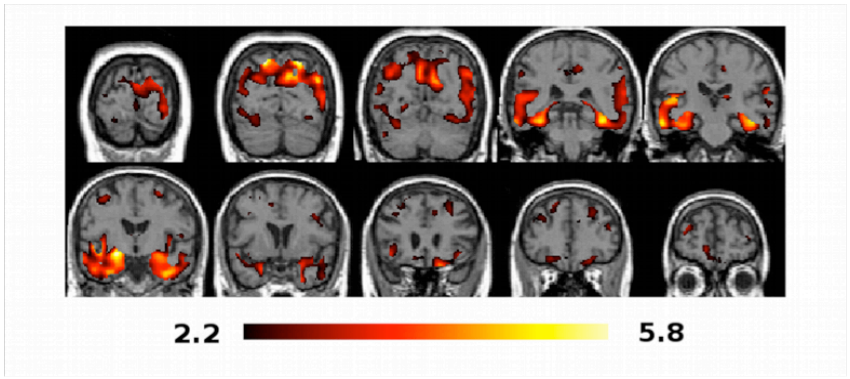

Figure 2: AD hypometabolism map, expressed in terms of t-scores. Significant GM hypometabolism was mainly located in the posterior cingulate cortex, in the inferior, medial temporal and temporoparietal lobes and, to a smaller extent, in the insula and restricted regions of the frontal lobe. Only regions of significant hypometabolism ($p<0.05$ FDR corrected) are shown in the figure

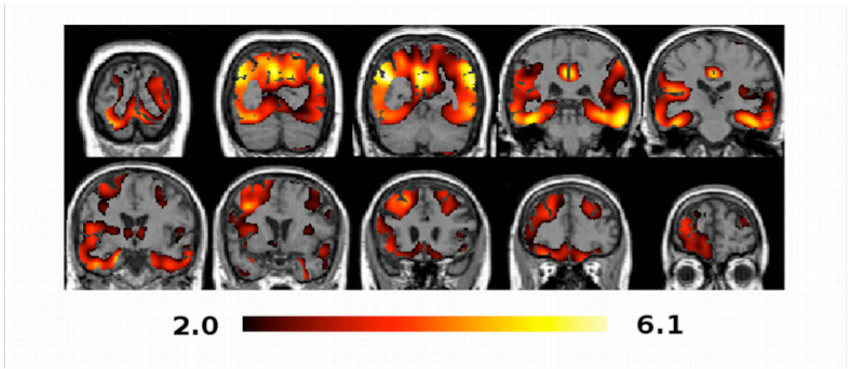

Figure 1 shows the pattern of GM atrophy in AD, expressed in terms of t values: temporoparietal and medial temporal lobes, insular regions and retrosplenial cortex bilaterally were found to be atrophic, as expected.

Similarly, figure 2 shows the pattern of significant GM hypometabolism in AD: reduced metabolism was mainly located in the retrosplenial cortex (BA 26, BA 29) and other areas of the posterior cingulate cortex, in the inferior, medial temporal, and temporo-parietal lobe, and, to a smaller extent, in the insula and restricted regions of the frontal lobe.

Figure 3: AD metabolic compensation map, obtained through BPM. Only significant regions ($p<0.05$ FDR corrected), located in the bilateral amygdala, mainly on the left side, are shown in the figure. The red arrow points to the small significant cluster located in the right amygdala, in order to make it notable

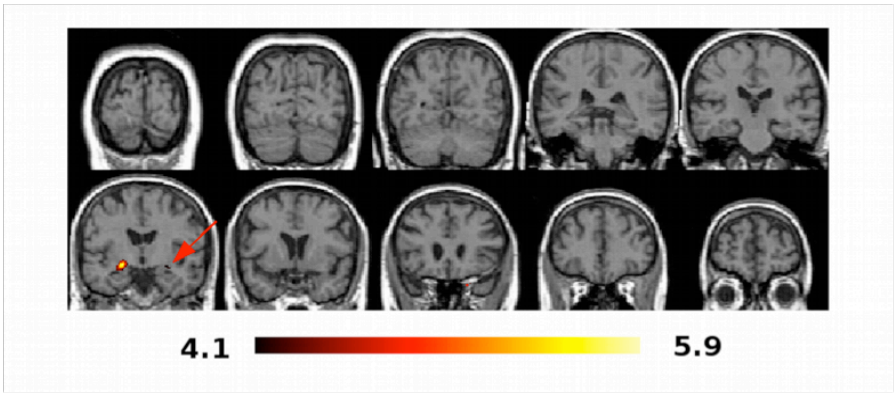

Figure 4: AD metabolic depression map, obtained through BPM. Only significant regions ($p<0.05$ FDR corrected), mainly located in the posterior cingulate cortex, in the inferior, medial temporal, and frontal lobes, are shown in the figure

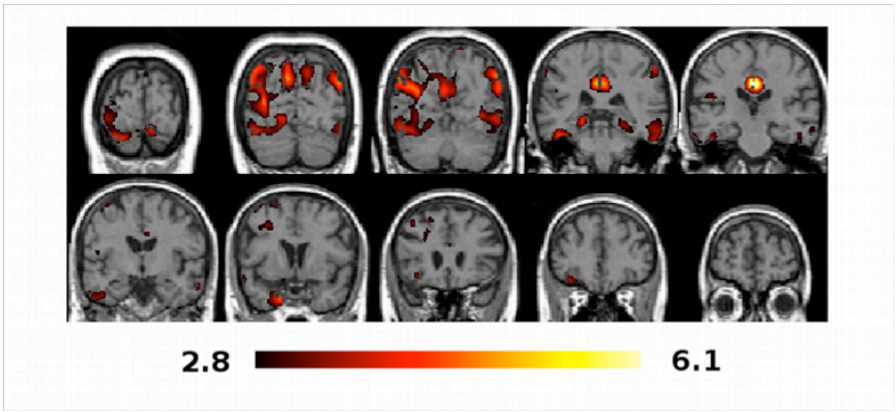

We found metabolic compensation in the amygdala bilaterally, mainly on the left side (Figure 3), while exceeding hypometabolism was mainly located in the retrosplenial cortex (BA 26, BA 29), in other areas of the posterior cingulate cortex and, to a smaller extent, in the inferior, medial temporal, and frontal lobes (Figure 4).
The additional analysis based on the masking procedure [9] confirmed the results obtained using BPM, showing pretty similar patterns of mismatch (data not shown).

Discussion

In this study we investigated the mismatch between atrophy and hypometabolism, in terms of metabolic compensation and depression, in AD using a voxel-based method. We found that GM atrophy and hypometabolism mapped to similar regions with variable degrees of severity. We found metabolic compensation in the amygdala, mainly on the left side, while metabolic depression mainly located in the posterior cingulate cortex.

GM atrophy and hypometabolism. GM atrophy and hypometabolism mapped to temporoparietal, retrosplenial, and medial temporal regions, as expected from the current knowledge about AD neuropathology and previous MR and PET findings throughout the last 20 years. Consistently with the notion that in AD functional antedate structural changes [21], we found a metabolic deficit more widespread than atrophy.

Metabolic compensation and depression. Several combined SPECT/PET and MR studies have investigated structural and functional changes, showing that GM tissue loss in AD is not the only responsible for functional reduction [6,9]. To further investigate the relationship between GM loss and hypometabolism, we used the BPM software for multimodality brain image analysis [20]: we found significant compensation (atrophy exceeding hypometabolism) in the amygdala, mainly on the left side; we found significant hypometabolism exceeding atrophy, denoting metabolic depression, mainly located in the posterior cingulate cortex and, to a smaller extent, in the inferior, medial temporal, and frontal lobes. These results are in good agreement with those reported in a recent PET study [6], finding hypometabolism significantly exceeding atrophy in most altered structures, mainly posterior cingulate, and atrophy exceeding hypometabolism in the amygdala. Our findings are also in line with a previous FDG-PET study [22] showing functional depression in parieto-temporal and

posterior cingulate regions, and disproportionate atrophy in the medial temporal lobe, and with two recent fMRI studies, finding decreased activation exceeding atrophy in early AD in the posterior cingulate cortex and precuneus [23], and preserved medial temporal activation, indicative of a compensatory capacity, in memory impairment [24].

As compared to compensation and depression patterns previously assessed in terms of perfusion [9], metabolic patterns partially overlap and partially do not. The discrepancy could reflect an existing divergence between defects of perfusion and glucose metabolism, which are correlated, but not always concurrent phenomena. However, there are several differences among the two studies which make the comparison of the results unreliable: perfusional and metabolic compensation were assessed on AD patients with different disease severity (MCI with preclinical AD for blood perfusion and moderate AD for glucose metabolism); FDG-PET imaging has higher resolution and provides better accuracy than SPECT [10]; PET and SPECT images highly depend on tracer used [25].

Metabolic compensation and depression: possible explanations. Metabolic depression in AD could be due to distant effects of atrophy on glucose metabolism, in part reflecting remote effects from the atrophied hippocampi [26], connected to the posterior cingulate through the cingulum bundle [26,27]. Furthermore, beta-amyloid protein has been shown to play a key role in the modulation of synaptic plasticity [28-30], and could thus cause synaptic dysfunction even in the absence of detectable atrophy [31]. Conversely, tau neurofibrillary tangles, seem to mainly cause cellular death rather than synaptic damage, thus leading to grey matter loss [31,32]. In the posterior cortical regions, denoted by greater amyloid than tau deposition, synaptic damage but neurons survival might occur, thus causing high hypometabolism but low atrophy. Conversely in the medial temporal lobe, denoted by higher tau deposition, the surviving neurons might have residual synaptic plasticity that could lead to compensatory synaptic sprouting and increased metabolism [33].

Strengths and limitations. Since native images and the customised PET and MR templates were coregistered, all normalised PET and MR images, as well as atrophy and hypometabolism maps themselves, were coregistered and could be reliably compared on a voxel-by-voxel level in order to study the relationship between the two processes.

We believe that the main strength of this study lies in the methodology used, which is simple, precise and less time consuming than methods previously used to investigate the relationship between structural and functional damage. BPM [20] is based on a voxel-wise general linear model, and enables to incorporate information obtained from other modalities as regressors in the analysis. Unlike standard voxel-based analysis tools based on the general linear model, such as SPM, in a BPM analysis each voxel has its own design matrix, with both scalar (e.g. age) and imaging voxel-specific (e.g. grey matter density) regressors. Hypometabolism detected after removing the variability due to GM intensity was interpreted as metabolic deficit, while GM atrophy detected after removing variability due to metabolism was considered as indicative of metabolic compensation. As BPM was originally developed for multimodal analysis of structural and functional MRI images, the current study represents the first application of BPM to the analysis of MR and FDG-PET data.

One of the limitations to be considered in the interpretation of the results is that control subjects were not matched for age, gender nor education compared to AD patients. Such differences could have potentially introduced a level of variance between the two groups which, although much lower than that due to the disease, could have partially influenced the results. In order to address this issue we found an age-matched subsample and a gender-matched one (age and sex likely being the main source of variability, beyond disease) and we repeated all the analysis in the two cases: new results pretty confirmed the original ones (in spite of decrease in significance, due to smaller sample size and to consequent statistical power reduction), showing that difference in either age or sex between the two groups, despite being significant, do not significantly influence the results. Age and sex-matched groups of adequate size would be needed to refine the analysis. To blur individual variations in gyral anatomy and increase the signal-to-noise ratio, all processed GM images and PET scans were smoothed using the standard Gaussian kernel of 12mm. Since the two data sets to be compared had different original spatial resolution, differential smoothing should be performed to obtain images of equivalent effective smoothness, and thus of identical resultant resolution; however, previous studies showed that the dimensions of the smoothing filters to be used for different data sets are really similar [6].

Future directions. The procedure presented in this paper to investigate the relationship between GM atrophy and hypometabolism has several others potential

applications of interest. It could be used to assess functional compensation at different stages of Alzheimer's disease, in order to map the time course of functional brain failure, hopefully opening the way to a more accurate disease marker than atrophy or metabolism alone or suggesting novel therapeutic strategies to improve the resilience of the brain to the neurodegenerative damage. Atrophy and metabolism patterns are expected to differ most at the earliest stages of the disease, and to converge more and more as the disease progresses. Moreover, the same methodology could be used to investigate functional compensation in other neurodegenerative diseases not due to amyloid deposition, such as fronto-temporal or Lewy body dementia.

References

1. Frisoni GB, Testa C, Zorzan A, et al. Detection of grey matter loss in mild Alzheimer's disease with voxel based morphometry. J Neurol Neurosurg Psychiatry 2002; 73:657-664.
2. Good CD, Scahill RI, Fox NC, et al. Automatic differentiation of anatomical patterns in the human brain: validation with studies of degenerative dementias. Neuroimage 2002; 17:29-46.
3. Karas GB, Burton EJ, Rombouts SA, et al. A comprehensive study of grey matter loss in patients with Alzheimer's disease using optimized voxel-based morphometry. Neuroimage 2003; 18:895-907.
4. Matsuda H, Kitayama N, Ohnishi T, et al. Longitudinal evaluation of both morphologic and functional changes in the same individuals with Alzheimer's disease. J Nucl Med 2002; 43:304-311.
5. Anchisi D, Borroni B, Franceschi M, et al. Heterogeneity of Brain Glucose Metabolism in Mild Cognitive Impairment and Clinical Progression to Alzheimer Disease. Arch Neurol 2005; 62:1728-1733.
6. Chetelat G, Desgranges B, Landeau B, et al. Direct voxel-based comparison between grey matter hypometabolism and atrophy in Alzheimer's disease. Brain 2008; 131:60-71.
7. Foster NL, Chase TN, Mansi L, et al. Cortical abnormalities in Alzheimer's disease. Ann Neurol 1984; 16:649–654.
8. Mosconi L. Brain glucose metabolism in the early and specific diagnosis of Alzheimer's disease. Eur J Nucl Med Mol Imaging 2005; 32:486-510.
9. Caroli A, Geroldi C, Nobili F, et al. Functional compensation in incipient Alzheimer's disease. Neurobiol Aging 2010; 31:387-397.
10. Dobert N, Pantel J, Frolich L, Hamscho N, Menzel C, Grunwald F. Diagnostic value of FDG-PET and HMPAO-SPET in patients with mild dementia and mild cognitive impairment: metabolic index and perfusion index. Dement Geriatr Cogn Disord 2005; 20:63-70.
11. Lezak M, Howieson D, Loring DW. Neuropsychological Assessment (fourth edition). Oxford: University Press 2004
12. Radloff LS. The CES-D scale: A self-report depression scale for research in the general population. Appl Psychol Measure 1997; 1:385-401.
13. McKhann G, Drachman D, Folstein M, Katzman R, Price D, Stadlan EM. Clinical diagnosis of Alzheimer's disease: report of the NINCDS-ADRDA Work Group under the auspices of Department of Health and Human Services Task Force on Alzheimer's Disease. Neurology 1984; 34:939-944.
14. Bartenstein P, Asenbaum S, Catafau A, et al; European Association of Nuclear Medicine. European Association of Nuclear Medicine Procedure Guidelines for Brain Imaging using [18F]FDG. Eur J Nucl Med 2002; 29:BP43–BP48.
15. Caroli A, Testa C, Geroldi C, et al. Brain perfusion correlates of medial temporal lobe atrophy and white matter hyperintensities in mild cognitive impairment. J Neurol 2007; 254:1000-1008.
16. Caroli A, Testa C, Geroldi C, et al. Cerebral perfusion correlates of conversion to Alzheimer's disease in amnestic mild cognitive impairment. J Neurol 2007; 254:1698-1707.
17. SPM, Statistical Parametric Mapping (computer program). Version 2: Functional Imaging Laboratory, 2002. Available at http://www.fil.ion.ucl/ac.uk/spm/software/spm2
18. Frisoni GB, Testa C, Sabattoli F, Beltramello A, Soininen H, Laakso MP. Structural correlates of early and

late onset Alzheimer's disease: voxel based morphometric study. J Neurol Neurosurg Psychiatry 2005; 76:112-114.

19. Ashburner J, Friston KJ. Why voxel-based morphometry should be used. Neuroimage 2001; 14:1238–43
20. Casanova R, Srikanth R, Baer A, et al. Biological parametric mapping: A statistical toolbox for multimodality brain image analysis. Neuroimage 2007; 34:137-143.
21. Small AS: Alzheimer disease, in living color. Nature Neuroscience 2005; 8:404-405.
22. Samuraki M, Matsunari I, Chen WP, et al. Partial volume effect-corrected FDG PET and grey matter volume loss in patients with mild Alzheimer's disease. Eur J Nucl Med Mol Imaging 2007; 34:1658-1669.
23. He Y, Wang L, Zang Y, Tian L, Zhang X, Li K, Jiang T. Regional coherence changes in the early stages of Alzheimer's disease: a combined structural and resting-state functional MRI study. Neuroimage 2007; 35:488-500.
24. Miller SL, Celone K, DePeau K, et al. Age-related memory impairment associated with loss of parietal deactivation but preserved hippocampal activation. Proc Natl Acad Sci USA 2008; 105:2181-2186.
25. Koyama M, Kawashima R, Ito H, et al. SPECT imaging of normal subjects with Technetium-99m-HMPAO and Technetium-99m-ECD. J Nucl Med 1997; 38:587-592.
26. Villain N, Desgranges B, Viader F, et al. Relationships between hippocampal atrophy, white matter disruption, and grey matter hypometabolism in Alzheimer's disease. J Neurosci 2008; 28:6174-6181.
27. Schmahmann JD, Pandya DN, Wang R, et al. Association fibre pathways of the brain: parallel observations from diffusion spectrum imaging and autoradiography. Brain 2007; 130:630-653.
28. Hu NW, Smith IM, Walsh DM, Rowan MJ. Soluble amyloid-beta peptides potently disrupt hippocampal synaptic plasticity in the absence of cerebrovascular dysfunction in vivo. Brain 2008; 131:2414-2424.
29. Rowan MJ, Klyubin I, Wang Q, Hu NW, Anwyl R. Synaptic memory mechanisms: Alzheimer's disease amyloid beta-peptide-induced dysfunction. Biochem Soc Trans 2007; 35:1219-23.
30. Shankar GM, Li S, Mehta TH, et al. Amyloid-beta protein dimers isolated directly from Alzheimer's brains impair synaptic plasticity and memory. Nat Med 2008; 14:837-842.
31. Josephs KA, Whitwell JL, Ahmed Z, et al. Beta-amyloid burden is not associated with rates of brain atrophy. Ann Neurol 2008; 63:204-212.
32. Whitwell JL, Josephs KA, Murray ME, et al. MRI correlates of neurofibrillary tangle pathology at autopsy. A voxel-based morphometry study. Neurology 2008; 71:743-749.
33. Cotman CW, Anderson KJ. Synaptic plasticity and functional stabilization in the hippocampal formation: possible role in Alzheimer's disease. Adv Neurol 1988; 47:313-335.
34. Guevara J, Dilhuydy H, Espinosa B, et al. Coexistence of reactive plasticity and neurodegeneration in Alzheimer diseased brains. Histol Histopathol 2004; 19:1075-1084.
35. Scheltens P, Leys D, Barkhof F, et al. Atrophy of medial temporal lobes on MRI in "probable" Alzheimer's disease and normal ageing: diagnostic value and neuropsychological correlates. J Neurol Neurosurg Psychiatry 1992; 55:967–572.
36. Wahlund LO, Barkhof F, Fazekas F, et al.; European Task Force of Age Related White Matter Changes. A new rating scale for age-related white matter changes applicable to MRI and CT. Stroke 2001; 32:1318–1322.

Chapter 8

General discussion

General discussion

Research is indeed very active in Alzheimer's disease, the most common form of dementia, which currently has no treatment to prevent or slow it. During the last years most of the AD research has been focused on the investigation of the early changes associated with AD, with the aim of identifying novel targets for pharmaceutical intervention which could delay disease progression. A number of AD biomarkers have been identified and validated through the years [1,2]. Among the others, neuroimaging markers have been shown to play a key role, enabling to diagnose and monitor AD in vivo since the earliest stages.

Chapter 2 reviews the main neuroimaging techniques currently available to accurately measure atrophy and subcortical vascular damage (structural imaging), perfusion, metabolism, and default network activity (functional imaging), and amyloid plaque deposition (amyloid imaging) in the brain. Despite some of them being really far from routine clinical practice and used in research only, due to the high technology required, most imaging biomarkers could become more and more helpful in clinics, and could potentially be included in the future in the AD diagnostic pathway. The research criteria for early AD recently formulated by Dubois et al [3] already stipulate that there must be at least one or more abnormal biomarkers, among medial temporal lobe atrophy (assessed on MR), temporo-parietal hypometabolism (assessed on FDG-PET), beta-amyloid (currently assessed by lobar puncture, and potentially assessed by amyloid imaging), and tau protein, beyond a clinical core of early and significant episodic memory impairment, further pointing out the relevance of imaging biomarkers in the early diagnosis of AD.

According to Dubois criteria even just one validated biomarker would be sufficient to diagnose AD. However, none of the proposed biomarkers has been adequately validated yet and a unique reliable biomarker still needs to be identified. As single imaging techniques enable to study single cerebral alterations, different techniques should be combined in order to investigate the overall cerebral damage. There is considerable promise that early and specific diagnosis of AD will be rendered possible through the identification of a specific overall "signature" of the disease, based on the combination of all available biomarkers.

A few studies have already tried to combine AD biomarkers, showing an increase in prognostic power [4,5] and diagnostic accuracy [6], but much work still needs to be

done to assess the relationship between different biomarkers.

Within this context, this thesis focuses on imaging, investigating the relationship between different imaging modalities using several multimodal analysis techniques. In particular, this thesis points attention to the imaging markers at the most advanced stage of validation: structural MRI, measuring cerebral atrophy, which can be considered a valid biomarker of neurodegeneration [7,8]; SPECT and FDG-PET, measuring cerebral perfusion and glucose metabolism, respectively, being valid indicators of the synaptic dysfunction that accompanies neurodegeneration [9-12]; and PIB uptake on PET, a valid biomarker for brain Aβ plaque load [13,14].

Clinical implications

Chapter 3 deals with the relevant clinical need of identifying MCI patients who will progress from those who will not. MCI represents an intermediate clinical state between the cognitive changes of aging and the very earliest features of Alzheimer's disease, with intermediate neuropathologic changes [15,16]. Moreover, about 50% of patients with MCI develop AD within 5 years [17]. Predicting AD at a preclinical stage would make it possible to implement strategies to prevent or delay dementia; furthermore, early therapeutical interventions are more likely to be effective. The study points out the prognostic relevance of both structural and functional neuroimaging since the preclinical stages, showing both significant hypoperfusion and significant atrophy in amnestic MCI converted to AD mainly located in the inferior and medial temporal lobe, in agreement with previous findings [18-21] and neurobiological knowledge [22,23]. Beyond this primary result, the study finds no overlap between hypoperfusion and atrophy patterns, suggesting that hypoperfusion is not due to volumetric loss only. The study separately investigates cerebral perfusion and atrophy correlates of conversion. However, predicting conversion to dementia is a multimodal task. The combination of several predictive markers from different fields of research could enable to increase the overall sensitivity and therefore the diagnostic accuracy of predicting conversion to dementia.

Chapter 4 studies the relationship between structural and functional damage in MCI patients. The investigation of the relationship between different alterations occurring in the brain from the earliest stages of the disease could enable to better understand the mechanisms that trigger the disease onset and drive its progression, to increase early

diagnostic accuracy and to lead to the identification of novel targets for pharmaceutical intervention which could delay disease progression. The study shows that both the neuropathological damage of AD in the medial temporal lobe and the white matter damage due to hypertensive or diabetic small vessel disease, previously reported in MCI [24-26] and often co-occurring in oldest patients, lead to reduced cerebral perfusion: medial temporal atrophy is associated with relevant local functional changes, while white matter hyperintensities are associated with remote cortical brain dysfunction. The study further suggests that not only in fully developed AD (as previously reported [27-29]) but also in earliest stages there is a significant correlation between biological severity of the disease (assessed by MTA rating) and hippocampal hypoperfusion.

Chapter 5 studies the local toxicity of amyloid deposition in AD, in terms of topographic relationship with grey matter atrophy. This relationship has relevant implications on current clinical trials with antiamyloid drugs, as brain atrophy is widely used as surrogate outcome in clinical trials of drugs that might delay or arrest AD progression [30] and, on the other hand, most current disease-modifying drugs for AD have been developed under the assumption that cognitive deterioration is due to amyloid deposition and that slowing or arresting amyloid deposition will lead to slowing or arresting cognitive deterioration [31]. Greater amyloid deposition was generally not associated with more severe grey matter atrophy except in the medial temporal lobe, in agreement with previous studies showing no relationship between synaptic integrity and amyloid deposition [32] and pathological data showing a correlation between amyloid load in the medial temporal lobe and cognitive performance [33]. Medial temporal lobe was among the regions with the lowest amount of amyloid deposition, indicating that different types of amyloid may deposit in the brain, different brain regions may be differentially susceptible to its toxic effects, or amyloid may be peripheral to neurodegeneration.

Chapter 6 and 7 investigate functional compensation and depression in terms of perfusion and glucose metabolism, respectively. A better understanding of compensatory mechanisms, taking into account the overall cerebral alteration rather than any specific structural or functional damage, could help to go more deep into the comprehension of the AD underlying pathology, hopefully opening the way to a more accurate disease marker than atrophy or perfusion and metabolism alone or

suggesting novel therapeutic strategies to improve the resilience of the brain to neurodegenerative damage. Chapter 6 investigates the relationship between structural and perfusional loss in incipient AD with a special focus on the regions affected by AD neuropathology, finding relatively preserved perfusion, indicative of compensation in the setting of neuronal loss, in the neocortex, and functional depression in the medial temporal lobe. A compensatory response to the beginning of AD pathology has been previously reported in terms of fMRI activation and hyperperfusion [34-36]. The neocortical perfusional compensation could reflect hyperperfusion due to vasodilation induced either by vasodilator agents (such as nitric oxid) released by the neuropathologically damaged tissue or by cholinergic neurons [37]. On the contrary, perfusional depression exceeding atrophy occurs in the medial temporal lobe as in this area, primarily affected by AD, the microcircle functional reserve was over. Chapter 7 investigates functional compensation and depression in terms of glucose metabolism in a cohort of mild AD patients, finding that GM atrophy and hypometabolism map to similar regions with variable degrees of severity, metabolic compensation is located in the amygdala, mainly on the left side, while metabolic depression is mainly located in the posterior cingulate cortex, in line with previous findings [38,39]. Metabolic depression can be due both to distant effects of atrophy and to additional hypometabolism-inducing factors, such as amyloid deposition. Conversely, metabolic compensation could reflect spared synaptic plasticity of the surviving neurons.

At a first glance, functional compensation and depression patterns presented in chapter 6 and 7 seem to be inconsistent. The discrepancy could reflect an existing divergence between defects of perfusion and glucose metabolism, which are correlated, but not always concurrent phenomena: metabolism is likely to be affected by the disease earlier than perfusion, as the biochemical mechanism leading up to progressive neuronal loss inducing local hypometabolism preceeds vessels damage. Moreover, there are several differences among the two studies which make the comparison of the results unreliable: perfusional and metabolic compensation were assessed on AD patients with different disease severity (preclinical AD for blood perfusion and mild to moderate AD for glucose metabolism); FDG-PET imaging has higher resolution and provides better accuracy than SPECT [40]; finally, PET and SPECT images highly depend on tracer used [41]. Despite all differences, both studies point out a compensatory mechanism taking place in the brain, trying and

counteracting the pathological changes of AD.

Some limitations should be taken into account in the interpretation of the results presented throughout this thesis. In the two studies involving AD patients (chapter 5 and 7) healthy controls were not matched for age and gender compared to AD patients, mainly due to the difficulty of finding out healthy elderly people willing to undergo SPECT/PET scan for research purposes. Such differences could have potentially introduced a level of variance between the two groups which, although much lower than that due to the disease, could have partially influenced the results. All studies included in this thesis involve relative small groups of patients and normal controls; larger groups would be needed to confirm the present results.

Methodological issues

In the studies presented in this thesis several methodologies have been adopted to measure atrophy, subcortical vascular damage, perfusion, glucose metabolism and PIB uptake, ranging from simple visual rating scales (the subjective medial temporal lobe atrophy [42] and age-related white matter changes [43] scales used in Chapter 4) to ROI-based methods (used in Chapter 5 to assess grey matter atrophy and PIB uptake in specific regions of interest) to more sophisticated automatic methods (voxel-based analysis by statistical parametric mapping [44] used in Chapters 3-8).

Beyond already in use image analysis techniques, there are a number of methods which have been developed specifically for this research project.

Chapter 4 introduces a novel optimised SPECT processing protocol. Prior to processing, each SPECT was coregistered to the pertinent MR image. A study-specific high resolution sixth generation MR template was generated using an iterative procedure. A study-specific SPECT template was generated averaging SPECT scans of patients under study, normalised to the MR template. SPECT scans were than spatially normalised to the SPECT customised template using a non linear two-step normalisation, in which the normalisation (first affine and then non-linear) parameters were assessed on smoothed images and applied to non-smoothed ones. SPECT customised template, generated using scans of patients under study, enables to account for central and cortical hypoperfusion effects frequently present in elderly patients. Moreover, the initial coregistration with MR scans and the usage of MR images during the SPECT template generation enable to improve the definition of the template, accounting for

anatomical definition. The two-step normalisation procedure enables to reach an accurate normalisation without introducing any blurring and thus without loosing any definition. Hypoperfusion patterns found in incipient AD patients, mainly involving the medial temporal and temporo-parietal lobes (chapter 3 and chapter 6), are in line with previous findings [45-48], proving the validity of the non-standard SPECT processing method proposed.

The optimised processing protocol developed for SPECT could be applied to PET images as well, and was further adopted to process both FDG-PET (chapter 7) and PIB-PET (chapter 5).

This preprocessing procedure enables to reliably compare functional and structural loss patterns assessed through SPM on a voxel-by-voxel basis: since native SPECT/PET scans were coregistered to their respective MR images, and the study-specific SPECT/PET template was coregistered to the high-definition MR template, all the normalised SPECT/PET and MR images used for the statistical analysis were coregistered to the SPM standard anatomical space, so that the hypoperfusion/hypometabolism/increased PIB uptake and grey matter atrophy patterns themselves were coregistered; furthermore, during processing, voxel size was resampled to 2 x 2 x 2 mm for all scans, and the resulting t maps could thus be compared on a voxel-by-voxel level.

Chapter 3 shows that grey matter atrophy and hypoperfusion patterns do not overlap, suggesting that the detected hypoperfusion is not due to volumetric loss only. Chapter 6 introduces a simple but innovative method to compare structural and functional loss on a voxel-by-voxel basis and to visualise functional compensation and depression. Since the regions of functional compensation are denoted by significant atrophy but non significant functional deficit, compensation t map was computed masking the significant grey matter atrophy map with non significant hypoperfusion. Conversely, perfusional depression t map was computed masking the significant hypoperfusion map with non significant atrophy.

Contemporarily with the publication of the study about perfusional compensation and depression in AD (chapter 6), a novel software for multimodality brain imaging analysis (Biological Parametric Mapping, BPM [49]) has been developed and made publicly available. BPM is based on a voxel-wise general linear model, and enables to incorporate in the analysis imaging regressors: unlike standard voxel-based analysis tools based on the general linear model, such as SPM, in a BPM analysis each voxel

has its own design matrix, with both scalar (e.g. age) and imaging voxel-specific (e.g. gray matter density) regressors. Chapter 7 describes the application of BPM to the multimodal analysis of MR and FDG-PET images. Hypometabolism detected after removing the variability due to GM intensity was interpreted as metabolic deficit, while GM atrophy detected after removing variability due to metabolism was considered as indicative of metabolic compensation. As BPM was originally developed for multimodal analysis of structural and functional MRI images, chapter 7 represents the first application of BPM to the analysis of MR and FDG-PET data. BPM is statistically more reliable than the method described in chapter 6 which, however, is still valid for the visualisation of functional compensation and depression; inspite of the large differences, the two methods showed pretty similar patterns of metabolic compensation and depression, further proving their validity.

Beyond the investigation of functional compensation and depression mechanisms, multimodal imaging enables to investigate the regional correlation between different cerebral phenomena. Chapter 5 introduces a method to investigate the voxel-wise correlation between grey matter density and [11C]-PIB uptake: Pearson's r coefficient was computed voxel-wise based on the grey matter atrophy and PIB uptake, a whole brain Pearson's r correlation map was created and voxel-by-voxel significance of the correlation was computed, using a Matlab script written specifically for this purpose. ROI-based correlation analysis confirms the validity of the voxel-based method.

Some methodological limitations should also be considered in the interpretation of this thesis results.

To blur individual variations in gyral anatomy and increase the signal-to-noise ratio, all processed GM images and SPECT/PET scans were smoothed using the standard Gaussian kernel of 12mm. Since the two data sets to be compared had different original spatial resolution, differential smoothing should be performed to obtain images of equivalent effective smoothness, and thus of identical resultant resolution; however, previous studies showed that the dimensions of the smoothing filters to be used for different data sets are really similar [50].

No partial volume effect correction was performed prior to SPECT/PET image analysis. In small atrophied structures such as the hippocampus, PVE could result in weaker signal due to the surrounding CSF, reduced perfusion and metabolism observed actually being an artifact of gray matter atrophy in the medial temporal lobe. However,

several previous studies showed that gray matter loss did not entirely explain the observed hypometabolism [51,52], and this thesis results further prove, by voxel-wise comparing structural and functional loss, that the detected functional reduction was not due to volumetric loss (chapter 3, 4, 6 and 7).

Future directions

The studies presented in this thesis point out the relevance and potential of multimodal imaging in studying the overall cerebral damage beyond single alterations, showing a number of applications and opening the way to several future directions. Multimodal imaging should aim to find out key prognostic indicators of conversion to dementia, early diagnostic markers and reliable indicators of disease progression based on the combination of different imaging techniques.

This thesis introduces several multimodal imaging analysis techniques. All of them were developed for the combined analysis of two imaging techniques; multimodal imaging tools able to manage more than two image modalities at a time need to be developed. Beyond the combination of imaging techniques only, it would be relevant to combine biomarkers from different fields of research, both imaging and not (e.g. memory performance on comprehensive neuropsychological tests, and concentrations of tau protein in the CSF). Multimodal analysis of imaging and non imaging information could help to identify novel combined markers, more accurate than each of the markers alone.

Further studies with larger groups of patients are needed to confirm the different hypotheses likely explaining the mismatch between grey matter atrophy and PIB uptake observed in chapter 5 (i.e. that different types of amyloid may deposit in the brain, different brain regions may be differentially susceptible to amyloid toxic effects, or that amyloid is peripheral to neurodegeneration), which could have relevant implications on current clinical trials with antiamyloid drugs.

Following up chapter 6 and 7, it would be interesting to assess functional compensation at different stages of the Alzheimer's disease, in order to map the time course of functional brain failure hopefully opening the way to a more accurate disease marker than atrophy or perfusion/metabolism alone or suggesting novel therapeutic strategies to improve the resilience of the brain to the neurodegenerative damage.

Multimodal analysis could be extremely useful in the investigation of the biomarker

dynamics. It has been recently pointed out [53] that biomarkers, reflecting individual aspects of the Alzheimer pathology, develop on their own time course. PIB retention already occurs in normal controls [54], further increases in prodromal AD and is almost stable in time in the clinical phases of the disease [55]; structural changes become appreciable later in the disease process, but correlate with cognitive progression as dementia worsens [54-56]; FDG-PET time course likely lies in between [53]. It would be now extremely important to compare biomarker dynamics, and order biomarker changes in time to express the disease process in terms of a series of testable biological indicators. This would enable to identify biomarkers which could be best used in clinical trials to select patients and measure disease-modifying drug effects, or even be used in future prevention trials. Furthermore, understanding the temporal order of each biomarker would make it possible to use a given marker for staging AD in vivo.

Conclusions

In conclusion, this thesis shows that structural damage, functional alterations, and protein build-up occurring at the cellular level, characterising Alzheimer's disease, are interrelated but not concurrent nor co-localised phenomena.

In particular, in incipient AD hypoperfusion and atrophy patterns do not overlap, and hypoperfusion in the medial and inferior temporal lobe could be considered as a prognostic indicator of conversion to dementia; in MCI, medial temporal lobe atrophy is associated with relevant local functional changes, while white matter hyperintensities seem to be associated with remote cortical brain dysfunction; greater amyloid deposition is generally not associated with more severe grey matter atrophy except in the medial temporal lobes, which might be highly susceptible to amyloid toxicity on the contrary of neocortical areas, which might be more resilient; in AD, grey matter atrophy and functional deficit map to similar regions with variable degrees of severity, functional compensatory mechanism appears to take place against atrophy and neuropathological damage in some regions of the brain, while functional depression exceeding atrophy appears to occur in others.

These results points out the need of using multimodal analysis techniques to further assess the relationship between different biomarkers from the earliest stages, in order to better understand the mechanisms that trigger the disease onset and drive its

progression, to increase early diagnostic accuracy and to lead to the identification of novel targets for pharmaceutical intervention which could delay disease progression.

References

1. Hampel H, Burger K, Teipel SJ, Bokde AL, Zetterberg H, Blennow K. Core candidate neurochemical and imaging biomarkers of Alzheimer's disease. Alzheimers Dement 2008; 4:38-48.
2. Shaw LM, Korecka M, Clark CM, Lee VM, Trojanowski JQ. Biomarkers of neurodegeneration for diagnosis and monitoring therapeutics. Nat Rev Drug Discov 2007; 6:295-303.
3. Dubois B, Feldman HH, Jacova C, et al. Research criteria for the diagnosis of Alzheimer's disease: revising the NINCDS-ADRDA criteria. Lancet Neurol 2007; 6:734-746.
4. Okamura N, Arai H, Maruyama M, et al. Combined Analysis of CSF Tau Levels and [(123)I]Iodoamphetamine SPECT in Mild Cognitive Impairment: Implications for a Novel Predictor of Alzheimer's Disease. Am J Psychiatry 2002; 159:474-476.
5. Borroni B, Anchisi D, Paghera B, et al. Combined 99mTc-ECD SPECT and neuropsychological studies in MCI for the assessment of conversion to AD. Neurobiol Aging 2006; 27:24-31.
6. Schmidt R, Ropele S, Pendl B, et al. Longitudinal multimodal imaging in mild to moderate Alzheimer disease: a pilot study with memantine. J Neurol Neurosurg Psychiatry 2008; 79:1312-1317.
7. Silbert LC, Quinn JF, Moore MM. Changes in premorbid brain volume predict Alzheimer's disease pathology. Neurology 2003; 61:487-492.
8. Frisoni GB, Fox NC, Jack CR Jr, Scheltens P, and Thompson PM. The clinical use of structural MRI in Alzheimer disease. Nat Rev Neurol 2010; 6:67-77.
9. Bonte FJ, Devous MD Sr, Holman BL. Single photon emission computed tomographic imaging of the brain. In: Sandler MP, Coleman RE, Wackers FJTh, Patton JA, Gottschalk A, Hoffer PB, eds. Diagnostic Nuclear Medicine. 4th ed. Baltimore MD: Williams and Wilkins. In press
10. Jagust W, Thisted R, Devous MD Sr, et al. SPECT perfusion imaging in the diagnosis of AD: a clinical-pathologic study. Neurology 2001; 56: 950–956.
11. Jagust WJ, Reed B, Mungas D, Ellis W, Decarli C. What does fluorodeoxyglucose PET imaging add to a clinical diagnosis of dementia? Neurology 2007; 69:871-877.
12. Hoffman JM, Welsh-Bohmer KA, Hanson M, et al. FDG PET imaging in patients with pathologically verified dementia. J Nucl Med 2000; 41:1920-1928.
13. Klunk WE, Engler H, Nordberg A, et al. Imaging brain amyloid in Alzheimer's disease with Pittsburgh Compound-B. Ann Neurol 2004; 55:306-319.
14. Ikonomovic MD, Klunk WE, Abrahamson EE, et al. Post-mortem correlates of in vivo PiB-PET amyloid imaging in a typical case of Alzheimer's disease. Brain 2008; 131:1630-1645.
15. Petersen RC, Doody R, Kurz A, et al. Current concepts in mild cognitive impairment. Arch Neurol 2001; 58:1985–1992.
16. Petersen RC. Early diagnosis of Alzheimer's disease: is MCI too late? Curr Alzheimer Res 2009; 6:324-330.
17. Frisoni GB, Padovani A, Wahlund LO. The predementia diagnosis of Alzheimer disease. Alzheimer Dis Assoc Disord 2004;18:51-53.
18. Baron JC, Chételat G, Desgranges B, et al. In vivo mapping of gray matter loss with voxel-based morphometry in mild Alzheimer's disease. Neuroimage 2001; 14:298-309.

19. Frisoni GB, Testa C, Zorzan A, et al. Detection of grey matter loss in mild Alzheimer's disease with voxel based morphometry. J Neurol Neurosurg Psychiatry 2002; 73:657-664.
20. Hirao K, Ohnishi T, Hirata Y, et al. The prediction of rapid conversion to Alzheimer's disease in mild cognitive impairment using regional cerebral blood flow SPECT. Neuroimage 2005; 28:1014-1021.
21. Ishiwata A, Sakayori O, Minoshima S, Mizumura S, Kitamura S, Katayama Y. Preclinical evidence of Alzheimer changes in progressive mild cognitive impairment: a qualitative and quantitative SPECT study. Acta Neurol Scand 2006; 114:91–96
22. Braak H, Braak E. Evolution of neuronal changes in the course of Alzheimer's disease. J Neural Transm Suppl 1998; 53:127-140.
23. Pennanen C, Kivipelto M, Tuomainen S, et al. Hippocampus and enthorinal cortex in mild cognitive impairment and early AD. Neurobiol Aging 2004; 25:303-310.
24. Petersen RC, Smith GE, Waring SC, Ivnik RJ, Tangalos EG, Kokmen E. Mild cognitive impairment: clinical characterization and outcome. Arch Neurol 1999; 56:303-308.
25. Morris JC, Storandt M, Miller JP, et al. Mild cognitive impairment represents early-stage Alzheimer disease. Arch Neurol 2001; 58:397–405.
26. De Carli C, Miller BL, Swan GE, Reed T, Wolf PA, Carmeli D. Cerebrovascular and brain morphologic correlates of mild cognitive impairment in the National Heart, Lung, and Blood Institute Twin Study. Arch Neurol 2001; 58:643-647.
27. Garrido GE, Furuie SS, Buchpiguel CA, et al. Relation between medial temporal atrophy and functional brain activity during memory processing in Alzheimer's disease: a combined MRI and SPECT study. J Neurol Neurosurg Psychiatry 2002; 73:508-516.
28. Yamaguchi S, Meguro K, Itoh M, et al. Decreased cortical glucose metabolism correlates with hippocampal atrophy in Alzheimer's disease as shown by MRI and PET. J Neurol Neurosurg Psychiatry 1997; 62:596-600.
29. Mosconi L, Tsui WH, De Santi S, et al. Reduced hippocampal metabolism in MCI and AD: automated FDG-PET image analysis. Neurology 2005; 64:1860-1867.
30. Frisoni GB, Caroli A. Neuroimaging outcomes for clinical trials. J Nutr Health Aging 2007; 11:348-352.
31. Hardy JA, Higgins GA. Alzheimer's disease: The amyloid cascade hypothesis. Science 1992; 256:184-185
32. Akram A, Christoffel D, Rocher AB, et al. Stereologic estimates of total spinophilin-immunoreactive spine number in area 9 and the CA1 field: Relationship with the progression of Alzheimer's disease. Neurobiol Aging 2008; 29:1296-1307.
33. Bussiere T, Friend PD, Sadeghi N, et al. Stereologic assessment of the total cortical volume occupied by amyloid deposits and its relationship with cognitive status in aging and Alzheimer's disease. Neuroscience 2002; 112:75-91.
34. Hamalainen A, Pihlajamaki M, Tanila H, et al. Increased fMRI responses during encoding in mild cognitive impairment. Neurobiol Aging 2007; 28:1889-1903.
35. Seidenberg M, Guidotti L, Nielson KA, et al. Semantic memory activation in individuals at risk for developing Alzheimer disease. Neurology 2009; 73:612-20.

36. Johnson KA, Moran EK, Becker JA, Blacker D, Fischman AJ, Albert MS. Single photon emission computed tomography perfusion differences in mild cognitive impairment. J Neurol Neurosurg Psychiatry 2007; 78:240-247.
37. Ionov ID. Specific mechanism for blood inflow stimulation in brain area proe to Alzheimer's disease lesions. Int J Neurosci 2007; 117:1425-1442.
38. Samuraki M, Matsunari I, Chen WP, et al. Partial volume effect-corrected FDG PET and grey matter volume loss in patients with mild Alzheimer's disease. Eur J Nucl Med Mol Imaging 2007; 34:1658-1669.
39. Chetelat G, Desgranges B, Landeau B, et al. Direct voxel-based comparison between grey matter hypometabolism and atrophy in Alzheimer's disease. Brain 2008; 131:60-71.
40. Dobert N, Pantel J, Frolich L, Hamscho N, Menzel C, Grunwald F. Diagnostic value of FDG-PET and HMPAO-SPET in patients with mild dementia and mild cognitive impairment: metabolic index and perfusion index. Dement Geriatr Cogn Disord 2005; 20:63-70.
41. Koyama M, Kawashima R, Ito H, et al. SPECT imaging of normal subjects with Technetium-99m-HMPAO and Technetium-99m-ECD. J Nucl Med 1997; 38:587-592.
42. Scheltens P, Leys D, Barkhof F, et al. Atrophy of medial temporal lobes on MRI in "probable" Alzheimer's disease and normal ageing: diagnostic value and neuropsychological correlates. J Neurol Neurosurg Psychiatry 1992; 55:967-972.
43. Wahlund LO, Barkhof F, Fazekas F, et al.; European Task Force on Age-Related White Matter Changes. A new rating scale for age-related white matter changes applicable to MRI and CT. Stroke 2001; 32:1318-1322.
44. SPM, Statistical Parametric Mapping, version 2 (2002). London: Functional Imaging Laboratory. Available at: http://www.fil.ion.ucl.ac.uk/spm/software/spm2
45. Foster NL, Chase TN, Mansi L, et al. Cortical abnormalities in Alzheimer's disease. Ann Neurol 1984; 16:649–654.
46. Holman BL, Johnson KA, Gerada B, Carvalho PA, Satlin A. The scintigraphic appearance of Alzheimer's disease: a prospective study using technetium-99m-HMPAO SPECT. J Nucl Med 1992; 33:181–185 (published erratum appears in J Nucl Med 33,484).
47. De Santi S, de Leon MJ, Rusinek H, et al. Hippocampal formation glucose metabolism and volume losses in MCI and AD. Neurobiol Aging 2001; 22:529-539.
48. Nestor PJ, Fryer TD, Smielewski P, Hodges JR. Limbic hypometabolism in Alzheimer's disease and mild cognitive impairment. Ann Neurol 2003; 54:343–351.
49. Casanova R, Srikanth R, Baer A, et al. Biological parametric mapping: A statistical toolbox for multimodality brain image analysis. Neuroimage 2007; 34:137-143.
50. Chetelat G, Desgranges B, Landeau B, et al. Direct voxel-based comparison between grey matter hypometabolism and atrophy in Alzheimer's disease. Brain 2008; 131:60-71.
51. Ibanez V, Pietrini P, Alexander GE, et al. Regional glucose metabolic abnormalities are not the result of atrophy in Alzheimer's disease. Neurology 1998; 50:1585-1593.
52. Matsuda H, Kanetaka H, Ohnishi T, et al. Brain SPET abnormalities in Alzheimer's disease before and after atrophy correction. Eur J Nucl Med Mol Imaging 2002; 29:1502-1505.

53. Jack CR Jr, Knopman DS, Jagust WJ, et al. Hypothetical model of dynamic biomarkers of the Alzheimer's pathological cascade. Lancet Neurol 2010; 9:119-128.
54. Jack CR Jr, Lowe VJ, Senjem ML, et al. 11C PiB and structural MRI provide complementary information in imaging of Alzheimer's disease and amnestic mild cognitive impairment. Brain 2008; 131:665-680.
55. Jack CR Jr, Lowe VJ, Weigand SD, et al; Alzheimer's Disease Neuroimaging Initiative. Serial PIB and MRI in normal, mild cognitive impairment and Alzheimer's disease: implications for sequence of pathological events in Alzheimer's disease. Brain 2009; 132:1355-1365.
56. Vemuri P, Wiste HJ, Weigand SD, et al.; Alzheimer's Disease Neuroimaging Initiative. MRI and CSF biomarkers in normal, MCI, and AD subjects: diagnostic discrimination and cognitive correlations. Neurology 2009; 73:287-293.

Chapter 9

Acknowledgments

First and foremost, I wish to thank Maastricht University, which gave me the possibility to defend this thesis to obtain the degree of Doctor, and in particular my promotor, Prof. Frans R.J. Verhey, who took charge of my application, kindly provided helpful advices, and accurately revised the current thesis.

I am specially thankful to both my co-promotores. Thanks to Dr Giovanni B Frisoni, unlimited source of creative research ideas, who has been leading my research activity at the Laboratory of Epidemiology and Neuroimaging (LENITEM) in Brescia for years, injecting part of his enthusiasm and supervising the writing of all scientific publications included in this thesis. Thanks to Dr. Andrea Remuzzi, currently leading my research activity at the Mario Negri Institute in Bergamo, who encouraged me to pursue a PhD degree, and gave me the possibility to achieve this goal, taking advantage of research activities performed in Brescia.

My PhD would not have been possible without the agreement in place between Maastricht University and Mario Negri Institute, which allowed me to perform the PhD research activity in Italy, and finally defend this thesis in Maastricht.

Special thanks to all present and past colleagues at LENITEM, with whom I have shared research activity throughout the PhD, and with whom it is really a pleasure to work and spend time. Thanks to all colleagues at Mario Negri Institute, in particular Luca and Katia, for always being supportive.

Last but not least, I wish to thank Mrs Elsa Misdom, who guided me through all steps required for the attainment of the doctoral degree with kindness and helpfulness.

Chapter 10

Summary

Alzheimer's disease is the most common form of dementia, affecting more than 35 million people worldwide, and represents a top priority public health problem with huge social and economic burdens. As the population is aging and the principal risk factor for AD is age, the projected AD growth is dramatic, pointing out the pressing need of effective drug therapies and the interrelated need of early diagnosis.

To date, AD can be definitively diagnosed only by histopathologic examination of brain tissue. Late-stage hallmarks have been identified, including amyloid plaques, neurofibrillary tangles, neuronal cell loss, and gliosis, but the initiating mechanisms that trigger disease onset and drive its progression have not been fully understood, yet. During the last ten years most of the AD research has been focused on finding biomarkers that could be reliably used to diagnose AD at the earliest stages, monitor its progression, and possibly predict its onset. Neuroimaging is playing a more and more relevant role in the identification and quantification of AD in vivo, especially in preclinical stages, when a therapeutical intervention could be more effective.

Chapter 2 reviews the main neuroimaging techniques currently available for AD research and clinical purposes. Structural imaging (mainly MRI) enables to investigate both regional atrophy, giving special attention to the medial temporal lobe, and subcortical cerebrovascular damage. Functional imaging (SPECT, FDG-PET and functional MRI) provides pathophysiological information on synapse dysfunction, enabling to assess the efficacy of treatments in attenuating or potentially compensating for disease progression since the earliest stages. Microstructural imaging (DTI and MTI) probes into the finest cerebral structures, providing information about brain microstructure which could help elucidating the AD pathophysiology. Finally, amyloid imaging (mainly PIB-PET and FDDNP-PET) enables in vivo quantification of amyloid plaque load in AD, hopefully replacing lobar puncture for the investigation of the pathological processes occurring at the cellular level. Throughout the years, several imaging tools have been developed, ranging from simple visual rating scales to sophisticated computerized algorithms; such tools might be used presently or in the future in clinical practice to help AD diagnosis.

Each imaging technique enables to study a single cerebral alteration; in order to investigate the overall cerebral damage, and thus to increase prognostic power and diagnostic accuracy, several techniques should be combined.

Chapter 3 investigates the hypoperfusion pattern in a group of 23 amnesic MCI

patients who underwent both MR and 99mTc ECD SPECT imaging, 9 of whom converted and 14 did not convert to AD (19±10 follow-up time). As compared to normal controls, converters showed hypoperfusion in the right parahippocampal gyrus and left inferior temporal and fusiform gyri, whereas non-converters showed hypoperfusion in the retrosplenial cortex, precuneus and occipital gyri, mainly on the left side. Parahippocampal and inferior temporal but not retrosplenial hypoperfusion could thus be considered as prognostic indicators of conversion to dementia. Comparing significant hypoperfusion with atrophy pattern no overlap was found, suggesting that the detected hypoperfusion was not due to volumetric loss.

Chapter 4 investigates the association of MR-based measures of medial temporal lobe atrophy (MTA) and white matter hyperintensities (WMHs), assessed through visual rating scales, with voxel-wise grey matter perfusion in a group of 56 MCI patients who underwent both MR and 99mTc ECD SPECT imaging. MTA was found to be associated with hippocampal hypoperfusion while WMHs with grey matter hypoperfusion in areas of the insula and temporal neocortex. These results confirm that MTA is associated with local functional changes and suggest that WMHs may be associated with remote brain cortical dysfunction.

Chapter 5 studies the relationship between grey matter atrophy and amyloid deposition (assessed through [11C]-PIB-PET imaging) in 23 AD patients and 17 healthy elderly subjects. Voxel-based analysis showed that in AD patients atrophy mapped to a restricted region corresponding to the hippocampus while increased PIB uptake to large frontal, parietal, and posterior cingulate cortical areas. ROI-based analysis confirmed these findings, showing the largest effect size for atrophy in hippocampus and amygdala and the highest effect size for PIB uptake in frontal, retrosplenial, insular and temporal regions. Significant correlations between atrophy and increased PIB uptake were found in the hippocampal and amygdalar ROIs but not in the frontal, temporal, posterior cingulate/retrosplenial, insular, and caudate ROIs, suggesting that the medial temporal lobe might be highly susceptible to amyloid toxicity while neocortical areas might be more resilient.

Chapter 6 and 7 investigate the functional compensation and depression mechanisms in the regions affected by AD neuropathology on a voxel-by-voxel basis. Chapter 6 studies such mechanisms in terms of perfusion in 9 amnesic MCI patients with incipient AD who underwent both MR scan and 99mTc ECD SPECT, compared with 17 elderly

healthy subjects. Relatively preserved perfusion, likely to be compensatory in the setting of neuronal loss, was found in the posterior cingulate, in the head of the hippocampus, in the amigdala, and in the insula bilaterally, while functional depression occurred bilaterally in the parahippocampal gyrus, suggesting that a perfusional compensatory mechanism takes place in the neocortex, trying and counteracting the pathological changes of AD.

Chapter 7 studies functional compensation and depression mechanisms in terms of glucose metabolism in 25 AD patients who underwent both MR scan and FDG-PET, compared with 21 elderly healthy subjects. GM atrophy and hypometabolism mapped to similar regions, with variable degrees of severity. Significant metabolic compensation, which could reflect spared synaptic plasticity of the surviving neurons, was found in the amygdala, while exceeding hypometabolism, likely due to distant effects of atrophy and to additional hypometabolism inducing factors, was mainly located in the posterior cingulate cortex.

In conclusion, this thesis shows that structural damage, functional alterations, and protein build-up occurring at the cellular level, characterising Alzheimer's disease, are interrelated but not concurrent nor co-localised phenomena. These results points out the need of using multimodal analysis techniques to further assess the relationship between different biomarkers from the earliest stages, in order to better understand the mechanisms that trigger the disease onset and drive its progression, to increase early diagnostic accuracy and to lead to the identification of novel targets for pharmaceutical intervention which could delay disease progression.

Curriculum vitae

Anna Caroli was born on October 25, 1979 in Bergamo, Italy. She attended the "Liceo scientifico L. Mascheroni" secondary school in Bergamo. She studied Mathematics at Milan University, spending a 6-month period at the Department of Mathematics of Strathclyde University in Glasgow, UK, and she graduated on July 14, 2003 with honours discussing a research thesis about computational electrocardiology. Thereafter she started to work as a researcher at the Laboratory of Epidemiology, Neuroimaging and Telemedicine of the IRCCS Centro San Giovanni di Dio - Fatebenefratelli in Brescia, the Italian National Centre for Research and Care of Alzheimer's and Mental Diseases, where she carried on her PhD research project. In 2005 she spent a 2-month training period at the Brain Imaging Center of the Montreal Neurological Institute in Montreal, Canada. During these years she has presented original research at many international meetings, and she has performed peer review activity for high ranked journals such as Neuroimaging and Neurobiology of Aging. Since January 2008 she works as a researcher at the Medical Imaging Unit, Bioengineering Department of the Mario Negri Institute for Pharmacological Research in Bergamo.

List of publications

- Duchesne S, Caroli A, Geroldi C, Frisoni GB, Collins DL. Predicting clinical variable from MRI features: application to MMSE in MCI. Med Image Comput Comput Assist Interv Int Conf Med Image Comput Comput Assist Interv. 2005; 8:392-399.
- Testa C, Caroli A, Roberto V, Frisoni GB. Structural brain imaging in patients with cognitive impairment in the year 2015. Future Neurology 2006; 1:77-86.
- Caroli A, Testa C, Geroldi C, Nobili F, Guerra UP, Bonetti M, Frisoni GB. Brain perfusion correlates of medial temporal lobe atrophy and white matter hyperintensities in mild cognitive impairment. J Neurol 2007;254:1000-1008.
- Frisoni GB, Caroli A. Neuroimaging outcomes for clinical trials. J Nutr Health Aging 2007;11:348-352.
- Caroli A, Testa C, Geroldi C, Nobili F, Barnden LR, Guerra UP, Bonetti M, Frisoni GB. Cerebral perfusion predictors of conversion to Alzheimer's Disease in amnestic Mild Cognitive Impairment. J Neurol 2007;254:1698-1707.
- Duchesne S, Caroli A, Geroldi C, Barillot C, Frisoni GB, Collins DL. MRI-Based Automated Computer Classification of Probable AD Versus Normal Controls. IEEE Trans Med Imaging 2008; 27:509-520.
- Nobili F, Frisoni GB, Portet F, Verhey F, Rodriguez G, Caroli A, Touchon J, Calvini P, Morbelli S, De Carli F, Van de Pol LA, Visser PJ. Brain SPECT in subtypes of mild cognitive impairment: findings from the 'DESCRIPA' multicenter study. J Neurol 2008; 255:1344-1353.
- Caroli A, Geroldi C, Nobili F, Barnden LR, Guerra UP, Bonetti M, Frisoni GB. Functional compensation in incipient Alzheimer's disease. Neurobiol Aging 2010; 31:387-397 (epub June, 12 2008).
- Frisoni GB, Lorenzi M, Caroli A, Kemppainen N, Någren K, Rinne JO. In vivo mapping of amyloid toxicity in Alzheimer's disease. Neurology 2009; 72:1504-1511.
- Nobili F, De Carli F, Frisoni GB, Portet F, Verhey F, Rodriguez G, Caroli A, Touchon J, Morbelli S, Guerra UP, Dessi B, Brugnolo A, Visser PJ. SPECT predictors of cognitive decline and Alzheimer's disease in mild cognitive impairment. J Alzheimers Dis. 2009; 17:761-772.
- Duchesne S, Caroli A, Geroldi C, Collins DL, Frisoni GB. Relating one-year cognitive change in mild cognitive impairment to baseline MRI features. Neuroimage 2009;

47:1363-1370.

- Morbelli S, Piccardo A, Villavecchia G, Dessi B, Brugnolo A, Piccini A, Caroli A, Frisoni G, Rodriguez G, Nobili F. Mapping brain morphological and functional conversion patterns in amnestic MCI: a voxel-based MRI and FDG-PET study. Eur J Nucl Med Mol Imaging; epub 07 Aug 2009.
- Caroli A, Frisoni GB. Quantitative evaluation of Alzheimer's disease. Exp Rev Med Dev 2009; 6:569-588.
- Boccardi M, Almici M, Bresciani L, Caroli A, Bonetti M, Monchieri S, Gennarelli M, Frisoni GB. Clinical and Medial Temporal Features in a Family with Mood Disorders. Neurosci Lett 2010; 468:93-97.
- Caroli A, Antiga L, Cafaro M, Fasolini G, Remuzzi A, Remuzzi G, Ruggenenti P. Reducing Polycystic liver volume in ADPKD: effects of the extended release somatostatin analogue Octreotide. Clin J Am Soc Nephrol; epub 25 Feb 2010.
- Caroli A, Lorenzi M, Geroldi C, Nobili F, Paghera B, Bonetti M, Cotelli M, Frisoni GB. Metabolic compensation and depression in Alzheimer's Disease. Dement Geriatr Cogn Disord 2010; 29:37-45.
- Perico N, Antiga L, Caroli A, Fasolini G, Cafaro M, Ondei P, Rubis N, Diadei O, Gherardi G, Prandini S, Panozo A, Flores Bravo R, Rodriguez De Leon F, Gaspari F1, Cortinovis M, Motterlini N, Ene-Iordache B, Ruggenenti P, Remuzzi A, and Remuzzi G. Sirolimus therapy to halt the progression of ADPKD. J Am Soc Nephrol 2010; 21:1031-1040.
- Caroli A, Frisoni GB, and the Alzheimer's Disease Neuroimaging Initiative. The dynamics of Alzheimer's disease biomarkers in the ADNI dataset. Neurobiol Aging 2010; 31:1263-1274.